Purely Organic Thermally Activated Delayed Fluorescence Materials for Organic Light-Emitting Diodes

*Michael Y. Wong and Eli Zysman-Colman**

The design of thermally activated delayed fluorescence (TADF) materials both as emitters and as hosts is an exploding area of research. The replacement of phosphorescent metal complexes with inexpensive organic compounds in electroluminescent (EL) devices that demonstrate comparable performance metrics is paradigm shifting, as these new materials offer the possibility of developing low-cost lighting and displays. Here, a comprehensive review of TADF materials is presented, with a focus on linking their optoelectronic behavior with the performance of the organic light-emitting diode (OLED) and related EL devices. TADF emitters are cross-compared within specific color ranges, with a focus on blue, green–yellow, orange–red, and white OLEDs. Organic small-molecule, dendrimer, polymer, and exciplex emitters are all discussed within this review, as is their use as host materials. Correlations are provided between the structure of the TADF materials and their optoelectronic properties. The success of TADF materials has ushered in the next generation of OLEDs.

1. Introduction

Organic light-emitting diodes (OLEDs) have been the object of intense research since their initial invention in 1987 by Tang and Van Slyke[1] as they represent an unprecedented advancement in both display and lighting technologies. Compared with existing liquid-crystal displays (LCDs), OLEDs provide improved image quality and contrast, faster response times/refresh rates, are viewable over wider viewing angles, and are thinner and lighter. Even more impressive is the capacity to fabricate these devices on flexible substrates, to the point where OLED displays can be rolled up like a poster, a characteristic unfathomable in older-generation displays. OLEDs are also more energy-efficient because they do not require a backlighting system. Given that lighting alone constitutes around 20% of the global electricity consumption, a significant amount of electricity can be saved if OLEDs are widely adopted as a lighting technology.[2]

M. Y. Wong, Dr. E. Zysman-Colman
Organic Semiconductor Centre
EaStCHEM School of Chemistry
University of St Andrews
St Andrews, Fife KY16 9ST, UK
E-mail: eli.zysman-colman@st-andrews.ac.uk

DOI: 10.1002/adma.201605444

The earliest account of electroluminescence, the process of converting electrical energy into light, using organic materials can be traced back to 1963 when Pope et al. applied a direct current to an anthracene single crystal under a bias of 400 V using silver-paste electrodes.[3] Although anthracene fluorescence was observed, a driving voltage of 400 V is evidently not viable in practical applications. The seminal breakthrough in the development of OLEDs appeared in 1987 when Tang and Van Slyke reported a double-layered device using tris(8-hydroxyquinoline)aluminum (Alq_3) as the emitting and electron-transporting layer.[1] The green-emitting device showed an external quantum efficiency (EQE) of about 1% when driven at less than 10 V. This marked the dawn of OLED development and tremendous interest and effort from both academia and industry have followed subsequent to this pioneering work, resulting in the ultimate wide-scale commercialization of OLEDs, particularly for display applications.

In order to make OLEDs commercially viable for lighting applications, where the cost per unit must be competitive with presently used technology, there are a number of challenges that must be overcome aside from reducing the production cost. The organic emitters should have high photoluminescence quantum yields (PLQYs), which directly impact the device efficiency. The energy levels of the frontier molecular orbitals (i.e., highest occupied and lowest unoccupied molecular oribitals (HOMOs and LUMOs)) of each of the layers in the device should be optimally relatively aligned in order to: i) minimize the barrier to charge injection, and ii) control the recombination region within the device, which greatly affects both the device efficiency and lifetime.[4] The organic materials must demonstrate sufficient thermal stability to be compatible with their vacuum deposition during device fabrication or produce thin films of suitable morphology when spin-coated during solution processing. Regardless of the fabrication method, the organic material must be morphologically stable during device operation when Joule heat is produced in the device.[5]

Aside from the aforementioned challenges, another key issue to address is the management of hole and electron recombination within the device, each possessing their own spin. Unlike photoexcitation, in which mainly singlet excited states are produced in the organic emitters, exciton formation through charge (hole and electron) recombination in OLED devices results in 25% singlets and 75% triplets, according to

spin statistics.[6] Whilst the former contributes to light emission by fluorescence (k_F, **Figure 1**) with short emission lifetimes (in the nanosecond regime), phosphorescence (k_P, Figure 1) from the latter with emission lifetimes extending to milliseconds occurs due to the spin-forbidden nature of the emission. The very long emission lifetime makes the triplet excitons vulnerable to nonradiative deactivation as heat loss to the surroundings. Assuming Lambertian emission and a light outcoupling efficiency of 20%, the maximum external quantum efficiency (EQE) for an OLED with a fluorescent emitter is only 25% of 20% = 5%.[7] As a response to this shortcoming in device efficiency, Baldo et al. in 1998 reported an OLED device in which a red-emitting organometallic complex, 2,3,7,8,12,13,17,18-octaethyl-21*H*,23*H*-porphyrine platinum(II) (PtOEP), was doped into a fluorescent host.[6] Through efficient energy transfer from the host to the emitter, both singlets and triplets were harvested for light emission with reported external and internal quantum efficiencies (IQE) of 4% and 23%, respectively. This seminal contribution can be regarded as the dawn of phosphorescence-based OLEDs. The value of employing organometallic complexes as emitters is their capacity to access triplet states via intersystem crossing (ISC) from the singlet excited state through strong spin–orbit coupling mediated by the heavy metal (e.g., Ir and Pt) in the complexes.[2,6,8] The phosphorescence emission decays in these complexes within a useful microsecond regime. Since 2001, devices based on organometallic complexes with nearly 100% IQE have been reported.[9] Commercial OLED devices for displays presently rely on green- and red-emitting cyclometalated iridium complexes.[10] However, the rarity of the heavy-metal salt reagents is a major detracting feature and contributes to increased cost of the device; potential environmental contamination of these heavy metals also is an element of concern. Moreover, while organometallic complexes exhibit impressive performance metrics in red and green-emitting devices, the corresponding blue-emitting complexes are thus far not satisfactory in terms of their combined stability, their color purity and their brightness during device operation.[11] Possible reasons for their poor performance include triplet–polaron annihilation (TPA), which results in the formation of: i) highly energetic polarons that cause device degradation,[11] and ii) unstable radical cations on the complex, which cause ligand dissociation or complex isomerization.[12] Bright, deep blue and stable emitters for OLEDs are urgently needed, and this is representative of the grand challenges in emitter design at present.

In response to this need, thermally activated delayed fluorescence (TADF) is the most promising exciton harvesting mechanism used in OLED devices. Since the first reported OLED based on an organic TADF emitter in 2011[13] tremendous attention in recent years has been devoted to improving their performance (**Figure 2**).[14] Similar to phosphorescent organometallic emitters, purely organic TADF emitters can recruit both singlet and triplet excitions for light emission and hence achieve 100% IQE.[14b] One important advantage of TADF emitters is that they can be purely organic, thus avoiding the problems associated with the use of heavy-metal-based organometallic complexes.[15] TADF relies on a small singlet–triplet energy gap, ΔE_{ST}, defined as the gap between the lowest energy triplet state (T_1) and the lowest energy singlet state (S_1). When ΔE_{ST} is sufficiently small, taken usually as <0.1 eV, thermal upconversion from the triplet state to the singlet state by reverse intersystem-crossing (RISC) becomes possible.[15a] TADF emitters typically show two types of photoluminescence (PL): the prompt fluorescence in which the history of the singlet exciton does not involve communication with the triplet manifold, and delayed fluorescence, which is the result of an initial ISC to the triplet state followed by repopulation of the singlet state via RISC.[15a]

In an organic TADF material, ΔE_{ST} is critical to the success of singlet harvesting because it governs the rate of RISC, k_{RISC}, according to the following Boltzmann distribution:[14a]

$$k_{RISC} \propto \exp\left(\frac{\Delta E_{ST}}{k_B T}\right) \quad (1)$$

Michael Yin Wong graduated from the Hong Kong University of Science and Technology with a B.Sc. in chemistry. He then obtained an M.Phil. in chemistry from the Hong Kong Baptist University under the supervision of Dr. Louis Leung Man Lay, working on stacking poly(dibenzofulvene)s and luminescent polymers and small molecules for optoelectronic devices. Currently, he is in the final year of his Ph.D. in chemistry under the guidance of Dr. Eli Zysman-Colman at the University of St Andrews, where he has been working on novel thermally activated delayed fluorescence (TADF) emitters for organic light-emitting diodes (OLEDs) and light-emitting electrochemical cells (LEECs).

Eli Zysman-Colman obtained his Ph.D. from McGill University in 2003 under the supervision of David N. Harpp where he conducted research in physical organic sulfur chemistry. He then completed two postdoctoral fellowships, one in supramolecular chemistry with Jay Siegel at the Organic Chemistry Institute, University of Zurich and the other in inorganic materials chemistry with Stefan Bernhard at Princeton University. After six years in Canada as an assistant professor, in 2013 he moved to the University of St Andrews, where he is presently Reader in Optoelectronic Materials. His research program focuses primarily on the rational design of luminophores for solid-state lighting based on organic light-emitting diode (OLED) and light-emitting electrochemical cell (LEEC) electroluminescent devices.

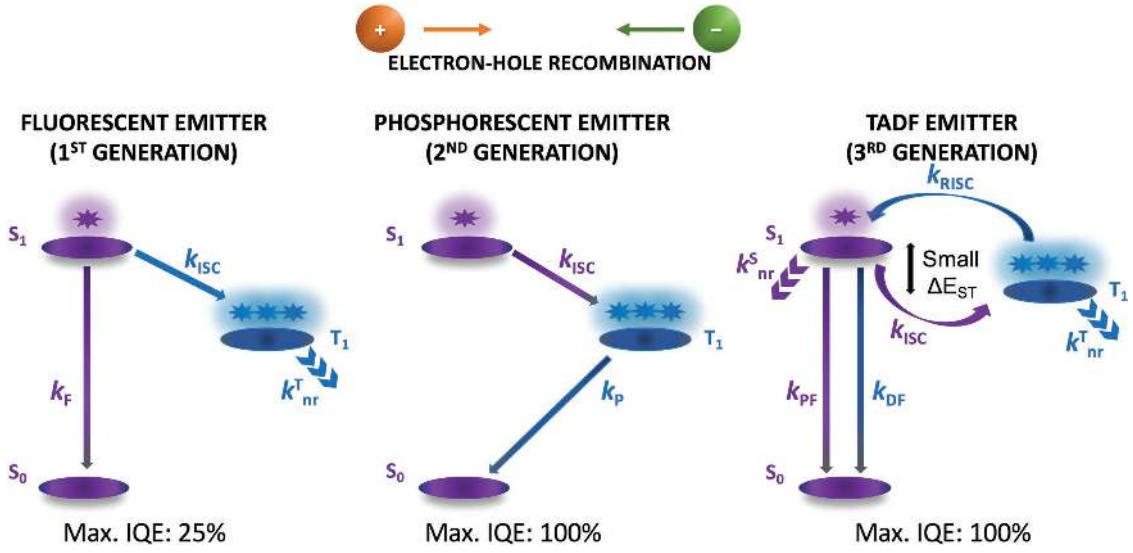

Figure 1. Comparison of emission mechanism in first-generation (fluorescent), second-generation (phosphorescent), and third-generation (TADF) emitters. F = fluorescence; P = phosphorescence; PF = prompt fluorescence; DF = delayed fluorescence; ISC = intersystem crossing; RISC = reverse intersystem crossing; ΔE_{ST} = the energy difference between the first excited singlet and triplet states; nr = nonradiative.

where k_{RISC} is the rate constant of RISC, k_B is Boltzmann's constant and T is the temperature. A consequence of Equation (1) is that a large ΔE_{ST} results in slow k_{RISC} and a correspondingly longer delayed fluorescence ($k_{DF} = 1/\tau_d$).[16] The delayed fluorescence lifetime, τ_d, has been found to decrease with either an increasing rate of ISC (k_{ISC})[17] or of RISC (k_{RISC}).[16] In particular, τ_d can be expressed mathematically as:[18]

$$\frac{1}{\tau_d} = k_{nr}^{T} + \left(1 - \frac{k_{ISC}}{k_r^s + k_{nr}^s + k_{ISC}}\right) k_{RISC} \tag{2}$$

where k_r^s ($k_r^s = k_{PF}$, Figure 1) and k_{nr}^s are the radiative and nonradiative decay rate constants of the S_1 state, respectively. In Cu(I) TADF compounds where k_{ISC}, k_{RISC}, and k_P are relatively fast as a result of the increased spin–orbital coupling due to the heavy atom effect of Cu metal (ζ: 857 cm^{-1}), which enhances the intersystem-crossing rate, an equilibrium between excited singlet and triplet states ensues, which is governed by a Boltzmann distribution, and the emission decay time τ is given by:[19]

$$\tau = \frac{3 + \exp\left(-\frac{\Delta E_{ST}}{k_B T}\right)}{\frac{3}{\tau(T_1)} + \left[\frac{1}{\tau(S_1)}\right] \exp\left(-\frac{\Delta E_{ST}}{k_B T}\right)} \tag{3}$$

In organic compounds, formally spin-forbidden processes are much slower. The key difference between Equation (2) and Equation (3) is the presence of "$\tau(T_1)$" such that in Cu(I) complexes phosphorescence from T_1 becomes kinetically competitive with both nonradiative quenching, k_{nr}^T, of the triplet state, and k_{RISC}, whereas in purely organic materials both of these processes are retarded.

Importantly, ΔE_{ST} is correlated with the structure of the emitter, as it is proportional to the exchange integral, J:[20]

$$\Delta E_{ST} = E_S - E_T = 2J \tag{4}$$

J in turn depends on the electron density overlap between the HOMO and LUMO, assuming that the S_1 and T_1 states are dominated by HOMO to LUMO transitions:

$$J = \iint \phi_{HOMO}(\mathbf{r}_1)\phi_{LUMO}(\mathbf{r}_2)\frac{1}{|\mathbf{r}_2 - \mathbf{r}_1|}\phi_{HOMO}(\mathbf{r}_2)\,\phi_{LUMO}(\mathbf{r}_1)\,d\mathbf{r}_{1d}\mathbf{r}_2 \tag{5}$$

where ϕ_{HOMO} and ϕ_{LUMO} are the spatial distributions of the HOMO and the LUMO, respectively, and $\mathbf{r}_1$ and $\mathbf{r}_2$ are position vectors (for a more detailed treatise see ref. [21]). It follows that reducing the overlap between the HOMO and the LUMO decreases the exchange integral (J) and hence ΔE_{ST}.

The normally spin-forbidden ISC and RISC processes in purely organic TADF emitters can therefore become efficient thanks to a small ΔE_{ST} and can be explained by Equation (6):[15a]

$$\lambda \propto \frac{H_{SO}}{\Delta E_{ST}} \tag{6}$$

where λ and H_{SO} are the first-order mixing coefficient between singlet and triplet states and the spin–orbital interaction, respectively. Thus, despite the small H_{SO} in purely organic materials, ISC and RISC processes can still occur readily if the ΔE_{ST} is sufficiently small.

The nature of the S_1 and T_1 states is also an important factor when determining the efficiency of the RISC process. El-Sayed's rule[22] broadly states that for ISC (and RISC) to efficiently occur there must be a change in the symmetry of the excited state. Thus, k_{ISC} and k_{RISC} will be fast if, for instance, T_1 were a locally excited (LE) state while S_1 were a charge-transfer (CT) state. However, there are cases when RISC can be efficient without El-Sayed's rule being rigorously followed. Indeed, excited states involved in the TADF process are not typically either pure CT

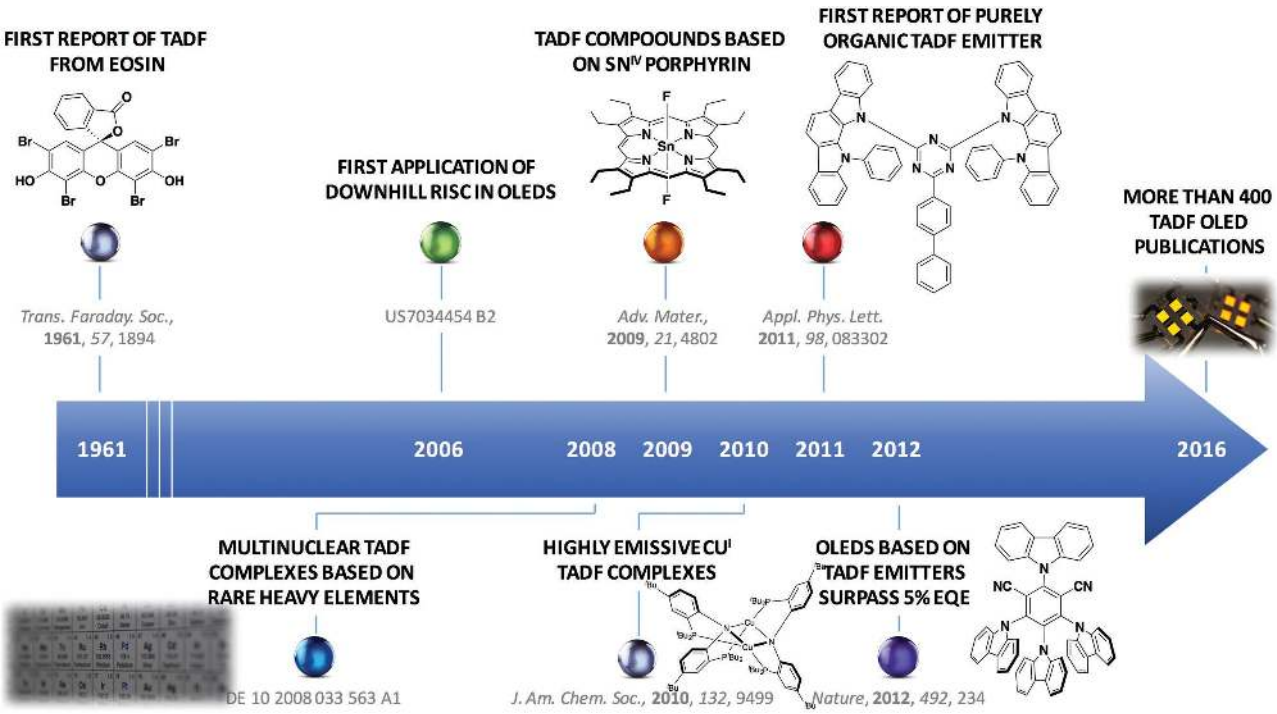

Figure 2. Timeline of developments of TADF-based OLEDs.

or LE states but mixed CT–LE with possibly different fractions of CT character. Therefore, El-Sayed's rule would not strictly apply.[23] If the ΔE_{ST} is very small, hyperfine-coupling (HFC) comes into play and El-Sayed rule does not have to be obeyed in this case.[24] Some organic TADF emitters have elements that are relatively heavier than typical C, H, N elements, and these elements assist ISC or RISC by the heavy-atom effect. A typical example is sulfur, which is commonly used in deep-blue or sky-blue TADF emitters.[15c] Finally, regardless of the nature of the lowest triplet state, it cannot be ruled out that there are higher triplet levels that are themselves lower in energy than the lowest singlet excited state. This permits a route governed by both reverse internal conversion (RIC) and RISC to harvest triplet excitons.

Indeed, TADF, also known as E-type delayed fluorescence in the early literature,[25] is a photophysical mechanism that was first reported in 1961, when eosin was observed to emit delayed fluorescence in ethanol at 70 °C (Figure 2). Other examples of organic molecules that have been shown to emit via TADF include benzophenone,[26] aromatic thiones,[27] thioketones[28] and 9,10-anthraquinone.[29] Although the vast majority of effort and attention is devoted to purely organic TADF emitters, the very first TADF emitters applied in OLED devices stemmed from more traditional organometallic complexes and, interestingly, the TADF-emitter development history showed a gradual transition from heavy metals (e.g., Ir and Pt) to lighter elements (e.g., C and N).[30] In 2008, Yersin and Monkowius filed a patent in which multinuclear complexes based on iridium, palladium, platinum, rhodium, and gold characterized by a small singlet–triplet energy gap (500–2000 cm^{-1}) between the lowest triplet state and the first higher lying singlet state were applied in OLEDs for singlet harvesting.[31] In 2009, Adachi et al. reported the use of a Sn^{4+} porphyrin as a TADF emitter in OLEDs, albeit in devices with very low efficiencies.[32] The following year, Deaton et al. reported the first example of a highly emissive TADF bis(phosphine)diarylamido dinuclear copper(I) complex,[24] work that has inspired much additional research into this class of emitters by the likes of Yersin,[33] Thompson,[33c,34] Bräse,[35] and others.[36] In 2011, the first purely organic TADF emitter, **PIC-TRZ**, was reported by Adachi et al.[13] The EQE of the OLED was 5.3%, which is still close to the theoretical limit of conventional fluorescent emitters[13] and thus not incontrovertible proof that the mechanism of emission in the device was TADF. Finally in 2012, a series of groundbreaking organic TADF emitters (**CDCBs**) were reported by the same group.[15a] These emitters are based on donor–bridge–acceptor architectures in which the donor carbazoles are in a highly twisted conformation relative to the phthalonitrile plane, resulting in a reduced overlap between the HOMO and the LUMO and a correspondingly small singlet–triplet energy gap, ΔE_{ST}. The best performing OLED in this study achieved an astonishing EQE of 19.3%, which clearly surpasses the expected theoretical maximum of 5% for electroluminescent (EL) devices employing ordinary fluorescent emitters. Such a high efficiency was the definitive demonstration that both singlet and triplet excitons were being harvested within the device. Since this report, organic TADF emitters for use in EL devices have become a red-hot topic of academic and industrial research, evidenced by more than 400 reports in this field to date (**Figure 3**).

This review aims to provide a comprehensive summary of the development of organic TADF emitters, together with their monochromatic device performance and their use in white OLEDs. We shall then discuss host materials designed for TADF emitters, which themselves can be employed as

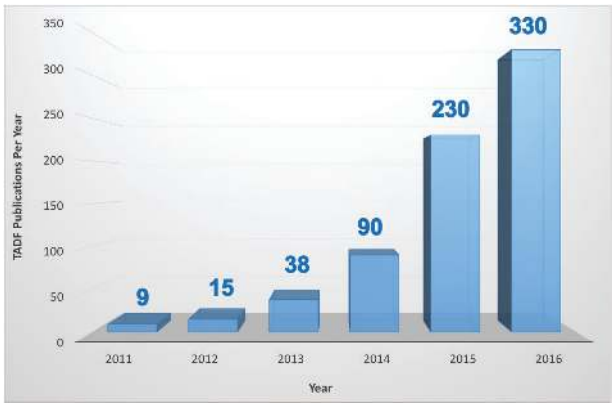

Figure 3. Number of TADF publications per year. Keyword: "thermally activated delayed fluorescence" or "TADF". Scifinder search conducted: 16/11/2016.

hosts for traditional fluorophores and phosphors. Finally, we shall introduce exciplex systems that show the TADF phenomenon.

2. TADF Emitters

The first purely organic TADF emitter **PIC-TRZ** (**Figure 4**) was reported in 2011 by Adachi et al.[13] Limited by its moderate PLQY of 39% in doped thin film (6 wt% in 1,3-bis(*N*-carbazolyl)benzene (mCP) and only 32% triplet utilization efficiency, the device (ITO/α-NPD/mCP/6 wt% **emitter**:mCP/BP4mPy/LiF/Al) (ITO = indium tin oxide; α-NPD = *N*,*N*′-di(1-naphthyl)-*N*,*N*′-diphenyl-(1,1′-biphenyl)-4,4′-diamine; BP4mPy = 3,3′,5,5′-tetra[(*m*-pyridyl)-phen-3-yl]biphenyl) shows an EQE of 5.3%. With the explosion of interest in the development of TADF emitters, there have been more than 100 new compounds reported over the past 3.5 years. As will be demonstrated below, the performance of OLEDs employing TADF emitters across the entire visible spectrum is comparable in terms of efficiency with those using organometallic phosphors. Device EQE can reach beyond 30% using TADF emitters.[37] Numerous other TADF devices show an EQE of greater than 20%. There have been several recently published reviews where there has been either a partial focus on TADF compounds or the reviews have been written to take a broad overview of the subject, including a discussion of organometallic TADF complexes.[14,19,38] Given the paradigm-shifting importance of TADF emitters in EL devices, now is the time to provide a comprehensive review of the field, organized herein as a function of EL emission color.

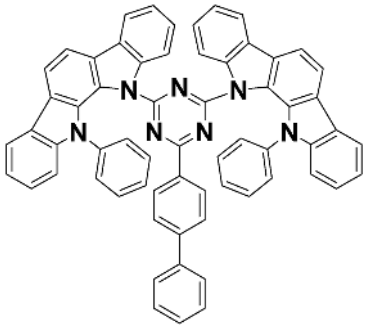

PIC-TRZ

Figure 4. Chemical Structure of **PIC-TRZ**.

2.1. Blue TADF Emitters

In this section, we define blue emitters as those compounds whose electroluminescence peak wavelength (EL_{max}) is shorter than 500 nm. This definition is used as EL_{max} data are always provided, whereas Commission Internationale De L'Éclairage (CIE) coordinates are only provided in about 50% of reports. We recognize that not all emitters in this section will produce blue light, but our stated threshold serves to aid in the categorization of the emitters within this review, one that we have successfully used in the past for phosphorescent iridium emitters.[39] The distribution of CIE coordinates for the OLEDs reported in this section is shown in **Figure 5** (vide infra). **Table 1** summarizes the photophysical properties of emitters in this section while **Table 2** summarizes the OLED device performance metrics. As blue phosphorescent complexes are widely recognized for their instability in EL devices,[11] great hope exists that blue TADF devices can address this weakness in OLED technology. In 2012, Adachi et al. reported the very first class of deep-blue TADF emitters (**1**–**3**) (**Figure 6**) based on diphenylsulfone as the acceptor.[15c] The best device within the study (ITO/α-NPD/TCTA/CzSi/10 wt% **emitter**:DPEPO/DPEPO/TPBI/LiF/Al) (TCTA = tris(4-carbazoyl-9-ylphenyl) amine; DPEPO = bis[2-(diphenylphosphino)phenyl] ether oxide; TPBI = 2,2′,2″-(1,3,5-benzinetriyl)-tris(1-phenyl-1-*H*-benzimidazole)) shows an EQE of 9.9% and CIE coordinates of (0.15, 0.07) with **3** (λ_{max}: 423 nm; PLQY: 80%; τ_d: 540 µs, 2600 µs in 10 wt% DPEPO; ΔE_{ST}: 0.32 eV) used as the emitter. The authors suggested that in order to achieve a small ΔE_{ST}, the energy gap between the lower energy triplet donor-centered locally excited π–π^* state (^{3}LE) and the higher-energy triplet charge-transfer state (^{3}CT) must be small. This hypothesis was verified by the appearance of delayed fluorescence when the medium of the emitter was changed from nonpolar hexane to polar methanol, where the ^{3}CT is significantly stabilized, evidenced by the positive solvatochromism. Under these conditions reverse internal conversion (RIC) occurs from ^{3}LE to ^{3}CT, followed by efficient RISC to ^{1}CT. Indeed, emitters **1** (λ_{max}: 421 nm; PLQY: 60%; τ_d: 850 µs in 10 wt% DPEPO; ΔE_{ST}: 0.54 eV) and **2** (λ_{max}: 430 nm; PLQY: 66%; τ_d: 840 µs, 8200 µs in 10 wt% DPEPO; ΔE_{ST}: 0.45 eV), while having a similar energy ^{1}CT state compared with **3** (λ_{max}: 423 nm), each possess a diphenylamine ^{3}LE state that is lower in energy than that with carbazole, thereby translating into compounds with larger ΔE_{ST} of 0.54 eV and 0.45 eV, respectively. Nevertheless, it is particularly challenging to design deep-blue TADF emitters that adhere to this ordering of excited states because of the high intrinsic energies of charge-transfer singlet and triplet states. Control of the conjugation length (e.g., through sterics[40] or substitution pattern[41]) and the choice of donor are important in this regard. However, Dias et al.

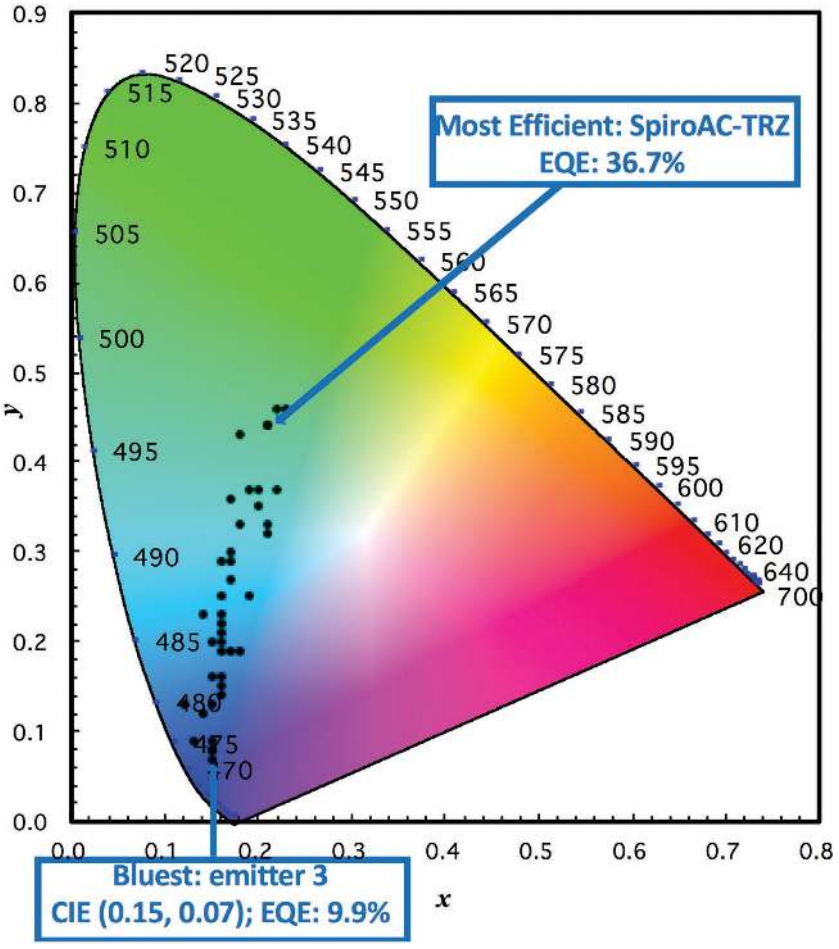

Figure 5. Summary of CIEs of blue TADF OLED.

proposed another plausible mechanism of RISC in this type of molecule.[42] They performed a detailed photophysical study on a series of emitters and found that, for emitters with ΔE_{ST} greater than 0.3 eV, RISC is still possible and may even be very efficient. For example, the molecule **DTC-DBT** (cf. **Figure 7**) possesses a high ΔE_{ST} of 0.35 eV, but 100% of the triplet excitons are harvested by the RISC process. The presence of heteroatom lone pairs form an important "hidden" ^{3}n–π^* state sandwiched between the higher ^{3}CT and the lower ^{3}LE state. Thus, up-conversion happens in an even more complex cascade manner: $^3\text{LE} \rightarrow {}^3\text{n}\pi^* \rightarrow {}^3\text{CT} \rightarrow {}^1\text{CT}$; however, the energy gap between the higher ^{3}CT and the ^{3}n–π^* depicted in their work is around 0.38 eV (**Figure 8**), which we believe is probably too high for an efficient up-conversion.

Indeed, Chen et al. pointed out that, for the molecule **DTC-DBT**, the lowest ^{3}LE state already has some mixing with the ^{3}n–π^* state.[43] Rather, they stressed the importance of non-adiabatic effects in butterfly-shaped donor–acceptor–donor (D–A–D) molecules such as **DTC-DBT**. When the donor and acceptor groups rotate such that they are all mutually orthogonal, a conical intersection (CI) between the low-lying excited states (i.e., between S_1 and S_2 as well as between T_1 and T_2) occurs. At the CI point, the non-adiabatic coupling (NAC) matrix element between two excited states becomes infinite, which is proportional to the RISC rate. It is important to note that this situation does not hold for antisymmetric donor–acceptor (D–A) molecules. A recent study by Etherington et al.[44] suggests that second order vibronic coupling between the ^{3}LE and ^{3}CT states facilitate the RISC process.

As a follow up to their pioneering blue TADF emitter **DTC-DPS** (Figure 6),[15c] Adachi et al. prepared a modified deep-blue emitter **DMOC-DPS** (λ_{max}: 455 nm; PLQY: 80%; τ_d: 114 µs in 10 wt% DPEPO; ΔE_{ST}: 0.21 eV) (Figure 6) in which the di-*tert*-butylcarbazole donor was replaced by the stronger electron-donating dimethoxycarbazole.[45] Given that the S_1 state is of charge-transfer character (^{1}CT), whereas the T_1 state is a locally excited state ($^3\text{LE} = {}^3\pi\pi^*$, as suggested by the structured phosphorescence at 77 K), the introduction of the more electron-donating methoxy groups lowers the S_1 state (λ_{max}: 455 nm for **DMOC-DPS** vs λ_{max}: 423 nm for **DTC-DPC**) while keeping the energy of T_1 relatively unchanged. As a result, a smaller ΔE_{ST} is achieved in **DMOC-DPS** (0.21 eV) compared with the parent **DTC-DPS** (0.32 eV). The smaller ΔE_{ST} results in a shorter delayed component lifetime (114 µs for **DMOC-DPS**, 540 and 2600 µs for **DTC-DPS**) and thus the **DMOC-DPS** device (ITO/α-NPD/TCTA/CzSi/10 wt% **emitter**:DPEPO/DPEPO/TPBI/LiF/Al) demonstrates lower efficiency roll-off, emitting deep-blue color (CIE coordinates: 0.16, 0.16) with an EQE of 14.5%. In another publication by the same group, a structurally similar blue TADF emitter **DMAC-DPS** (λ_{max}: 464 nm; PLQY: 80%; τ_d: 3.1 µs in 10 wt% mCP; ΔE_{ST}: 0.08 eV) device (ITO/α-NPD/TCTA/CzSi/10 wt% **emitter**:DPEPO/DPEPO/TPBI/LiF/Al) showed an EQE of 19.5%.[15b] The choice of the dimethylacridan donor results in a higher ^{3}LE state than ^{3}CT state, producing a small ΔE_{ST} of 0.08 eV. The emitter has also been applied in nondoped devices, which demonstrate more facile device fabrication and higher device reliability.[46] The methyl groups on the acridan moiety of **DMAC-DPS** prevent intermolecular interactions in its neat film. Moreover, the Stokes shift of the emitter is sufficiently large to prevent self-quenching by Förster resonance energy transfer (FRET). As a result, both PLQYs and delayed component emission lifetimes of **DMAC-DPS** in neat (88%) and doped film (80%) are fairly similar. The best non-doped device (ITO/MoO_3/mCP/neat **emitter**/DPEPO/LiF/Al) of **DMAC-DPS** in the study shows an EQE of 19.5%. A similar TADF emitter, **DMAC-BP** (λ_{max}: 506 nm; PLQY: 85%; τ_d: 2.7 µs as neat emitter; ΔE_{ST}: 0.07 eV) (Figure 6) also performs extraordinarily well in a nondoped configuration with an EQE of 18.9%, albeit its green emission being due to the stronger acceptor strength of the benzophenone. Lee, Song, and Lee reported a deep blue TADF emitter **DMTDAc** (PLQY: 100%; τ_d: 1.2 µs

Table 1. Summary of photophysical and electrochemical properties of blue TADF emitters (EL_{max} < 500 nm).

Emitter	Solution PL_{max}/PLQY/$\tau^{a)}$ (medium) [nm/%/µs]	Solid State PL_{max}/PLQY/$\tau^{a)}$ (medium) [nm/%/µs]	ΔE_{ST} [eV]	HOMO [eV]	LUMO [eV]	Ref.
1	402/57/90 (PhMe)	421/60/850 (10 wt% in DPEPO)	0.54	5.89	2.62	[15c]
3	404/69/270 (PhMe)	423/80/540,2600 (10 wt% in DPEPO)	0.32	5.81	2.52	[15c]
2	419/65/140 (PhMe)	430/66/840,8200 (10 wt% in DPEPO)	0.45	5.65	2.46	[15c]
DTC-mBPSB	–/69.3/– ($CHCl_3$)	434/71.0/1.16 (10 wt% in DPEPO)	0.24	5.47	2.49	[48]
Cz2BP	438/21/– (PhMe)	444/55/710 (6 wt% in DPEPO)	0.21	5.74	2.64	[49]
SPXZPO	467/45/–	470/42/95 (10 wt% in DPEPO)	0.26	5.57	2.24	[81]
DMTDAc	≈460/–/– (PhMe)	–/100/1.2 (UGH3:TSPO1)	0	6.10	3.35	[85]
2PXZ-TAZ	462/15.2/28.9 (PhMe)	467/52/2090 (6 wt% in DPEPO)	0.23	–	–	[86]
CNBPCz	458/46/–	–/37/24.3 (5 wt% in DPEPO)	0.27	–	–	[75]
DCzTrz	≈440/43/3.1 (PhMe)	–/–/–	0.25	5.88	2.86	[53]
DABNA-1	462/89/– (DCM)	460/88/93.7 (1 wt% in mCBP)	0.18	5.58	2.91	[80]
DMOC-DPS	445/56/93 (PhMe)	≈455/80/114 (10 wt% in DPEPO)	0.21	5.55	–	[45]
DPXZPO	471/57/–	476/55/31 (10 wt% in DPEPO)	0.19	5.57	2.57	[81]
CzBPCN	453/76/–	–/94/48.2 (5 wt% in DPEPO)	0.27	–	–	[75]
DCzIPN	–/–/–	447/87/1.2 (1 wt% in polystyrene)	0.05	6.26	3.56	[87]
3CzFCN	443/76/– (PhMe)	≈470/74/28 (10 wt% in SiCz)	0.06	6.38	3.56	[76]
TPXZPO	474/65/–	478/67/17 (10 wt% in DPEPO)	0.11	5.57	2.66	[81]
DMAC-PXB	472/–/– (PhMe)	440/98/2.36 (6 wt% in polystyrene)	0.013	5.81	2.46	[77]
DDCzTrz	≈450/66/2.8 (PhMe)	–/–/–	0.27	6.01	2.90	[53]
DTPDDA	≈460/–/– (PhMe)	≈470/74/0.1,2.3,25.4 (16 wt% in mCP:TSPO1)	0.14	5.57	2.80	[57]
DABNA-2	470/85/– (DCM)	469/90/65.3 (1 wt% in mCBP)	0.14	5.38	2.75	[80]
DMAC-DPS	460/80/7.1 (PhMe)	464/80/3.1 (10 wt% in mCP)	0.08	5.92	2.92	[15b]
4CzFCN	453/81/– (PhMe)	≈480/100/17 (10 wt% in SiCz)	0.06	6.31	3.49	[76]
44TCzPN	444/61/4.2 (PhMe)	–/–/–	0.21	6.38	3.54	[88]
34TCzPN	448/66/3.0 (PhMe)	–/–/–	0.16	6.30	3.52	[88]
TMCPOB	451/56/2.1 (PhMe)	–/–/–	0.06–0.12	5.8	2.9	[79]
SXDPAPOB	443/86/3.5 (PhMe)	–/–/–	0.06–0.12	5.9	2.9	[79]
P3	427,491/18.4/5.4 (PhMe)	470/27.5/2.4 (neat)	–	–	–	[89]
CzAcSF	–/71/5.6 (THF)	≈450/–/– (in DPEPO)	0.14	5.89	3.00	[90]
TCzTrz	–/100/13.5 (PhMe)	≈460/100/– (30 wt% in DPEPO)	0.16	5.40	2.18	[55]
SFDPAPOB	456/76/4.0 (PhMe)	–/–/–	0.06–0.12	5.8	2.9	[79]
DTC-pBPSB	–/56.3/– ($CHCl_3$)	461/66.6/1.23 (10 wt% in DPEPO)	0.05	5.50	2.65	[48]
DMAC-DPS	–/–/–	470/88/3.0 (neat)	–	–	–	[46]
2CzPN	473/46.5/166 (PhMe)	–/–/–	–	–	–	[15a]
TB-1PXZ	–/11/–	478/12/5.9 (10 wt% in CzSi)	0.12	5.08	2.24	[91]
5CzCF3Ph	481/43/15.3 (PhMe)	495/–/– (10 wt% in mCP)	0.02	5.57	2.75	[84]
CC2BP	462/38/– (PhMe)	475/73/460 (6 wt% in DPEPO)	0.14	5.65	2.63	[49]
mPTC	455/–/–(cyclohexane)	498/54.9/12.9 (6.5 wt% in mCP)	0.01	5.12	2.84	[92]
m-ATP-ACR	490/36/– (PhMe_	483/52/– (6 wt% in mCBP)	0.13	5.9	3.1	[63,93]
BFCz-2CN	–/94.6/– (PhMe)	≈500/85/2.6 (1 wt% in mCP)	0.13	6.19	3.58	[66]
BTCz-2CN	–/94.0/– (PhMe)	≈500/85/2.0 (1 wt% in mCP)	0.17	6.17	3.58	[66]
35IPNDCz	470/50/145 (PhMe)	≈500/58/– (6 wt% in DPEPO)	0.14	–	–	[72]
DCBPy	490/13.6/0.6 (PhMe)	514/88/– (5 wt% in CzPS)	0.07	5.75	2.88	[50]
DAC-Mes_3B	477/91/– (PhMe)	477/87/– (16 wt% in DPEPO)	0.062	5.4	2.7	[78]
Ac-MPM	478/–/– (PhMe)	489/80/26.2 (10 wt% in DPEPO)	0.19	5.66	2.85	[62]

Table 1. Continued.

Emitter	Solution PL_{max}/PLQY/$\tau^{a)}$ (medium) [nm/%/μs]	Solid State PL_{max}/PLQY/$\tau^{a)}$ (medium) [nm/%/μs]	ΔE_{ST} [eV]	HOMO [eV]	LUMO [eV]	Ref.
DMAC-TRZ	–/–/–	495/90/1.9 (8 wt% in mCPCN)	0.046	5.30	2.78	[56]
SpiroAC-TRZ	479/67.8/3 (PhMe)	480/100/2.1 (12 wt% in mCPCN)	0.072	5.72	3.10	[61]
PPZ–4TPT	495/3/– (PhMe)	474/12/28000 (10 wt% in mCP)	0.43	4.85	2.06	[15b]
ACRPOB	475/100/1.6 (PhMe)	–/–/–	0.06–0.12	5.8	3.0	[79]
CCT2A	–/–/–	–/–/–	0.06	–	–	[59]
CPC	474/–/– (PhMe)	≈490/49.7/46.6 (13 wt% in mCP)	0.04	6.25	3.47	[71]
BCzT	460/–/– (PhMe)	483/95.6/33 (6 wt% in DPEPO)	0.29–0.33	–	–	[52]
2DAC-Mes_3B	495/84/– (PhMe)	487/100/– (16 wt% in DPEPO)	0.058	5.4	2.6	[78]
DCN-3	482/49/3.26 (PhMe)	–/–/–	0.13	5.57	3.26	[73]
P6	427,491/18.5/5.1 (PhMe)	479/27.2/2.5 (neat)	–	–	–	[89]
DAC-BTZ	496/65/– (PhMe)	496/82/660, 4600 (6 wt% in DPEPO)	0.18–0.22	5.4	2.7	[94]
DCzmCzTrz	–/84/9.7 (PhMe)	≈510/100/– (30 wt% in DPEPO)	0.20	5.26	2.15	[55]
ATP-ACR	503/26/– (PhMe)	492/49/– (6 wt% in mCP)	0.16	5.8	3.0	[93]
TB-2PXZ	–/20/–	484/47/2.9 (10 wt% in CzSi)	0.05	5.08	2.29	[91]
DDCzIPN	477/91/2.8 (PhMe)	–/–/–	0.13	6.40	3.88	[95]
P9	427,491/20.0/6.1 (PhMe)	491/33.7/2.2 (neat)	–	–	–	[89]
Ac-PPM	484/–/– (PhMe)	498/79/20.7 (10 wt% in DPEPO)	0.19	5.65	2.85	[62]
Ac-HPM	489/–/– (PhMe)	498/77/21.4 (10 wt% in DPEPO)	0.18	5.65	2.84	[62]
DPAA-AF	–/–/2.4 (PhMe)	≈510/70/4.3 (6 wt% in mCP)	0.021	–	–	[82]
m-ATP-CDP	532/77/18.1 (PhMe)	499/77/– (6 wt% in mCP)	0.26	5.7	3.1	[63,93]
ACRSA	≈510/70/– (PhMe)	≈500/45/5.3 (neat)	0.03	–	–	[83]

[a)]Lifetime of delayed component.

in 30 wt% UGH3:TSPO1 (UGH3 = 1,3-bis(triphenylsilyl) benzene); ΔE_{ST}: 0 eV) (Figure 6) based on an acridan donor and 9,9-dimethyl-9*H*-thioxanthene-10,10-dioxide acceptor.[47] Compared with **DMAC-DPS**, which shows a relatively broad emission, the additional methylene group linking the phenyl rings of the thioxanthene-dioxide core reduces vibrational motion and thus narrows the emission spectrum. The device (ITO/PEDOT:PSS/TAPC/mCP/30 wt% **emitter**:UGH3:TSPO1/TSPO1/TPBI/LiF/Al) (PEDOT:PSS = poly(3,4-ethylenedioxythiophene)-poly(styrenesulfonate); TAPC = 4,4′-cyclohexylidenebis[*N*,*N*-bis(4-methylphenyl)benzenamine]) with **DMTDAc** gives an impressively deep-blue emission with an EQE of 19.8% and CIE coordinates of (0.15, 0.13).

A modified DAAD (donor–acceptor–acceptor–donor) emitter system inspired by **DTC-DPS** was reported by Kido et al., who replaced the original diphenylsulfone acceptor with a *p*-bis(phenylsulfonyl)benzene unit to afford **DTC-pBPSB** (λ_{max}: 461 nm; PLQY: 67%; τ_d: 1.23 μs in 10 wt% DPEPO; ΔE_{ST}: 0.05 eV) and **DTC-mBPSB** (λ_{max}: 434 nm; PLQY: 71%; τ_d: 1.16 μs in 10 wt% DPEPO; ΔE_{ST}: 0.24 eV) (Figure 6).[48] Compared with the parent **DTC-DPS** with a ΔE_{ST} of 0.32 eV, **DTC-pBPSB** and **DTC-mBPSB** show smaller ΔE_{ST} values of 0.05 eV and 0.24 eV, respectively. Given the more pronounced bathochromic shift in emission wavelength of **DTC-pBPSB** (λ_{max}: 461 nm) compared with **DTC-mBPSB** (λ_{max}: 434 nm), it can be deduced that the effective conjugation length is longer in the former. The smaller ΔE_{ST} value of the former is probably due to its lower ^{1}CT state and hence a smaller gap with respect to the lowest localized triplet state. Therefore, the connection mode of the emitter molecule strongly affects its photophysical properties. The use of **DTC-pBPSB** and **DTC-mBPSB** translates to sky-blue (0.18, 0.19) and deep-blue (0.15, 0.08) devices (ITO/NPB/TCTA/CzSi/10 wt% **emitter**:DPEPO/DPEPO/TPBI/LiF/Al) (NPB = *N*,*N*′-di(1-naphthyl)-*N*,*N*′-diphenyl-(1,1′-biphenyl)-4,4′-diamine) with EQEs of 11.7% and 5.5%, respectively.

Among the original diphenylsulfone-based deep-blue TADF emitters (**1**–**3**, **DMOC-DPS**, and **DMAC-DPS**), **DMAC-DPS** is the most promising due its smallest ΔE_{ST} (0.08 eV) and high solid state PLQY (80%) amongst this series of sulfone emitters. This suggests the use of acridan donors is preferable to using carbazole (**3** and **DMOC-DPS**) or diphenylamine (**1** and **2**) donors. This can be attributed to the electron richness of the acridan donor, which promotes greater HOMO and LUMO separation, along with its highly rigid structure, which contributes to reducing nonradiative decay paths from the excited state. Compared with **DMAC-DPS**, the use of 9,9-dimethyl-9*H*-thioxanthene-10,10-dioxide as the acceptor (**DMTDAc**) results in an even higher solid-state PLQY (100%), probably due to a greater rigidity of the acceptor moiety, and a vanishing ΔE_{ST} (0 eV). Invoking a dimerization strategy produces improved blue TADF emitters (compare **DTC-mBPSB** and **DTC-pBPSB** vs **3**) because of their slightly redshifted emission energies (i.e., a lower-energy S_1 state, which is the lowest-energy ^{1}CT state), which

Table 2. Summary of device structures and performances of blue TADF emitters (EL_{max} < 500 nm).

Emitter	Device structure	EL_{max} [nm]	CIE	V_{on} [V]	EQE/PE/CE[a] [%/lm W^{-1}/cd A^{-1}]	Ref.
1	ITO/α-NPD /TCTA/CzSi/10 wt% **emitter**:DPEPO/DPEPO/TPBI/LiF/Al	421	–	–	2.9/–/–	[15c]
3		423	(0.15, 0.07)	–	9.9/–/5.0	[15c]
2		430	–	–	5.6/–/–	[15c]
DTC-mBPSB	ITO/NPB/TCTA/CzSi/10 wt% **emitter**:DPEPO/DPEPO/TPBI/LiF/Al	≈440	(0.15, 0.08)	–	5.5/–/4.4	[48]
Cz2BP	ITO/α-NPD/mCP/6 wt% **emitter**:DPEPO/DPEPO/TPBi/LiF/Al	446	(0.16, 0.14)	4.3	8.1/–/9.3	[49]
SPXZPO	ITO/MoO_3/NPB/mCP/10 wt% emitter:DPEPO/DPEPO/Bphen/LiF/Al	448	(0.16, 0.12)	4	6.3/7.6/7.3	[81]
DMTDAc	ITO/PEDOT:PSS/TAPC/mCP/30 wt% **emitter**:UGH3:TSPO1/TSPO1/TPBI/LiF/Al	451	(0.15, 0.13)	3.9	19.8/23.3/22.6	[85]
2PXZ-TAZ	ITO/α-NPD/mCP/6 wt% **emitter**:DPEPO/DPEPO/TPBi/LiF/Al	456	(0.16, 0.15)	–	6.4/–/–	[86]
CNBPCz	ITO/PEDOT:PSS/TAPC/mCP/5 wt% **emitter**:DPEPO/TSPO1/TPBI/LiF/Al	456	–	–	4.8/–/–	[75]
DCzTrz	ITO/PEDOT:PSS/TAPC/mCP/25 wt% **emitter**:DPEPO/TSPO1/TPBI/LiF/Al	459	(0.15, 0.16)	5.9	17.8/22.4/26.8	[53]
DABNA-1	ITO/NPD/TCTA/mCP/1 wt% **emitter**:mCBP/mCBP/TSPO1/LiF/Al	459	(0.13, 0.09)	–	13.5/8.3/10.6	[80]
DMOC-DPS	ITO/α-NPD/TCTA/CzSi/10 wt% **emitter**:DPEPO/DPEPO/TPBI/LiF/Al	460	(0.16, 0.16)	4.0	14.5/–/–	[45]
DPXZPO	ITO/MoO_3/NPB/mCP/10 wt% emitter:DPEPO/DPEPO/Bphen/LiF/Al	460	(0.16, 0.17)	3.5	10.6/16.9/16.1	[81]
CzBPCN	ITO/PEDOT:PSS/TAPC/mCP/5 wt% emitter:DPEPO/TSPO1/TPBI/LiF/Al	460	(0.14, 0.12)	–	14.0/–/–	[75]
DCzIPN	ITO/PEDOT:PSS/TAPC/mCP/15 wt% **emitter**:mCP/TSPO1/LiF/Al	462	(0.17, 0.19)	3.5	16.4/–/–	[87]
3CzFCN[b]	ITO/PEDOT:PSS/PVK/10 wt% **emitter**:SiCz/TPBI/LiF/Al	463	(0.16, 0.19)	–	17.8/–/26.9	[76]
TPXZPO	ITO/MoO_3/NPB/mCP/10 wt% emitter:DPEPO/DPEPO/Bphen/LiF/Al	464	(0.17,0.20)	3.5	15.3/23.6/26.4	[81]
DMAC-PXB	ITO/PEDOT:PSS/α-NPD/mCP/6 wt% **emitter**:DPEPO/DPEPO/TPBi/Al	466	–	–	15.1/–/–	[77]
DDCzTrz	ITO/PEDOT:PSS/TAPC/mCP/25 wt% **emitter**:DPEPO/TSPO1/TPBI/LiF/Al	467	(0.16, 0.22)	5.9	18.9/26.2/31.3	[53]
DTPDDA	ITO/4 wt% ReO_3:mCP/mCP/16 wt% **emitter**:mCP:TSPO1/TSPO1/4 wt% Rb_2CO_3:TSPO1/Al	468	(0.15, 0.20)	3.0	22.3/30.4/35.6	[57]
DABNA-2	ITO/NPD/TCTA/mCP/1 wt% **emitter**:mCBP/mCBP/TSPO1/LiF/Al	468	(0.12, 0.13)	–	20.2/15.1/21.1	[80]
DMAC-DPS	ITO/α-NPD/TCTA/CzSi/10 wt% **emitter**:DPEPO/DPEPO/TPBI/LiF/Al	470	(0.16, 0.20)	3.7	19.5/–/–	[15b]
4CzFCN[b]	ITO/PEDOT:PSS/PVK/15 wt% **emitter**:SiCz/TPBI/LiF/Al	471	(0.16, 0.25)	–	20.0/–/36.1	[76]
44TCzPN	ITO/PEDOT:PSS/TAPC/mCP/10 wt% **emitter**:DPEPO/TSPO1/TPBI/LiF/Al	473	(0.16, 0.23)	–	19.5/23.0/32.9	[88]
34TCzPN	ITO/PEDOT:PSS/TAPC/TCTA/mCP/10 wt% **emitter**:DPEPO/TSPO1/TPBi/LiF/Al	475	(0.17, 0.29)	–	21.8/30.2/38.5	[88]
TMCPOB	ITO/HAT-CN/α-NPD/CCP/20 wt% **emitter**:PPF/PPF/TPBi/LiF/Al	≈475	(0.15, 0.09)	–	20.1/–/–	[79]
SXDPAPOB		≈475	(0.15, 0.08)	–	13.3/–/–	[79]
P3[b]	ITO/PEDOT:PSS/poly-TPD/neat **polymer**/TmPyPB/Ba/Al	478	(0.19, 0.25)	3.5	1.2/1.7/2.0	[89]
CzAcSF	ITO/PEDOT:PSS/TAPC/TCTA/mCP/20 wt% **emitter**:DPEPO/TSPO1/TPBI/LiF/Al	≈480	(0.16, 0.21)	5.1	20.7/33.7/33.1	[90]
TCzTrz	ITO/PEDOT:PSS/TAPC/mCP/40 wt% **emitter**:DPEPO/TSPO1/TPBI/LiF/Al	480	(0.18, 0.33)	–	25.0/42.7/–	[55]
SFDPAPOB	ITO/HAT-CN/α-NPD/CCP/20 wt% **emitter**:PPF/PPF/TPBi/LiF/Al	≈480	(0.14, 0.12)	–	19.0/–/–	[79]
DTC-pBPSB	ITO/NPB/TCTA/CzSi/10 wt% **emitter**:DPEPO/DPEPO/TPBI/LiF/Al	≈480	(0.18, 0.19)	–	11.7/–/19.4	[48]
DMAC-DPS	ITO/MoO_3/mCP/neat **emitter**/DPEPO/LiF/Al	480	(0.16, 0.29)	4.3	19.5/19/–	[46]
2CzPN	ITO/α-NPD/mCP/5 wt% **emitter**:PPT/PPT/LiF/Al	≈480	–	–	8.0/–/–	[15a]
TB-1PXZ	ITO/PEDOT:PSS/10 wt% **emitter**:CzSi/TmPyPB/Liq/Al	480	(0.19, 0.29)	8.9	1.0/0.7/1.7	[91]
5CzCF3Ph[b]	ITO/PEDOT:PSS/10 wt% **emitter**:mCP/TmPyPB/LiF/Al	484	(0.21, 0.33)	3.9	5.2/–/11.8	[84]
CC2BP	ITO/α-NPD/mCP/6 wt% **emitter**:DPEPO/DPEPO/TPBi/LiF/Al	484	(0.17, 0.27)	4.4	14.3/–/25.5	[49]
mPTC	ITO/TAPC/TCTA/6.5 wt% **emitter**:mCP/TmPyPb/LiF/Al	484	(0.18, 0.32)	3.2	17.4/35.8/39.9	[92]
m-ATP-ACR	ITO/α-NPD/mCP/6 wt% **emitter**:mCP/PPT/TPBi/LiF/Al	486	–	4.8	8.7/6.2/13.1	[63,93]
BFCz-2CN	ITO/PEDOT:PSS/TAPC/mCP/1 wt% **emitter**:mCP/TSPO1/LiF/Al	486	–	–	12.1/–/–	[66]
BTCz-2CN		486	–	–	11.8/–/–	[66]
35IPNDCz	ITO/α-NPD/mCP/10 wt% **emitter**:DPEPO/TPBi/LiF/Al	487	–	–	9.2/–/–	[72]

Table 2. Continued.

Emitter	Device structure	EL_{max} [nm]	CIE	V_{on} [V]	EQE/PE/CE[a] [%/lm W^{-1}/cd A^{-1}]	Ref.
DCBPy	ITO/NPB/mCP/5 wt% **emitter**:CzPS/DPEPO/TmPyPb/LiF/Al	488	(0.17, 0.36)	3.0	24.0/57.2/54.7	[50]
DAC-Mes$_3$B	ITO/TAPC/16 wt% **emitter**:DPEPO/BmPyPhB/Liq/Al	488	(0.17, 0.30)	–	14.0/–/–	[78]
Ac-MPM	ITO/TAPC/10 wt% **emitter**:mCP/10 wt% **emitter**:DPEPO/B3PyPB/LiF/Al	489	(0.19, 0.37)	2.8	24.5/61.6/–	[62]
DMAC-TRZ	ITO/PEDOT:PSS/TAPC/mCP/8 wt% **emitter**: mCPCN/DPPS/3TPYMB/LiF/Al	≈490	–	≈3	26.5/65.6/66.8	[56]
SpiroAC-TRZ	ITO/MoO_3/TAPC/mCP/12 wt% emitter:mCPCN/3TPYMB/LiF/Al	≈490	(0.18, 0.43)	≈2	36.7/98.4/94	[61]
PPZ–4TPT	ITO/α-NPD/TCTA/CzSi/10 wt% **emitter**:DPEPO/DPEPO/TPBI/LiF/Al	≈490	–	–	≈2/–/–	[15b]
ACRPOB	ITO/HAT-CN/α-NPD/CCP/50 wt% **emitter**:PPF/PPF/TPBi/LiF/Al	≈490	(0.14, 0.23)	–	21.7/–/–	[79]
CCT2A	ITO/α-NPD/mCP/6 wt% **emitter**:DPEPO/DPEPO/TPBi/LiF/Al	490	–	–	11/–/–	[59]
CPC	ITO/TAPC/TCTA/13 wt% **emitter**:mCP/TmPyPB/LiF/Al	490	(0.20, 0.35)	3.2	21.2/42.8/47.7	[71]
BCzT	ITO/α-NPD/m-CBP/6 wt% **emitter**:DPEPO/TPBi/LiF/Al	492	–	–	21.7/–/–	[52]
2DAC-Mes$_3$B	ITO/TAPC/16 wt% **emitter**:DPEPO/BmPyPhB/Liq/Al	492	(0.18, 0.43)	–	21.6/–/–	[78]
DCN-3	ITO/HAT-CN/NPB/TAPC/10 wt% **emitter**:PPT/PPT/TPBi/LiF/Al	492	(0.20, 0.37)	5.9	13.3/8.1/15.3	[73]
P6[b]	ITO/PEDOT:PSS/poly-TPD/neat **polymer**/TmPyPB/Ba/Al	492	(0.21, 0.32)	3.7	1.1/1.8/2.2	[89]
DAC-BTZ	ITO/α-NPD/m-CBP/6 wt% **emitter**:DPEPO/DPEPO/TPBi/LiF/Al	493	–	–	10.3/–/–	[94]
DCzmCzTrz	ITO/PEDOT:PSS /TAPC/mCP/20 wt% **emitter**:DPEPO/TSPO1/TPBI/LiF/Al	496	(0.23, 0.46)	–	21.3/42.4/–	[55]
ATP-ACR	ITO/α-NPD/mCP/6 wt% **emitter**:mCP/PPT/TPBi/LiF/Al	496	–	4.8	7.5/5.7/11.5	[63,93]
TB-2PXZ	ITO/PEDOT:PSS/10 wt% **emitter**:CzSi/TmPyPB/Liq/Al	496	(0.18, 0.40)	5.8	8.9/13.8/21.0	[91]
DDCzIPN	ITO/PEDOT:PSS/TAPC/mCP/**emitter**:mCP:BmPyPb/TSPO1/TPBI/LiF/Al	497	(0.22, 0.46)	3.5	18.9/38.3/–	[95]
P9[b]	ITO/PEDOT:PSS/poly-TPD/neat **polymer**/TmPyPB/Ba/Al	498	(0.22, 0.37)	3.2	4.0/9.4/9.0	[89]
Ac-PPM	ITO/TAPC/10 wt% **emitter**:DPEPO/B3PyPB/LiF/Al	498	(0.21, 0.44)	2.9	19.0/52.8/49.2	[62]
Ac-HPM		499	(0.21, 0.44)	2.9	20.9/60.3/54.7	[62]
DPAA-AF	ITO/α-NPD/mCP/6 wt% **emitter**:mCP/PPT/TPBi/LiF/Al	499	–	–	9.6/–/–	[82]
m-ATP-CDP	ITO/α-NPD/mCP/6 wt% **emitter**:mCP/PPT/TPBi/LiF/Al	499	–	4.8	7.5/6.4/13.4	[63,93]
ACRSA	ITO/α-NPD/mCP/20 wt% **emitter**:DPEPO/DPEPO/TPBi/LiF/Al	≈500	–	–	16.5/–/–	[83]

[a]Maximum values for EQE, power efficiency (PE), and current efficiency (CE); [b]Solution-processed device.

results in a smaller ΔE_{ST} (the energy gap between the ^{1}CT state and the ^{3}LE state). This agrees well with previous findings from Adachi et al., which suggest lowered emission energies for blue TADF emitters help to decrease ΔE_{ST}.[15c,45]

A benzophenone-type acceptor can also be used in the design of blue TADF emitters. Lee et al.[49] fabricated two blue devices (ITO/α-NPD/mCP/6 wt% **emitter**:DPEPO/DPEPO/TPBi/LiF/Al) using **Cz2BP** (λ_{max}: 444 nm; PLQY: 55%; τ_d: 710 µs in 6 wt% DPEPO; ΔE_{ST}: 0.21 eV) and **CC2BP** (λ_{max}: 475 nm; PLQY: 73%; τ_d: 460 µs in 6 wt% DPEPO; ΔE_{ST}: 0.14 eV) (**Figure 9**) as the emitters. The OLEDs obtained EQEs of 8.1% and 14.3% at CIE coordinates of (0.16, 0.14) and (0.17, 0.27), respectively. **CC2BP**, with an extended carbazole donor system, exhibits a smaller ΔE_{ST} than **Cz2BP** by 0.07 eV. This also enhances the donor strength in **CC2BP** (HOMO: –5.65 eV) compared with **Cz2BP** (HOMO: –5.74 eV) and results in a significant redshifted emission (31 nm, 1470 cm^{-1}). Rajamalli et al.[50] reported two novel TADF emitters based on a benzoylpyridine acceptor **DCBPy** (λ_{max}: 514 nm; PLQY: 88%; τ_d: 0.6 µs in 5 wt% 9,9′-(sulfonylbis(4,1-phenylene))bis(9*H*-carbazole) (CzPS); ΔE_{ST}: 0.07 eV) and **DTCBPy** (λ_{max}: 518 nm; PLQY: 91%; τ_d: 1.0 µs in 5 wt% 4,4′-bis(*N*-carbazolyl)-1,1′-biphenyl (CBP); ΔE_{ST}: 0.08 eV) (Figure 9). The only difference between these two emitters is the presence of *tert*-butyl groups in the **DTCBPy**. Given their modest electron-donating nature, **DTCBPy** shows a small redshift in emission wavelength by only 4 nm (150 cm^{-1}). The other photophysical properties seem to be unaffected. Intramolecular through-space interaction between the *ortho*-carbazole donor and the benzoylpyridine acceptor is believed to induce efficient TADF. The interaction also suppresses intermolecular aggregation in the solid state, and thus the PLQY in the solid state is greatly enhanced in doped film (up to 91.4%) compared with solution (14–36%). **DCBPy** (ITO/NPB/mCP/5 wt% **emitter**:CzPS/DPEPO/TmPyPb/LiF/Al) and **DTCBPy** (ITO/NPB/TAPC/5 wt% **emitter**:CBP/PPT/TmPyPb/LiF/Al) (TmPyPb = 1,3,5-tri(*m*-pyridin-3-ylphenyl)benzene; PPT = 2,8-bis(diphenylphosphoryl)dibenzo-[*b*,*d*]thiophene) give sky-blue and green devices with EQEs of 24.0% and 27.2% with CIE coordinates of (0.17, 0.36) and (0.30, 0.64), respectively.

Compared with the **Cz2BP** and **CC2BP** series, **DCBPy** and **DTCBPy** have redshifted emission due to the enhanced acceptor strength conferred by the pyridine group in these molecules, which is evidenced by their deeper LUMO levels. For example, the LUMO levels of the **BP** series are from –2.63 eV to –2.64 eV, while those of

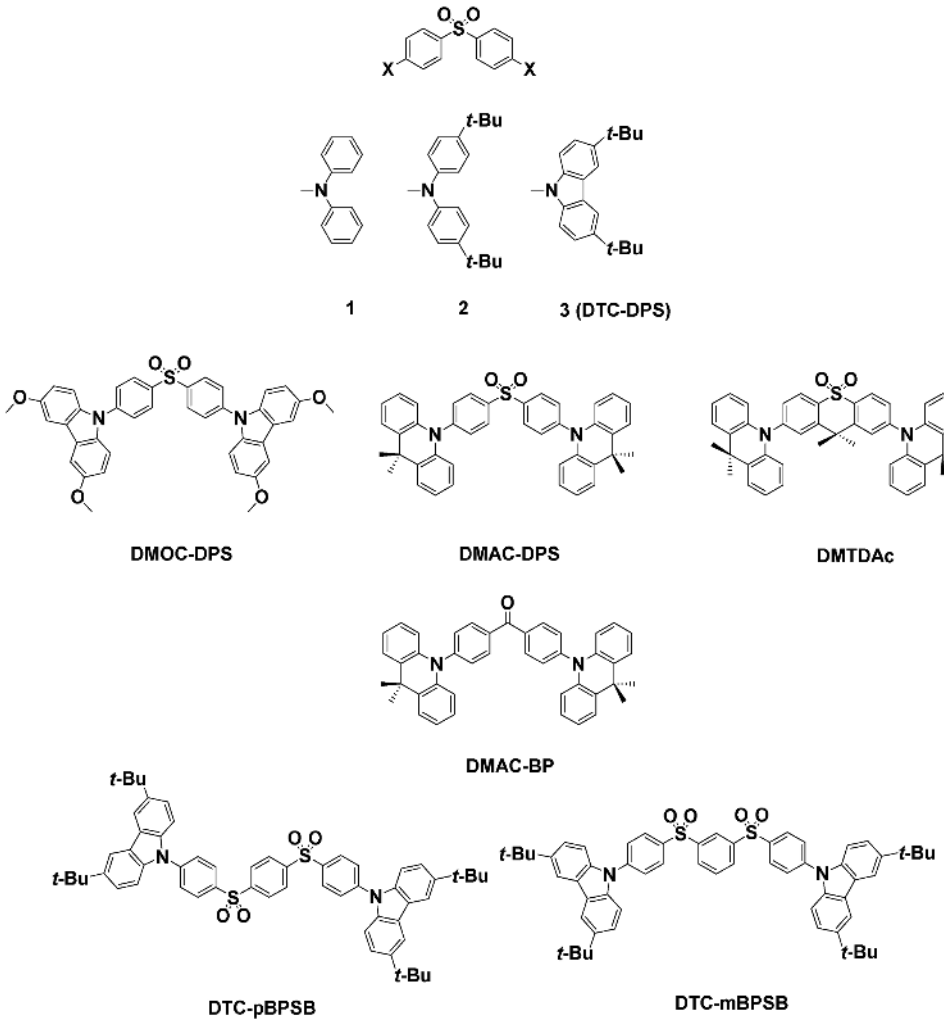

Figure 6. Chemical structures of sulfone-based blue TADF emitters and **DMAC-BP** as the benzophenone analogue of **DMAC-DPS**.

the **BPy** series are from –2.87 eV to –2.88 eV. In addition, the latter family of emitters has smaller ΔE_{ST}, most likely due to *ortho*-carbazole substitution that increases the torsion between the donor and acceptor moieties due to increased steric hindrance between carbazoles, resulting in greater localization of the HOMO and LUMO, a feature that is absent in the **Cz2BP** and **CC2BP** series.

Apart from the popular diphenylsulfone moiety, the 1,3,5-triazine is one of the most common acceptors used for blue TADF emitters. A blue-greenish TADF emitter **CzT** (λ_{max}: 502 nm; PLQY: 40%; τ_d: 42.6 µs in 3 wt% DPEPO; ΔE_{ST}: 0.09 eV) (**Figure 10**) was employed in an OLED device (ITO/α-NPD/TCTA/CzSi/3 wt% **emitter**:DPEPO/DPEPO/TPBi/LiF/Al), which showed an EQE of 6% at CIE coordinates of (0.23, 0.40).[51] However, a structurally similar emitter **PhCzTAZ** (PhCzTAZ = 3-(2′-(4,6-diphenyl-1,3,5-triazin-2-yl)-[1,1′-biphenyl]-2-yl)-9-phenyl-9H-carbazole) does not show TADF because of the absence of charge-transfer emission, probably due to limited HOMO and LUMO communication restricted by steric hindrance around the biphenyl bridge. To improve on the low PLQY of the **CzT** emitter, **BCzT** (λ_{max}: 483 nm; PLQY: 96%; τ_d: 33 µs in 6 wt% DPEPO; ΔE_{ST}: 0.29–0.33 eV) was then developed, in which the overlap density between the excited state and the ground state (ρ_{10}) was increased.[52] The presence of an additional phenyl-ring bridge increases the overlap integral between the HOMO and the LUMO as its presence mediates increased conjugation. As a result, the ρ_{10} in **BCzT** is more widely distributed than in **CzT**, and the transition dipole moment of the former is consequently larger than the latter, resulting in a higher radiative rate constant (k_r). It should be noted that the addition of the phenyl-ring bridge increases the ΔE_{ST}, but triplet-to-light efficiency (defined as the ratio of PLQY contribution by delayed component (Φ_d) to triplet formation yield (Φ_T)) in **BCzT** (76.2%) is much higher than **CzT** (25%). We believe this is due to a much higher k_r in **BCzT** that decreases the cycling between singlet and triplet states and thus eliminates the probability of nonradiative decay in both singlet and triplet states. Therefore, for efficient TADF to occur, both high RISC rate (k_{RISC}) and radiative rate constants (k_r) are essential. The device with **BCzT** gives a sky-blue emission (ITO/α-NPD/m-CBP/6 wt% **emitter**:DPEPO/TPBi/LiF/Al) with an EQE of 21.7% and EL_{max} at 492 nm, which is far improved compared to the 6% EQE obtained by the OLED with **CzT**.

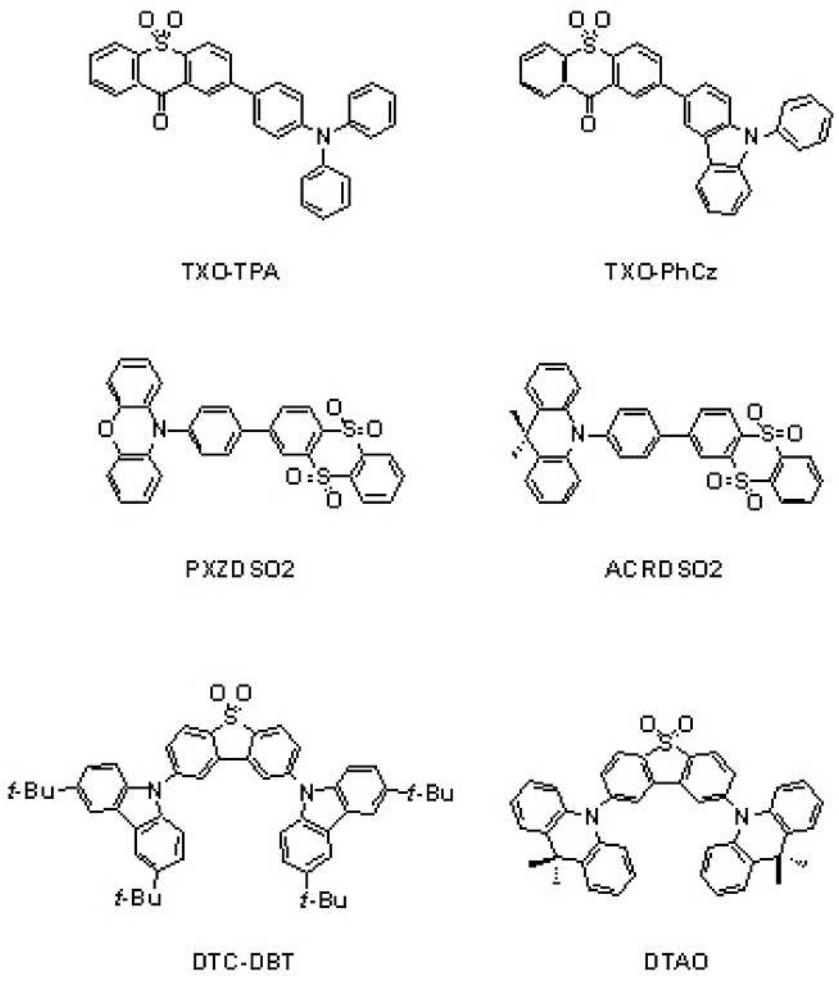

Figure 7. Chemical structures of sulfone-based green TADF emitters.

In 2015, Kim et al. reported two blue TADF emitters **DCzTrz** (λ_{max}: ≈420 nm; PLQY: 43%; τ_d: 3.1 µs in toluene; ΔE_{ST}: 0.25 eV) and **DDCzTrz** (λ_{max}: ≈430 nm; PLQY: 66%; τ_d: 2.8 µs in toluene; ΔE_{ST}: 0.27 eV) (Figure 10) with the only difference being two additional carbazole moieties attached to the phenyl ring in a *meta* fashion in **DDCzTrz**. As "*meta* linkages" limit conjugation length, the two emitters have similar emission energies and ΔE_{ST}. The OLED (ITO/PEDOT:PSS/TAPC/mCP/25 wt% **emitter**:DPEPO/TSPO1/TPBI/LiF/Al) using the latter has an impressive EQE of 18.9% at CIE coordinates of (0.16, 0.22).[53] In particular, this device shows an LT_{80} (the time required for the luminance to drop to 80% of its initial value) of 52 h, which is approximately three times longer than the blue phosphorescent analog using tris[1-(2,4-diisopropyldibenzo[b,d]furan-3-yl)-2-phenyl-1H-imidazole]-iridium(III), **[Ir(dbi)$_3$]**. The authors attributed the stability to three main factors: firstly, the carbazole and triazine moieties are robust and the nearly planar structure of the molecule gives the peripheral carbazole moiety further stabilization through conjugation with the triazine; Secondly, the nature of charge transfer makes the excited state resemble a pair of positive carbazole and negative triazine polarons, which are known to be stable; lastly, the excellent thermal stability of the emitters (glass-transition temperature (T_g) for **DCzTrz** and **DDCzTrz**: 160 °C and 218 °C, respectively) contributes positively to the device stability. However, based on the above reasoning, one would expect the device stability to be similar for **DCzTrz** and **DDCzTrz**. Indeed, while **DDCzTrz** shows an LT_{80} of 52 h, **DCzTrz** has an LT_{80} of only 5 h. The authors asserted that the higher emission energy of **DCzTrz** was responsible for the poorer stability. We believe that the poorer stability is due to the intrinsic structure of the emitters, which are designed using the well-known "*meta*-linkage" interconnection mode. This approach effectively limits the conjugation length of the whole molecule as the number of π-conjugated systems keeps increasing in order to avoid redshifts in the emission and lowering of the triplet energy level.[41,54] Therefore, the emission energy of the emitters is expected to be similar, which, experimentally, is the case where the PL and EL spectra of these two emitters are essentially the same. The authors later modified **DCzTrz** through addition of more carbazole donors to the emitter to generate three new compounds: **TCzTrz** (λ_{max}: ≈450 nm; PLQY: 100%; τ_d: 13.5 µs in 30 wt% DPEPO; ΔE_{ST}: 0.16 eV), **TmCzTrz** (λ_{max}: ≈470 nm; PLQY: 100%; τ_d: 13.3 µs in 30 wt% DPEPO; ΔE_{ST}: 0.07 eV) and **DCzmCzTrz** (λ_{max}: ≈490 nm; PLQY: 98%; τ_d: 9.7 µs in 30 wt% DPEPO; ΔE_{ST}: 0.20 eV) (Figure 10).[55] By comparing these emitters with the parent **DCzTrz**, the authors suggested that having more carbazole donors present in the emitter helps to reduce the ΔE_{ST} (e.g., one additional carbazole in **TCzTrz** lowers the ΔE_{ST} by 0.09 eV compared with **DCzTrz**), while uneven distribution of the electron density in the HOMO increases ΔE_{ST} (e.g., the HOMO is localized on the dimethylcarbazole moieties in **DCzmCzTrz** due to the electron-donating nature of methyl groups, conferring **DCzmCzTrz** with a larger ΔE_{ST} than that of **TCzTrz** and **TmCzTrz** by 0.04 eV and 0.13 eV, respectively). Among these emitters, the OLED (ITO/PEDOT:PSS/TAPC/mCP/40 wt% **emitter**:DPEPO/TSPO1/TPBI/LiF/Al) with **TCzTrz** is sky-blue with an impressive EQE of 25.0% at CIE coordinates of (0.18, 0.33). The devices(ITO/PEDOT:PSS/TAPC/mCP/30 wt% **emitter**:DPEPO/TSPO1/TPBI/LiF/Al) with **TmCzTrz** and **DCzmCzTrz** are green with EQEs of 25.5% and 21.3% and CIE coordinates of (0.25, 0.50) and (0.23, 0.46), respectively.

Tsai et al. reported a sky-blue TADF emitter **DMAC-TRZ** (λ_{max}: 495 nm; PLQY: 90%; τ_d: 1.9 µs in 8 wt% 9-(3-(9*H*-carbazol-9-yl)phenyl)-9*H*-carbazole-3-carbonitrile (mCPCN); ΔE_{ST}: 0.05 eV) (Figure 10), which, when doped in 9-(3-(9*H*-carbazol-9-yl)phenyl)-9*H*-carbazole-3-carbonitrile (**mCPCN**), gave a highly efficient device (ITO/PEDOT:PSS/TAPC/mCP/8 wt% **emitter**:mCPCN/DPPS/3TPYMB/LiF/Al) (3TPYMB = tris(2,4,6-trimethyl-3-(pyridin-3-yl)phenyl)borane; DPPS = diphenylbis(4-(pyridin-3-yl)phenyl)silane) with an EQE of 26.5% and EL_{max}

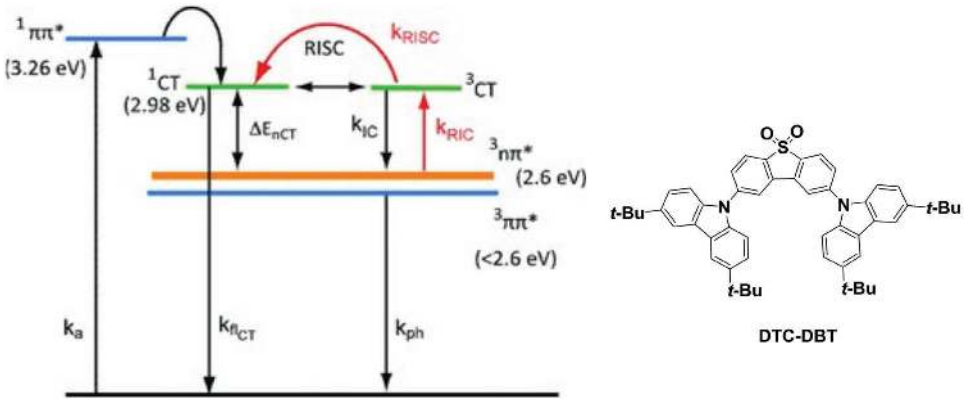

Figure 8. Simplified Jablonski diagram of important states in TADF process in **DTC-DBT** proposed by Dias et al. Reproduced with permission.[42] Copyright 2013, Wiley-VCH.

at ≈490 nm.[56] Acridan, being a stronger donor than carbazole, redshifts the **DMAC-TRZ** compared with carbazole-based triazine TADF emitters. Interestingly, the emitter also demonstrates an excellent EQE of 20% in the absence of a host. Indeed, the PLQYs of the emitter in doped thin film (90%) and neat film (83%) are very similar, which is attributed to the methyl groups on the acridan unit that serve via sterics to suppress intermolecular interactions, similar to that observed for **DMAC-DPS** (Figure 6).[46] Sun et al.[57] reported a potent deep-blue TADF emitter **DTPDDA** (λ_{max}: 444 nm; PLQY: 74%; τ_d: 0.1, 2.3, 25.4 µs in 16 wt% mCP:TSPO1; ΔE_{ST}: 0.14 eV) whose device (ITO/4 wt% ReO_3:mCP/mCP/16 wt% **emitter**:mCP:TSPO1/TSPO1/4 wt% Rb_2CO_3:TSPO1/Al) performance reaches an outstanding EQE of 22.3% with CIE coordinates of (0.15, 0.20). Silicon was chosen for its rigid tetrahedral configuration, which, due to its size, effectively suppresses nonradiative decay pathways and enhances the morphological stability of the molecule. Beneficially, the HOMO of the azasiline (–5.57 eV) is lowered compared with the carbon analog **DMAC-TRZ** (HOMO: –5.30 eV) because of the longer Si–C bond that limits the antibonding interactions between the two azasiline carbons bonded to the silicon atom.[58] The lowering of the HOMO energy level increases the bandgap and contributes to the deep-blue emission of the device.

Aside from designing emitters that can attain 100% IQE, the efficiency of the device can be improved by increasing the light-outcoupling efficiency, which is generally around only 20% for typical emitters. Mayr et al.[59] designed a largely planar sky-blue TADF emitter **CC2TA** (λ_{max}: ≈490 nm; PLQY: 62%; τ_d: 22 µs in 6 wt% DPEPO; ΔE_{ST}: 0.06 eV). It has previously been demonstrated that planar, long, linear molecules have preferential horizontal orientations on the substrate due to favourable intermolecular interactions with the host during film deposition. The horizontal placement of emitters in the film orients their transition dipole more optimally, thereby enhancing light outcoupling.[60] The outcoupling efficiency of the **CC2TA** emitting layer was found to be 31.3% and the device (ITO/α-NPD/mCP/6 wt% **emitter**:DPEPO/DPEPO/TPBi/LiF/Al) achieved an EQE of 11% with EL_{max} at 490 nm. Very recently, Lin et al.[61] reported a novel triazine-based blue TADF emitter, **spiroAC-TRZ** (λ_{max}: 480 nm; PLQY: 100%; τ_d: 2.1 µs in 12 wt% mCPCN; ΔE_{ST}: 0.07 eV), which shows a strong horizontal dipole ratio, $\Theta_{//}$, (where $\Theta_{//}$ is defined as the horizontal emitting dipole/total emitting dipoles) as high as 83%. In comparison with structurally similar **DMAC-TRZ**, the phenyl rings attached on the acridan moiety in **spiroAC-TRZ** weaken the electron-donating capacity of the donor inductively, thus producing a modest blueshift of 15 nm in the emission. The PLQY of **spiroAC-TRZ** (100%) was also higher than that of **DMAC-TRZ** (90%), which was attributed to the more planar conformation of the acridan moiety, as confirmed by single-crystal X-ray diffraction, which showed that the dihedral angles between the acridan phenyl planes were 0° and 11°, respectively.[61] Together with both

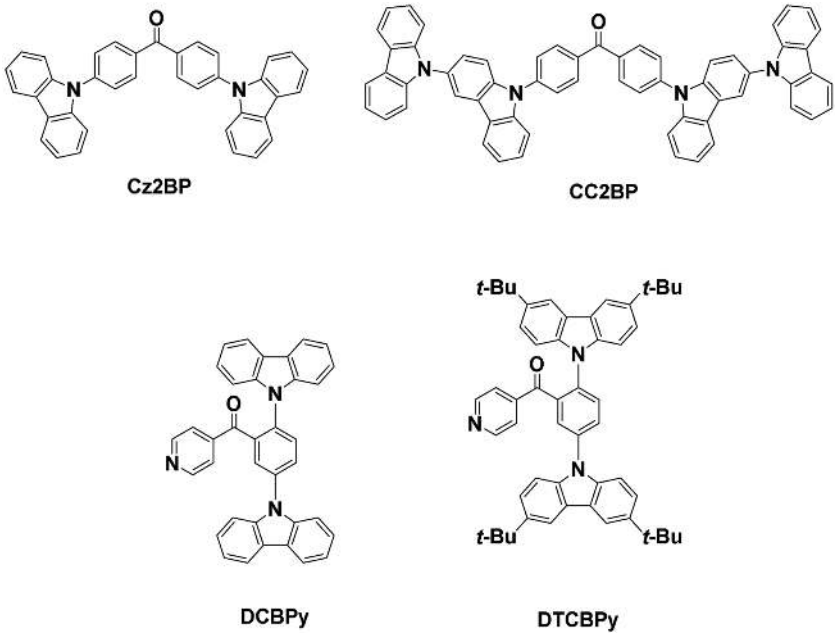

Figure 9. Chemical structures of benzophenone-based blue TADF emitters.

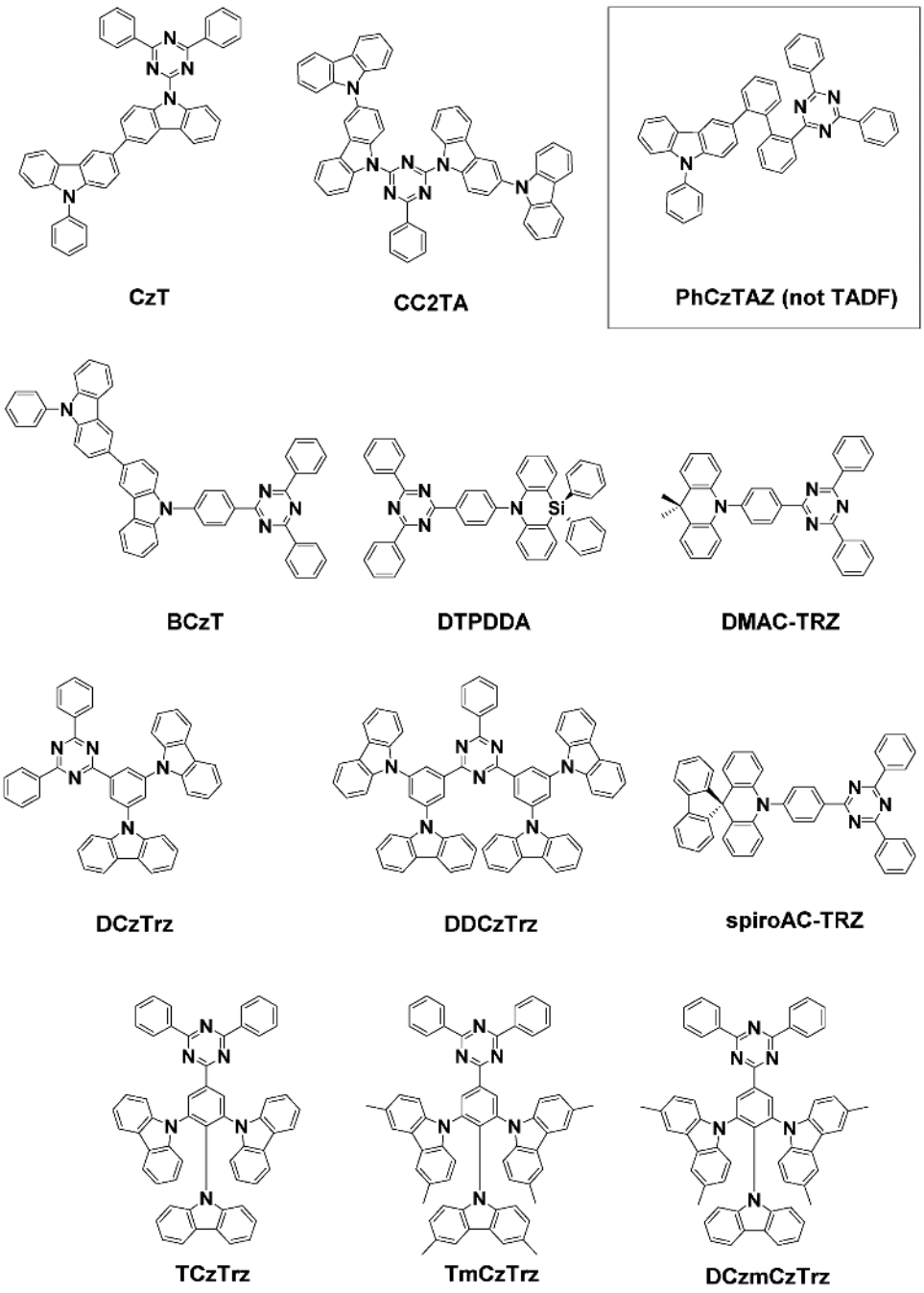

Figure 10. Chemical structures of 1,3,5-triazine-based blue TADF emitters.

100% PLQY and IQE, a high-performance blue device (ITO/MoO_3/TAPC/mCP/12 wt% **spiroAC-TRZ**:mCPCN/3TPYMB/LiF/Al) with an EQE of 37% and CIE coordinates of (0.18, 0.43) was obtained, making it the best blue TADF device reported so far, despite the large *y*-ordinate CIE value.

Similar to diphenyl-sulfone-based blue TADF emitters, the employment of an acridan donor (**DTPDDA**, **DMAC-TRZ**, and **spiroAC-TRZ**) results in improved emitter performance, primarily as a result of smaller ΔE_{ST} values than the corresponding carbazole congener (**BCzT**). The use of the diphenylsilane group in **DTPDDA**, though bulkier, actually promotes a decreased PLQY compared to the dimethyl analog **DMAC-TRZ** (74% vs 90%). The horizontal orientation increases from isotropic **DTPDDA** ($\Theta_{//}$ = 0.66),[57] to **DMAC-TRZ** ($\Theta_{//}$ = 0.72), to **spiroAC-TRZ** ($\Theta_{//}$ = 0.83), which is likely the result of an enhancement of the glass-transition temperature[61] and increased planarity of the acridan moiety[60,61] across the series. **DMAC-TRZ** and **spiroAC-TRZ** show a significantly smaller ΔE_{ST} (0.046 eV and 0.072 eV, respectively) than **DTPDDA** (0.14 eV), which can be explained by the lower

emission energies of the former (51 nm and 36 nm redshifted, respectively, compared to **DTPDDA**), similar to that which was evidenced with the diphenyl sulfone blue TADF emitter materials (vide supra). However, this does not hold for **BCzT**, which has a similar emission energy (483 nm) but possesses a much larger ΔE_{ST} (≈0.2 eV larger). The use of 1,3-dicarbazoylphenyl as the donor (**DCzTrz** and **DDCzTrz**) does not significantly modulate ΔE_{ST} compared with the use of the 4-carbazoylphenyl donor (**BCzT**). However, when one additional carbazole donor is inserted between the two carbazoles (**TCzTrz**, **TmCztrz**, and **DCzmCzTrz**), a much smaller ΔE_{ST} can be realized as a function of a more delocalized HOMO; excellent solid-state PLQY values are nonetheless maintained (98–100%).

Komatsu et al. reported a series of three sky-blue emitters (**Ac-RPM**s, **Figure 11**) by modifying the triazine acceptor to pyrimidine.[62] As expected, the photophysics properties of these three emitters are highly similar because the different substituents have little impact on the energies of the LUMO. Devices of all these emitters are characterized by low turn-on voltages (<3.0 V), among which **Ac-MPM** (λ_{max}: 489 nm; PLQY: 80%; τ_d: 26.2 µs in 10 wt% DPEPO; ΔE_{ST}: 0.19 eV) gives the most efficient double-emission-layer (DEML) device (ITO/TAPC/10 wt% **emitter**:mCP/10 wt% **emitter**:DPEPO/B3PyPB/LiF/Al) (B3PyPB = 1,3-bis(3,5-dipyrid-3-ylphenyl)benzene) with an EQE of 24.5% and CIE coordinates of (0.19, 0.37) at a turn-on voltage as low as 2.80 V.

Takahashi et al.[63] reported a series of TADF emitters **ATP-ACR**, **m-ATP-ACR**, **m-ATP-CDP**, **m-ATP-PXZ**, and **ATP-PXZ** based on a 1,4-diazatriphenylene acceptor (**Figure 12**), which itself possesses a high triplet energy level (E_T: 2.9 eV) that is beneficial for the design of blue TADF emitters. The device using ***m*-ATP-ACR** (λ_{max}: 492 nm; PLQY: 49% in 6 wt% 3,3-di(9-*H*-carbazol-9-yl)biphenyl (mCBP); ΔE_{ST}: 0.16 eV) as the emitter shows sky-blue emission with an EQE of 8.7% and EL_{max} at 486 nm (ITO/α-NPD/mCP/6 wt% **emitter**:mCPB/PPT/TPBi/LiF/Al). On the other hand, the device with ***m*-ATP-PXZ** (λ_{max}: 524 nm; PLQY: 81% in 6 wt% mCP; ΔE_{ST}: 0.04 eV), where acridan (ACR) (HOMO: −5.9 eV) is replaced by the stronger donor phenoxazine (PXZ) (HOMO: −5.7 eV), emits in the green with an EQE of 12.6% and EL_{max} at 516 nm (ITO/α-NPD/mCP/6 wt% **emitter**:CPB/TPBi/LiF/Al).

Cyano-based acceptors are some of the most common building blocks used for blue TADF emitters. The very first of these reported by Adachi et al. is **2CzPN** (λ_{max}: ≈473 nm; PLQY: 47%; τ_d: 166 µs in toluene) (**Figure 13**), which generated a sky-blue device (ITO/α-NPD/mCP/5 wt% **emitter**:PPT/PPT/LiF/Al) with a decent EQE of 8.0% and EL_{max} at ≈480 nm. By doping the emitter in a *p*-type host (mCP) to prevent exciplex formation between the hole-transporting layer and the emitting layer, a higher EQE of 13.6% (ITO/α-NPD/mCP/6 wt% **emitter**:mCP/PPT/TPBi/LiF/Al) was achieved by the same group.[64] Sun et al. recently reported an excellent EQE of 21.8% (ITO/4 wt% ReO_3:mCP/5 wt% **emitter**:mCP:PO15/4 wt% Rb_2CO_3:PO-15/Al) (PO-15 = poly[*N*,*N*′-bis(4-butylphenyl)-*N*,*N*′-bisphenylbenzidine]) by using a mixed co-host system (mCP:PO15 = 1:1) for maximum charge balance to minimize electrical loss.[65] Nevertheless, the device suffered from serious efficiency roll-off at higher current density, and the best 21.8% EQE was only achieved at 0.01 mA cm^{-2}.

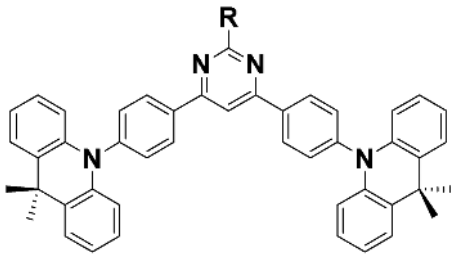

R = H, Ac-HPM
R = PhAc-PPM
R = MeAc-MPM

Figure 11. Chemical structures of **Ac-RPM**s.

Later, Lee et al.[66] prepared two derivatives of **2CzPN**[15a] by replacing carbazole with benzofurocarbazole and benzothienocarbazole (**BFCz-2CN** (λ_{max}: ≈480 nm; PLQY: 85%; τ_d: 2.6 µs in 1 wt% mCP; ΔE_{ST}: 0.13 eV) and **BTCz-2CN** (λ_{max}: ≈480 nm; PLQY: 85%; τ_d: 1.98 µs in 1 wt% mCP; ΔE_{ST}: 0.17 eV) (Figure 13). These derivatives have higher PLQYs but similar emission energies (94.6% and 94.0%, respectively in degassed PhMe, compared with 47% for **2CzPN** in degassed PhMe), probably due to the higher rigidity of benzofurocarbazole and benzothienocarbazole donors in addition to more efficient RISC processes (deduced from their shorter delayed emission lifetime components). The albeit increased conjugation of the fused structure of the donor and the presence of electron-donating oxygen and sulfur atoms, which all increase the HOMO level (from −6.17 to −6.19 eV) nevertheless still contribute to produce sky-blue emission in a doped thin film and the device. While the authors obtained an EQE of 5.0% for the OLED using the parent emitter **2CzPN**, the devices (ITO/PEDOT:PSS/TAPC/mCP/1 wt% **emitter**:mCP/TSPO1/LiF/Al) with **BFCz-2CN** and **BTCz-2CN** showed enhanced EQEs of 12.1% and 11.8%, respectively (they have the same EL_{max} at 486 nm). Our group[67] has prepared a charged analog of **2CzPN**, **TL-2** (Figure 13), bearing tethered charged imidazolium hexafluorophosphate groups. **TL-2** was conceived to work as an emitter in a light-emitting electrochemical cell (vide infra). **TL-2** was also tested as an emitter in solution-processed OLEDs (ITO/PEDOT:PSS/PVK/**emitter**/B3PYMPM/Ca/Al) (PVK = poly(*N*-vinylcarbazole); B3PYMPM = 4,6-bis(3,5-di(pyridin-3-yl)phenyl)-2-methylpyrimidine), where it was employed as a neat emitting layer, affording a device with an EQE of 5.1% with EL_{max} at 546 nm and CIE coordinates of (0.41, 0.53), making it amongst the best solution-processed, nondoped small-molecule-based TADF OLEDs reported, which includes **red-1b**[68] (red, (0.65, 0.33), EQE: 1.75%) and the **G3TAZ** dendrimer[69] (bluish-green, (0.27, 0.49), EQE: 3.4%) (vide infra). Solution-processed but doped **2CzPN** devices (**mCP** as host) can reach an EQE of 8.1%.[70] Liu et al.[71] prepared a sky-blue TADF emitter **CPC** (λ_{max}: ≈500 nm; PLQY: 50%; τ_d: 46.6 µs in 13 wt% mCP; ΔE_{ST}: 0.04 eV) with a very small ΔE_{ST} of 0.04 eV, resulting in a very efficient device (ITO/TAPC/TCTA/13 wt% **emitter**:mCP/TmPyPB/LiF/Al) with an EQE of 21.2% at CIE coordinates of (0.20, 0.35). Li et al.[72] compared two TADF emitters **26IPNDCz** (λ_{max}: ≈490 nm; PLQY: 72%; τ_d: 9.2 µs in 10 wt% DPEPO; ΔE_{ST}: 0.06 eV) and **35IPNDCz**

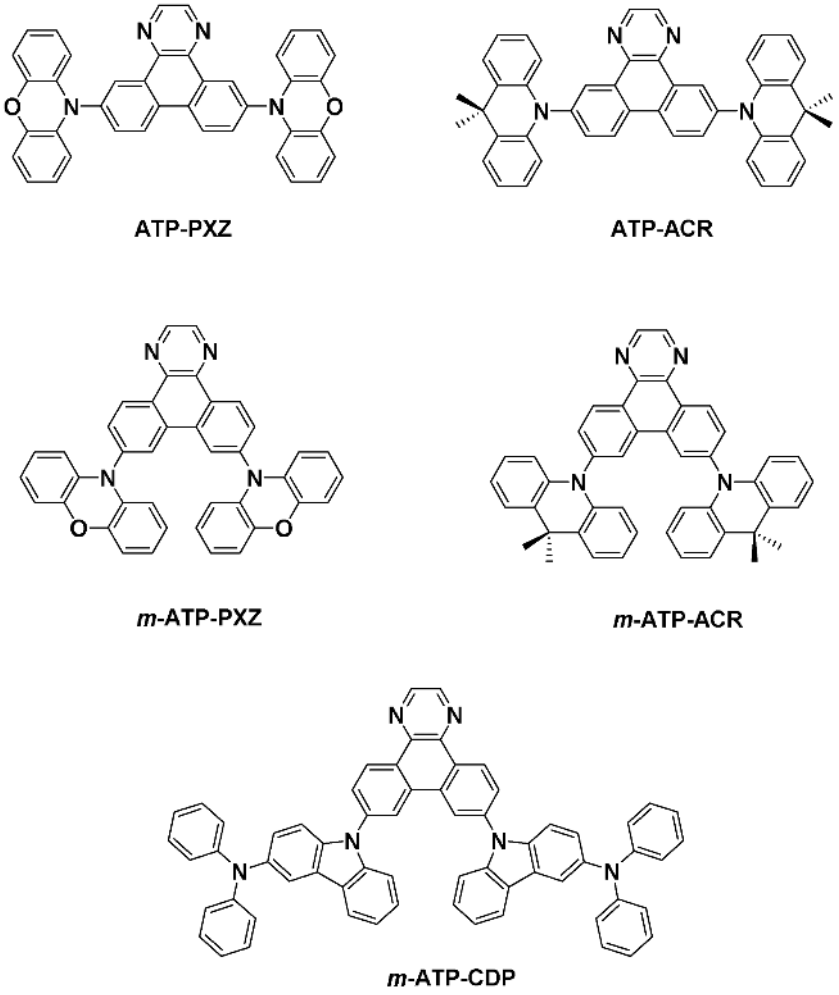

Figure 12. Chemical structures of 1,4-diazatriphenylene-based blue TADF emitters.

(λ_{max}: ≈500 nm; PLQY: 58%; τ_d: 145 µs in 10 wt% DPEPO; ΔE_{ST}: 0.14 eV) (Figure 13) to study the effect of the nitrile substituent position on the photophysical properties and device performance. With *ortho* substitution, the dihedral angle between the dicyanobenzene acceptor and the 3,3′-bicarbazolyl donor in **26IPNDCz** (69°) is larger than **35IPNDCz** (50°) due to the steric interactions between the nitriles and the donor moiety. Thus, a reduced exchange integral between the HOMO and the LUMO is realized in **26IPNDCz**, resulting in a smaller ΔE_{ST}, evidenced by the markedly shorter delayed component lifetime (9.2 µs) than that of **35IPNDCz** (145 µs). The larger dihedral angle in **26IPNDCz** also limits the conjugation length, resulting in a slightly blueshifted emission compared with **35IPNDCz**. In doped thin film (10 wt% DPEPO), the PLQYs of **26IPNDCz** and **35IPNDCz** are 58% and 72%, respectively. The devices (ITO/α-NPD/mCP/10 wt% **emitter**:DPEPO/TPBi/LiF/Al) employing these two emitters are blue-greenish (EL_{max}: 487 nm for **35IPNDCz** and 501 nm for **26IPNDCz**) with similar EQEs (9.2% for **35IPNDCz** and 9.6% for **26IPNDCz**). According to the authors, the key distinguishing feature is the reduced efficiency roll-off observed in the device with **26IPNDCz** due to its shorter triplet lifetime as a result of faster RISC rate.

Park et al.[73] designed a series of three related compounds (**DCN1–3**) (Figure 13) as potential TADF emitters for OLED applications. While TADF is observed in **DCN3** (λ_{max}: 482 nm; PLQY: 49%; τ_d: 3.26 µs in toluene; ΔE_{ST}: 0.13 eV), **DCN1** and **DCN2** do not demonstrate any TADF properties, which according to the authors, is based on their large ΔE_{ST} values. Though a reasonable assertion, no experimental ΔE_{ST} values are provided in the study. As the molecular scaffold of these molecules is basically the same, the increased spacing of the HOMO to the peripheral carbazoles in **DCN3** with respect to the isophthalonitrile-localized LUMO should be responsible for the realization of TADF. This is in line with the theoretical studies from, independently, Adachi et al.[74] and Sancho-Gracíer et al.[21] The former group compared TADF emitters **DACQ** and **CZQ** (Figure 13) and found that the installation of diphenylamino groups in **DACQ** promotes further localization of the HOMO density toward the periphery of the molecule, thereby further spatially separating the HOMO and LUMO, resulting in a smaller ΔE_{ST}. The latter team performed a theoretical study comparing three non-TADF against three known TADF emitters and proposed an inverse relationship between Δr(NTO) and ΔE_{ST}, where Δr(NTO) is a measure of the electron–hole separation after excitation (NTO = natural transition orbital) (**Figure 14**). The OLED (ITO/HAT-CN/NPB/TAPC/10 wt% **emitter**:PPT/PPT/TPBi/LiF/Al) (HAT-CN = 1,4,5,8,9,11-hexaazatriphenylenehexacarbonitrile) with **DCN3** gave sky-blue emission with an EQE of 13.3% at CIE coordinates of (0.20, 0.37). Very recently, Cho et al.[75] reported two biphenyl-based blue TADF emitters **CNBPCz** (λ_{max}: 458 nm; PLQY: 46%; τ_d: 24.3 µs in PhMe; ΔE_{ST}: 0.27 eV) and **CzBPCN** (λ_{max}: 453 nm; PLQY: 76%; τ_d: 48.2 µs in PhMe; ΔE_{ST}: 0.27 eV), whose OLED devices (ITO/PEDOT:PSS/TAPC/mCP/5 wt% **emitter**:DPEPO/TSPO1/TPBI/LiF/Al) gave EQEs of 4.8% and 14.0%, respectively. While **CNBPCz** and **CzBPCN** devices demonstrated similar emission maxima (456 nm and 460 nm, respectively), **CzBPCN** displayed a much sharper emission profile (full width at half maximum (FWHM): 48 nm) than **CNBPCz** (FWHM: 76 nm), which was attributed to the "donor interlock" molecular design of **CzBPCN** that relates to a much larger rotational barrier of the biphenyl as a result of increased *ortho*-substitution. This resulted in a deep blue device with CIE coordinates of (0.14, 0.12) with **CzBPCN** as the emitter.

Cho et al.[76] reported two solution-processable blue TADF emitters **3CzFCN** (λ_{max}: ≈440 nm; PLQY: 74%; τ_d: 28 µs in 10 wt% diphenyldi(4-(9-carbazolyl)phenyl)silane (SiCz); ΔE_{ST}: 0.06 eV) and **4CzFCN** (λ_{max}: ≈460 nm; PLQY: 100%; τ_d: 17 µs in 10 wt% SiCz; ΔE_{ST}: 0.06 eV) (Figure 13). The presence of fluorine atoms in these emitters promotes increased hydrophobicity

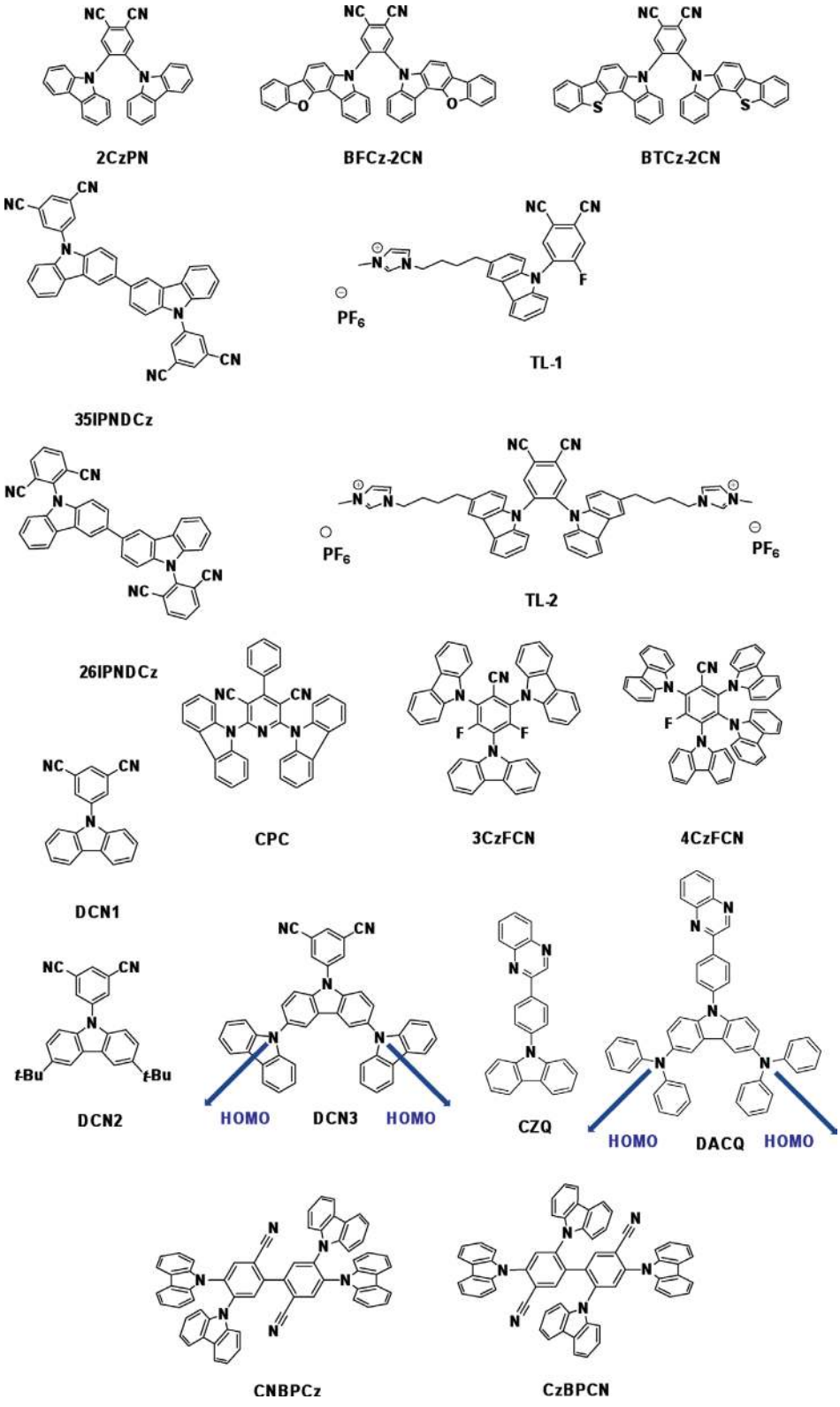

Figure 13. Chemical structures of cyano-based blue TADF emitters.

and increases solubility in aromatic solvents (e.g., toluene). Additionally, the weaker electron-withdrawing ability of fluorine compared to nitrile blueshifts the emission. The OLED (ITO/PEDOT:PSS/PVK/15 wt% **emitter**:SiCz/TPBI/LiF/Al) using **4CzFCN** as the emitter has an EQE of 20.0%, particularly high for a solution-processed device, with CIE coordinates of (0.16, 0.26).

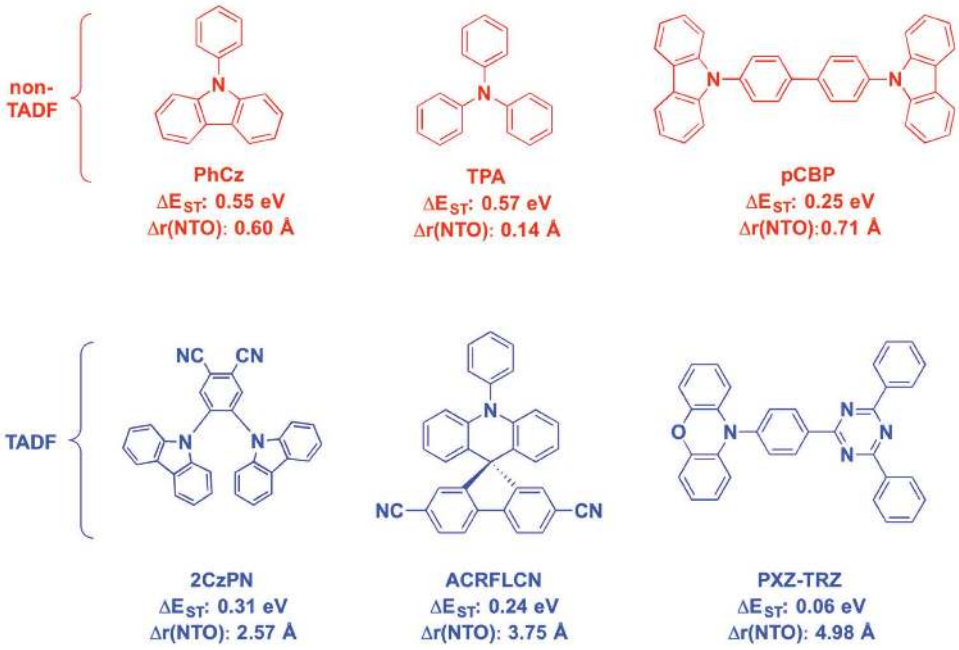

Figure 14. Comparison between TADF and non-TADF compounds in terms of Δr(NTO) and ΔE_{ST} values. Δr(NTO) is defined as the electron–hole separation after excitation and calculated using the Tamm–Dancoff approximation (TDA). The ΔE_{ST} values listed are experimental results.

The use of more rigid and bulkier donors in the **2CzPN** scaffold results in a boost in the PLQY by nearly a factor of two in toluene (compare **BTCz-2CN** and **BFCz-2CN** with **2CzPN**), which is probably due to the suppression of nonradiative decay modes conferred by these rigid structures. Additionally, the ΔE_{ST} decreases significantly (0.13 eV and 0.17 eV for **BFCz-2CN** and **BTCz-2CN**, respectively, while it is 0.31 eV for **2CzPN** in PhMe)[21] which results in more efficient RISC. Steric hindrance about the donor in these emitters is important, which is evidenced by the turn-off of TADF in **DCN1** and **DCN2** where, in these emitters, the carbazole donor has no adjacent groups to provide the steric bulk required to generate sufficient HOMO and LUMO separation. However, this analysis does not apply for **35IPNDCz** and **26IPNDCz**. A possible reason for this incoherence is due to their A–D–A symmetric molecular scaffold, which may promote more efficient TADF emitters, similar to that which is observed for D–A–D analogs. Steric hindrance about the donor is not necessary for TADF. By designing donor units that effectively extend the HOMO to the periphery of the molecule and away from the location of LUMO, as demonstrated in **DCN3**, TADF too can be realized This result agrees with the inverse relationship between Δr(NTO) and ΔE_{ST} values suggested by the theoretical work by Sancho-Gracíer et al.

A number of blue-to-green TADF emitters have been built with boron-based acceptors. TADF emitters **DMAC-PXB** (λ_{max}: 440 nm; PLQY: 98%; τ_d: 2.36 µs in 6 wt% DPEPO; ΔE_{ST}: 0.01 eV) and **PXZ-PXB** (λ_{max}: 482 nm; PLQY: 99%; τ_d: 1.87 µs in 5 wt% mCP; ΔE_{ST}: 0.03 eV) based on 10*H*-phenoxaboryl were reported by Kitamoto et al. (**Figure 15**).[77] The much redshifted emission in **PXZ-PXB** is due to the phenoxazine donor (HOMO: –5.60 eV) being much stronger than acridan in **DMAC-PXB** (HOMO: –5.81 eV). Devices employing **DMAC-PXB** (ITO/PEDOT:PSS/α-NPD/mCP/6 wt% **emitter**:DPEPO/DPEPO/TPBi/Al) and **PXZ-PXB** (ITO/PEDOT:PSS/α-NPD/mCP/6 wt% **emitter**:mCP/PPT/TPBi/LiF/Al) show blue and green emission with EQEs of 15.1% and 22.1% and EL_{max} at 466 nm and 503 nm, respectively. Another class of boron-based TADF emitters **PXZ-Mes$_3$B** (λ_{max}: 504 nm; PLQY: 92% in 16 wt% CBP; ΔE_{ST}: 0.07 eV), **2DAC-Mes$_3$B** (λ_{max}: 487 nm; PLQY: 100% in 16 wt% DPEPO; ΔE_{ST}: 0.06 eV) and **DAC-Mes$_3$B** (λ_{max}: 477 nm; PLQY: 87% in 16 wt% DPEPO; ΔE_{ST}: 0.06 eV) uses triarylboron as the acceptor (Figure 15).[78] Similar to that observed between **DMAC-PXB** and **PXZ-PXB**, the phenoxazine analog **PXZ-Mes$_3$B** demonstrated the most redshifted emission of the three emitters in the study due to its strong electron-donating power. **2DAC-Mes$_3$B** shows slightly redshifted emission by 10 nm (431 cm^{-1}) compared with **DAC-Mes$_3$B** due to the enhanced conjugation, which results from the additional diphenylamine in the former. Regardless of the donor, all three compounds are highly emissive in doped films and exhibit similarly small ΔE_{ST}. Devices using these emitters give bluish-green emission with EQEs ranging from 14.0% to 22.8% and CIE coordinates from (0.17, 0.30) to (0.22, 0.55), respectively. Numata et al.[79] reported a series of blue TADF emitters (**ACRPOB**, **SFD-PAPOB**, **SXDPAPOB**, and **TMCPOB**, Figure 15) based on a 10*H*-phenoxaborin acceptor and either an acridan or carbazole donor. There is effective suppression of intermolecular interactions that contribute to quenching of their emission because of the large dihedral angle between the 10*H*-phenoxaborin and the acridan moieties. The best device using emitter **ACRPOB** (λ_{max}: 475 nm; PLQY: 100%; τ_d: 1.6 µs in toluene; ΔE_{ST}: 0.06–0.12 eV) demonstrates an EQE of 21.7% (ITO/HAT-CN/α-NPD/CCP/50 wt% **emitter**:PPF/PPF/TPBi/LiF/Al) (CCP = 9-phenyl-9*H*-3,9′-bicarbazole; PPF = 2,8-bis(diphenylphosphoryl)-dibenzo[*b*,*d*]furan) at CIE coordinates of (0.14, 0.23).

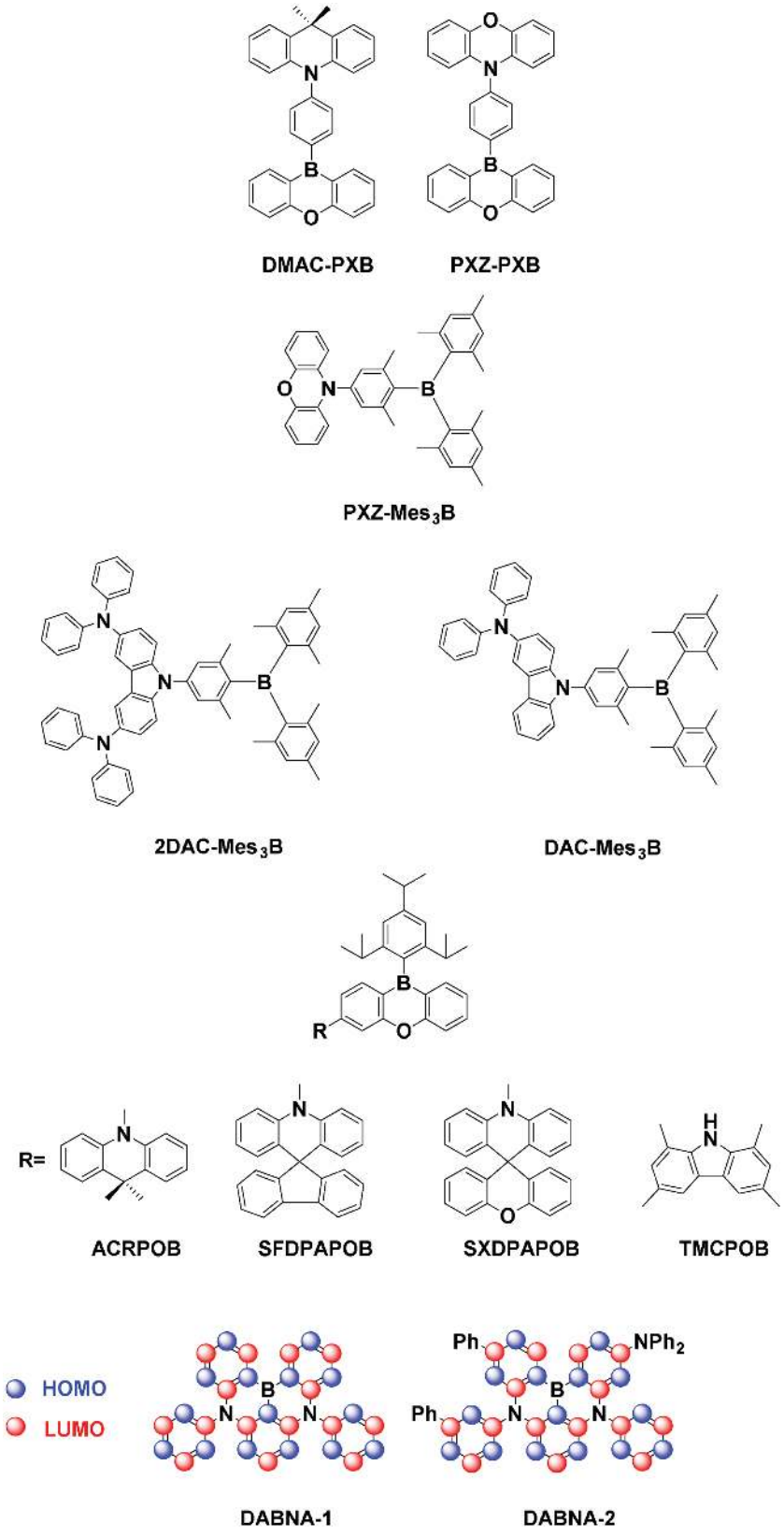

Figure 15. Chemical structures of boron-based blue TADF emitters.

Very recently, Hatakeyama et al.[80] reported two blue TADF emitters **DABNA-1** (λ_{max}: 460 nm; PLQY: 88%; τ_d: 8.8 µs in 1 wt% mCBP; ΔE_{ST}: 0.18 eV) and **DABNA-2** (λ_{max}: 469 nm; PLQY: 90%; τ_d: 6.0 µs in 1 wt% mCPB; ΔE_{ST}: 0.14 eV) (Figure 15). In these interesting molecules, HOMO and LUMO separation is realized by "multiple resonance effects" where the LUMO is localized on the boron atom, its *ortho* and *para* position, whereas the HOMO is localized on the nitrogen atom and *meta* to the boron atom. The merit of this multiple resonance effect strategy is that it sharpens the emission spectrum (smaller FWHM), which is a common drawback of donor–acceptor-based TADF emitters. These two emitters have basically the same photophysical properties, with **DABNA-2** showing a slightly redshifted emission (9 nm, 420 cm^{-1}), which is due to an enhanced conjugation length due to the additional phenyl and diphenylamino moieties. **DABNA-2** gives a more efficient deep-blue device ITO/NPD/TCTA/mCP/1 wt% **emitter**:mCBP/mCBP/TSPO1/LiF/Al with an EQE of 20.2% at (0.12, 0.13).

In general, most of the above boron-based blue TADF emitters show small ΔE_{ST} (<0.18 eV), probably because of the strong LUMO localization effect induced by the boron atom. Additionally, the majority of these emitters exhibit excellent PLQYs in the solid state (87–100%). These results suggest that boron-based TADF scaffold is a potent avenue for blue TADF emitters. The **DABNA** series is of particular interest, as the emission profiles are considerably sharper. This is due to the distinct strategy of localizing the HOMO and the LUMO as a function of the regiochemistry of the donor and acceptor.

Duan et al.[81] demonstrated that phosphine oxides can act as weak acceptors toward blue TADF emitters (**Figure 16**). The photophysical and electrochemical properties of the three emitters were found to be basically the same. However, the triply substituted **TPXZPO** (λ_{max}: 478 nm; PLQY: 67%; τ_d: 17 µs in 10 wt% DPEPO; ΔE_{ST}: 0.11 eV) maximizes the intramolecular charge-transfer (ICT) (a term synonymous with CT in the context of this review) character and thus the smallest ΔE_{ST} compared with the mono- and disubstituted analogs (ΔE_{ST} = 0.26 eV and 0.19 eV, respectively). OLEDs (ITO/MoO_3/NPB/mCP/10 wt% **emitter**:DPEPO/DPEPO/Bphen/LiF/Al) (Bphen = 4,7-diphenyl-1,10-phenanthroline) using **TPXZPO** as the emitter showed

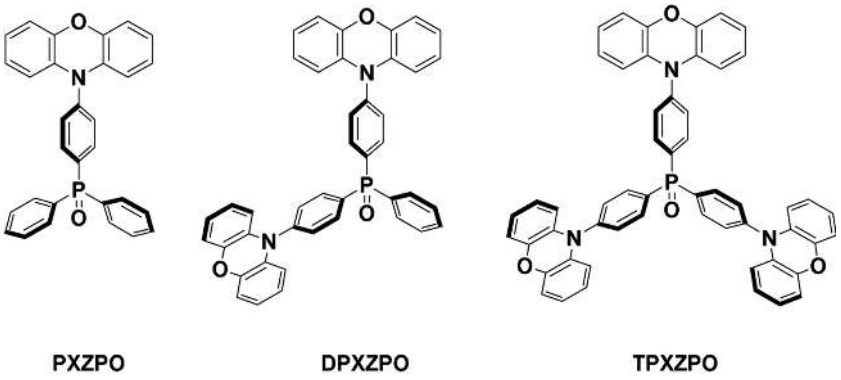

Figure 16. Chemical Structures of phosphine-oxide-based TADF emitters.

slightly blueshifted λ_{EL} at 464 nm, 100% exciton utilization efficiency, and an EQE of 15.3% with CIE values of (0.17, 0.20).

A blue-green device (ITO/α-NPD/mCP/6 wt% **emitter**:mCP/PPT/TPBi/LiF/Al) with an EQE of 9.6% and EL_{max} at 499 nm was reported using **DPAA-AF** (λ_{max}: ≈500 nm; PLQY: 70%; τ_d: 4.3 µs in 6 wt% mCP; ΔE_{ST}: 0.02 eV) (**Figure 17**) as the emitter, in which spiro-diazafluorene is used as the acceptor, where the spiro architecture effectively separates the HOMO and LUMO.[82] Another TADF emitter based on the spiro-anthracenone acceptor **ACRSA** (λ_{max}: ≈500 nm; PLQY: 81%; τ_d: 5.3 µs in 20 wt% DPEPO; ΔE_{ST}: 0.03 eV) also gave a blue-greenish device (ITO/α-NPD/mCP/20 wt% **emitter**: DPEPO/DPEPO/TPBi/LiF/Al) with an EQE of 16.5% and EL_{max} at ≈500 nm.[83]

Mei et al.[84] employed an inductively electron-withdrawing trifluoromethyl group as the acceptor in two blue TADF emitters, **4CzCF$_3$Ph** (λ_{max}: 445 nm; PLQY: 14%; τ_d: 9.3 µs in toluene; ΔE_{ST}: 0.24 eV) and **5CzCF$_3$Ph** (λ_{max}: 495 nm; PLQY: 43%; τ_d: 15.3 µs in toluene; ΔE_{ST}: 0.02 eV) (**Figure 18**). The number of carbazoles plays a crucial role in this scaffold by modulating ΔE_{ST} wherein it is much smaller for **5CzCF$_3$Ph** (0.02 eV) than for **4CzCF$_3$Ph** (0.24 eV). Theoretical calculations suggest that the charge-transfer character in the triplet excited state is greater in **5CzCF$_3$Ph** than in **4CzCF$_3$Ph**, resulting a much smaller ΔE_{ST} in the former. A solution-processed device with **5CzCF$_3$Ph** (ITO/PEDOT:PSS/10 wt% **emitter**:mCP/TmPyPB/LiF/Al) (EQE: 5.2% and CIE coordinates of (0.21, 0.33)) performs much better than that with **4CzCF$_3$Ph** (EQE: 0.7%).

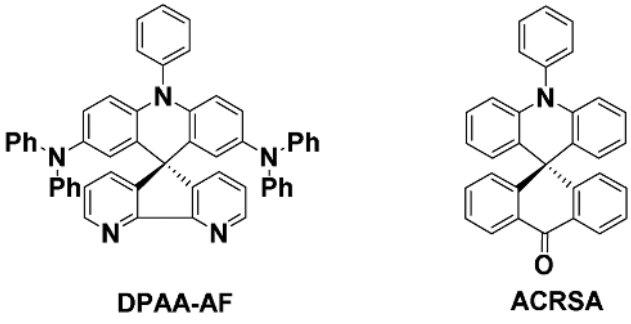

Figure 17. Chemical structures of **DPAA-AF** and **ACRSA**.

2.2. Green–Yellow TADF Emitters

In this section, we define green-to-yellow emitters as those whose electroluminescence peak wavelength (EL_{max}) lies between 500 nm and 580 nm. The distribution of CIE coordinates for the OLEDs reported in this section is shown in **Figure 19** (vide infra). **Table 3** summarizes the photophysical properties of emitters in this section while **Table 4** summarizes the OLED device performance metrics. A vast majority of green-to-yellow TADF emitters contain cyano-based acceptors. For example, in the pioneering report by Adachi et al.[15a] the emitters consisted of carbazole donors and a dicyanobenzene (phthalonitrile) acceptor. The molecular design is based on the presence of a twisted conformation of the donor carbazoles with respect to the phthalonitrile plane, which confers a well-separated HOMO and LUMO, and thus a small ΔE_{ST}. Depending on the regiochemistry of the donor carbazoles and the acceptor nitriles about the central benzene ring, this family of molecules can emit across the visible spectrum. The best-performing device in the report used the green emitter **4CzIPN** (λ_{max}: ≈510 nm; PLQY: 82%; τ_d: 3370 µs in 6 wt% CBP; ΔE_{ST}: 0.08 eV) (**Figure 20**), with an EQE as high as 19.3% and EL_{max} at ≈510 nm (ITO/α-NPD/5 wt% **emitter**:CBP/TPBi/LiF/Al). Since their initial report, **4CzIPN** has become the representative green TADF emitter and has been frequently used in photophysical,[96] mechanistic,[24,97] host[98] and device-optimization studies.[70,99] Lee et al.[100] modified **4CzIPN** by adding solubilizing *tert*-butyl groups in **t4CzIPN** (λ_{max}: ≈520 nm; PLQY: 78%; τ_d: 2.9 µs in 3 wt% SiCz) (Figure 20), an emitter that is now much more easily solution processable and exhibits less aggregation in the doped thin film. The solution-processed device (ITO/PEDOT:PSS/PVK/1 wt% **emitter**:SiCz/TSPO1/LiF/Al) using **t4CzIPN** (EQE: 18.3%) shows a markedly enhanced performance compared with the parent **4CzIPN** (EQE: 8.1%).

Taneda et al.[101] prepared a highly efficient TADF material **3DPA3CN** (λ_{max}: 533 nm; PLQY: 100%; τ_d: 550 µs in 6 wt% DPEPO; ΔE_{ST}: 0.10 eV) (Figure 20), which demonstrates both 100% PLQY and 100% efficiency of triplet utilization via RISC. The HOMO and LUMO are each strongly localized based on the molecular design. **3DPA3CN** is also found to have a preferential horizontal orientation in the **DPEPO** host, resulting in enhanced light outcoupling. The green device (ITO/α-NPD/mCBP/6 wt% **emitter**:DPEPO/TPBI/LiF/Al) shows an excellent EQE of 21.4% with EL_{max} at ≈540 nm.

Nakagawa et al.[102] reported a yellow TADF emitter **spiro-CN** (λ_{max}: ≈540 nm; PLQY: 27%; τ_d: 14 µs in 6 wt% mCP; ΔE_{ST}: 0.06 eV) (Figure 20) based on a spirobifluorene scaffold, which was chosen for its excellent thermal and color stability. A very small ΔE_{ST} of 57 meV was achieved due to the well-separated diphenylamine donor and cyano acceptor groups on the two different fragments of the spirobifluorene unit. Despite its efficient RISC, the low PLQY of the emitter (27%) in doped film (6 wt% in **mCP**) limits the device efficiency (ITO/α-NPD/6 wt% **emitter**:mCP/Bphen/MgAg/Ag) with a relatively low EQE of 4.4% and EL_{max} at ≈550 nm. Shortly

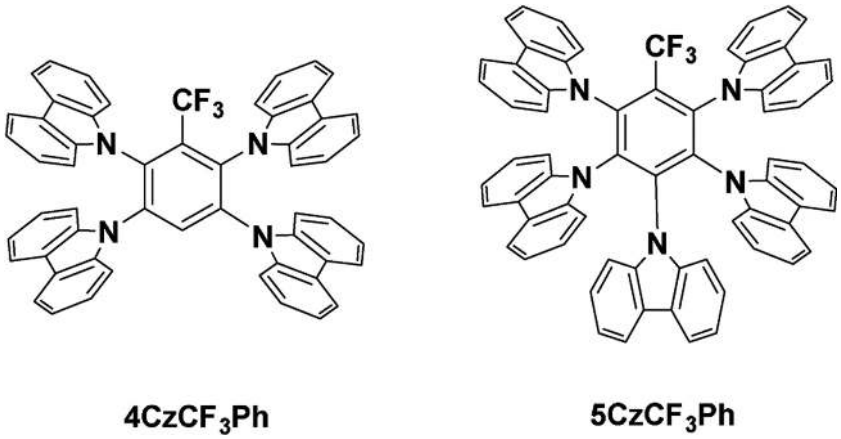

Figure 18. Chemical structures of **4CzCF$_3$Ph** and **5CzCF$_3$Ph**.

thereafter, the group reported another similarly structured green TADF emitter **ACRFLCN** (λ_{max}: 485 nm; PLQY: 67%; τ_d: 160, 940, 3900 µs in 6 wt% triphenyl-(4-(9-phenyl-9*H*-fluoren-9-yl)phenyl)silane (TPSi-F); ΔE_{ST}: 0.10 eV) (Figure 20) in which the spiro acridine moiety is used to separate the donor amine and acceptor nitrile groups.[103] The PLQY of the emitter is 67%, resulting in a higher EQE of 10.1% with EL$_{max}$ at ≈500 nm (ITO/TAPC/mCP/6 wt% **emitter**:TPSi-F/TmPyPB/LiF/Al).

Kawasumi et al.[104] reported two TADF emitters **TPA-QNX(CN)$_2$** (λ_{max}: 487 nm; PLQY: 44%; τ_d: 2.4 µs in cyclohexane; ΔE_{ST}: 0.11 eV) and **TPA-PRZ(CN)$_2$** (λ_{max}: 475 nm; PLQY: 55%; τ_d: 6.5 µs in cyclohexane; ΔE_{ST}: 0.08 eV) (Figure 20) based on an unusual triptycene scaffold in which a small ΔE_{ST} is realized by installing the diphenylamine donor and dicyanoquinoxaline or dicyanopyrazine acceptors on different arms of the propeller triptycene, which communicate with each other electronically by homoconjugation (i.e., a through-space interaction). Indeed, homoconjugation has already been employed in several previously reported spiro-based TADF emitters, although the term "homoconjugation" is not invoked explicitly.[82,102,103] Although the choice of dicyanoquinoxaline or dicyanopyrazine acceptor results in little impact on the photophysics of the emitters, it is interesting to note that their device performance differs greatly. OLEDs (ITO/MoO$_3$/TCTA/10 wt% **emitter**:mCP/TmPyPb/LiF/Al) with **TPA-QNX(CN)$_2$** and **TPA-PRZ(CN)$_2$** produce yellow and green light with EQEs of 9.4% and 4.0% and CIE coordinates of (0.45, 0.54) and (0.43, 0.55), respectively.

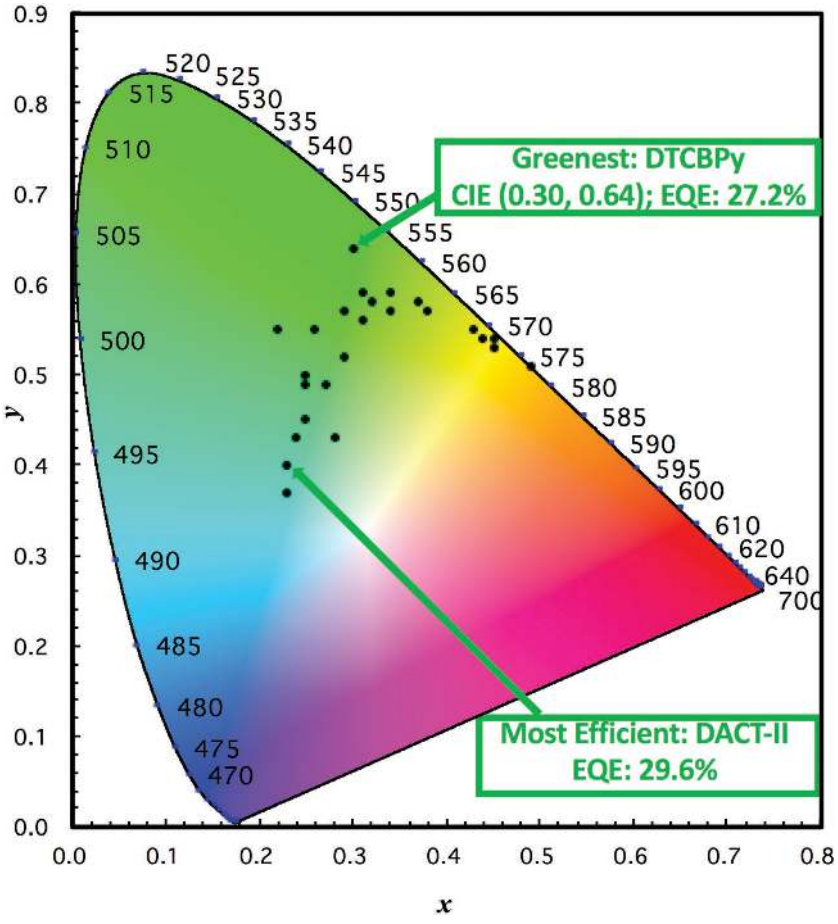

Figure 19. Summary of CIEs of green TADF OLED.

Tang et al.[105] fabricated a solution-processed green device using the emitter **4CzCNPy** (λ_{max}: 560 nm; PLQY: 55%; τ_d: 8.4 µs in toluene; ΔE_{ST}: 0.07 eV) (Figure 20) based on a 4-cyanopyridine acceptor. The device (ITO/PEDOT:PSS/8 wt% **emitter**:mCP/TmPyPB/LiF/Al) gave an EQE of 11.3% and CIE coordinates of (0.34, 0.59). The cyano group on **4CzCNPy** is important, without which there is no TADF observed in this molecule. The cyano group is also believed to be essential in boosting the PLQY compared with its analog **4CzPy** whose n–π^* state quenches the emission, whereas for **4CzCNPy**, the emission is dominated by ICT states.

Cho et al.[95] introduced a new emitter design strategy called a "dual emitting core", in which two emitting chromophores are joined together to enhance the molar absorptivity and also the emission efficiency due to an increased transition dipole moment. They justified their approach by comparing the PLQYs and device performance between **DDCzIPN** (dual-core) (λ_{max}: 477 nm; PLQY: 91%; τ_d: 2.8 µs in toluene; ΔE_{ST}: 0.13 eV) and **DCzIPN**[87] (ordinary single-core) (λ_{max}: 447 nm; PLQY: 87%; τ_d: 1.2 µs in 15 wt% mCP; ΔE_{ST}: 0.05 eV) (Figure 20). The PLQYs of the dual-core and single-core emitters in degassed toluene are 91% and 67%, respectively, in

Table 3. Summary of photophysical and electrochemical properties of green to yellow TADF emitters (500 nm < EL_{max} < 580 nm).

Emitter	Solution PL_{max}/PLQY/$\tau^{a)}$ (medium) [nm/%/µs]	Solid State PL_{max}/PLQY/$\tau^{a)}$ (medium) [nm/%/µs]	ΔE_{ST} [eV]	HOMO [eV]	LUMO [eV]	Ref.
oPTC	455/–/– (cyclohexane)	511/46.6/57.9 (6.5 et% in mCP)	0.02	5.11	2.85	[92]
BOX	504/22/– (PhMe)	–/75/– (6 wt% in mCBP)	0.067	–	–	[117]
PIC-TRZ	–/35/120 (PhMe)	≈500/39/230 (6 wt% in mCP)	0.11	–	–	[13]
TmCzTrz	–/99/13.3 (PhMe)	≈470/98/– (30 wt% in DPEPO)	0.07	5.19	2.11	[55]
ACRFLCN	–/–/–	485/67/160,940,3900 (6 wt% in TPSi-F)	0.10	6.07	2.53	[103]
PTSOPO	–/–/–	≈460/80/– (30 wt% in DPEPO)	0.09	5.78	3.06	[47]
G2TAZ	473/94/– (PhMe)	≈500/52/0.06, 0.85, 8.4 (neat)	0.03	5.76	3.01	[69]
G3TAZ	473/100/– (PhMe)	≈500/31/0.07,1.12,4.7 (neat)	0.06	5.72	2.97	[69]
G4TAZ	473/94/– (PhMe)	≈500/8.5/0.08,0.89,6.3 (neat)	0.06	5.68	2.80	[69]
pCzBP	472/28/–	508/23/74 (10 wt% in TAPC:TCTA)	0.18	5.64	2.76	[124]
26IPNDCz	488/72/9.2 (PhMe)	≈490/72/– (10 wt% in DPEPO)	0.06	–	–	[72]
PXZ-Mes_3B	509/44/– (PhMe)	504/92/– (16 wt% in CBP)	0.071	5.5	3.1	[78]
PXZ-PXB	522/–/– (PhMe)	482/99/1.87 (6 wt% in polystyrene)	0.028	5.60	2.53	[77]
AcPmBPX	496/20/– (PhMe)	492/46/925 (6 wt% in mCBP)	0.05	5.8	2.9	[119]
***t*-BuCz-DBPHZ**	457/61/– (cyclohexane)	509/31/– (10 wt% in CBP)	0.33	5.79	3.37	[125]
P12	427,491/20.4/4.1 (PhMe)	494/33.7/2.4 (neat)	–	–	–	[89]
2PXZ-OXD	502/43.1/13.3 (PhMe)	517/87/520 (6 wt% in DPEPO)	0.15	–	–	[86]
DMAC-BP	–/–/–	506/85/2.7 (neat)	0.07	–	–	[46]
TB-3PXZ	–/65/–	509/95/1.3 (10 wt% in CzSi)	0.01	5.08	2.38	[91]
TXO-PhCz	–/–/–	520/90/– (5 wt% in mCP)	0.073	5.78	3.58	[113]
4CzIPN	507/93.8/5.1 (PhMe)	≈510/81.8/– (5 wt% in CBP)	0.083	–	–	[15a]
33TCzPN	470/87/2.4 (PhMe)	–/–/–	0.11	6.11	3.50	[88]
BT	512/33/– (PhMe)	–/72/– (6 wt% in mCBP)	0.071	–	–	[117]
cis-BOX2	514/62/– (PhMe)	–/98/– (6 wt% in mCBP)	0.033	–	–	[117]
DTCBPy	508/30.3/1.0 (PhMe)	518/91.4/– (5 wt% in CBP)	0.08	5.61	2.87	[50]
m-ATP-PXZ	546/30/– (PhMe)	524/81/– (6 wt% in mCP)	0.04	5.7	3.1	[93]
HAP-3MF	520/26/– (PhMe)	520/–/– (6 wt% in DPEPO)	0.165	6.0	3.4	[121]
3ACR-TRZ	511/94/– (PhMe)	504/98/6.7 (16 wt% in CBP)	0.015	5.9	3.2	[110]
CzT	512/45.6/42.6 (PhMe)	502/39.7/– (3 wt% in DPEPO)	0.090	–	–	[51]
DACT-II	–/63.7/– (PhMe)	≈520/100/– (9 wt% in CBP)	0.009	5.5	3.2	[37]
PXZ-DPS	507/81/2.5 (PhMe)	505/90/2.6 (10 wt% in mCP)	0.08	5.59	2.79	[15b]
m4CzIPN	≈520/–/– (PhMe)	≈530/67/2.6 (1 wt% in SiCz)	–	–	–	[100]
4CzCNPy	536/54.9/8.4 (PhMe)	–/–/–	0.07	5.72	3.26	[105]
PXZ-POB	–/–/–	492/92/2.69 (1 wt% in PMMA)	0.06	5.50	2.93	[120]
PXZ-TRZ	545/29.5/0.68 (PhMe)	≈540/65.7/– (6 wt% in CBP)	0.070	5.5	3.1	[106]
ATP-PXZ	546/24/1.9 (PhMe)	529/63/– (6 wt% in CBP)	0.09	5.6	3.1	[93]
PXZPM	535/–/3.14 (PhMe)	≈530/88/2.56 (6 wt% in CBP)	0.08	5.10	2.42	[122]
PXZMePM	524/–/1.80 (PhMe)	≈530/89/2.11 (6 wt% in CBP)	0.10	5.10	2.41	[122]
PXZPhPM	528/–/1.82 (PhMe)	≈530/91/1.99 (6 wt% in CBP)	0.03	5.09	2.41	[122]
trans-BOX2	533/32/– (PhMe)	–/81/– (6 wt% in mCBP)	0.050	–/	–	[117]
PPZ-3TPT	528/7/33 (PhMe)	520/42/4900 (10 wt% in mCP)	0.30	4.85	2.20	[15b]
t4CzIPN	≈520/–/– (PhMe)	≈530/78/3.2 (1 wt% in SiCz)	–	–	–	[100]
PTZ-TRZ	409,562/17/– (PhMe)	≈420,520/65.8/– (2 wt% in mCBP)	0.18	5.5	3.0	[107]
ACRDSO2	≈520/34/– (PhMe)	520/71/8.3 (6 wt% in CBP)	0.058	5.26	2.65	[115]

Table 3. Continued.

Emitter	Solution PL_{max}/PLQY/$\tau^{a)}$ (medium) [nm/%/μs]	Solid State PL_{max}/PLQY/$\tau^{a)}$ (medium) [nm/%/μs]	ΔE_{ST} [eV]	HOMO [eV]	LUMO [eV]	Ref.
Bis-PXZ-TDZ	–/–/–	≈540/68.5/7,56,311 (6 wt% in DPEPO)	0.11	5.6	3.2	[116]
Px2BP	509/44/– (PhMe)	538/70/12 (6 wt% in mCP)	0.01	5.44	2.92	[49]
3DPA3CN	506/82/– (PhMe)	533/100/550 (6 wt% in DPEPO)	0.103	–	–	[101]
DTC-DBT	–/–/–	521/53/0.39-0.55 (in TAPC)	0.35	–	–	[111]
TP-AEN	–/–/–	≈540/43.6/1-50000 (neat)	0.22	–	–	[126]
BT2	546/51/– (PhMe)	–/80/– (6 wt% in mCBP)	0.054	–	–	[117]
PxPmBPX	510/10/– (PhMe)	530/57/314 (6 wt% in mCBP)	0.02	5.6	2.8	[119]
TPA-PRZ(CN)2	475/55/6.5 (cyclohexane)	–/–/–	0.075	5.23	2.48	[104]
DHPZ-2BI	550/24.1/5.7 (PhMe)	537/67.6/50 (6 wt% in mCBP)	0.19	5.30	2.85	[16a]
DHPZ-2BN	545/8.4/1.88 (PhMe)	541/35.2/7 (6 wt% in mCBP)	0.10	5.34	3.02	[16a]
DPA-TRZ	565/45/– (PhMe)	540/100/160 (6 wt% in mCBP)	0.11	–	–	[108]
p-Px2BBP	600/10/– (PhMe)	555/36/2.9 (6 wt% in mCBP)	0.06	5.62	3.13	[49]
pAcBP	550/26/–	540/46/10 (10 wt% in TAPC:TCTA)	0.10	5.41	2.78	[124]
Spiro-CN	–/–/–	≈540/27/14 (6 wt% in mCP)	0.057	–	–	[102]
TXO-TPA	–/–/–	580/83/<78 (5 wt% in mCP)	0.052	5.37	3.49	[113]
bis-PXZ-TRZ	560/23-29/1.33 (PhMe)	–/64/– (6 wt% in mCBP)	0.054	5.7	3.4	[109]
tri-PXZ-TRZ	568/23-29/1.10 (PhMe)	–/58/– (6 wt% in mCBP)	0.065	5.7	3.4	[109]
PPZ-DPO	577/12/0.52 (PhMe)	550/45/2.4 (10 wt% in mCP)	0.08	4.92	2.49	[15b]
PXZDSO2	≈580/37/– (PhMe)	540/62/5.0 (6 wt% in CBP)	0.048	5.06	2.67	[115]
DPXZ-*as*-TAZ	–/–/–	553/43/0.98 (1.5 wt% in CBP)	0.08	5.08	2.92	[123]
TPXZ-*as*-TAZ	–/–/–	555/53/1.10 (1.5 wt% in CBP)	0.03	5.08	2.99	[123]
TPA-QNX(CN)2	487/44/2.4 (cyclohexane)	–/–/–	0.111	5.22	2.57	[104]
b3	558/60/17 (PhMe)	550/65/16,156 (1 wt% in CBP)	–	6.1	3.6	[127]

[a)]Lifetime of delayed component.

line with the improved EQE of the former (18.9% at (0.22, 0.46); ITO/PEDOT:PSS/TAPC/mCP/**emitter**:mCP:BmPyPb/TSPO1/TPBI/LiF/Al) (BmPyPb = 1,3-bis(3,5-dipyrid-3-ylphenyl)benzene) compared with that of the latter (16.4% at (0.17, 0.19); ITO/PEDOT:PSS/TAPC/mCP/15 wt% **emitter**:mCP/TSPO1/LiF/Al). However, linking two chromophores together results in extended conjugation and unwanted redshifting of the emission. The same group later reported a series of dual-core TADF emitters **33TCzPN** (λ_{max}: 470 nm; PLQY: 87%; τ_d: 2.35 μs in 10 wt% DPEPO; ΔE_{ST}: 0.11 eV), **34TCzPN** (λ_{max}: 448 nm; PLQY: 66%; τ_d: 2.96 μs in 10 wt% DPEPO; ΔE_{ST}: 0.16 eV), and **44TCzPN** (λ_{max}: 444 nm; PLQY: 61%; τ_d: 4.21 μs in 10 wt% DPEPO; ΔE_{ST}: 0.21 eV) (Figure 20), whose structures vary with respect to the regiochemistry of the interconnection pattern.[88] According to the optimized structures determined by density functional theory (DFT) calculations, the dihedral angles between the central two carbazoles for **33TCzPN**, **34TCzPN**, and **44TCzPN** are 40°, 56°, and 87°, respectively, and therefore, while the two emitter moieties in **33TCzPN** are conjugated, in **34TCzPN** and **44TCzPN** they are not. This is evidenced by a redshifted emission of **33TCzPN** (λ_{max}: 470 nm) while the emission maxima (λ_{max}: 444–448 nm) of **34TCzPN** and **44TCzPN** are similar to two isolated **DCzIPN** chromophores. A green device (ITO/PEDOT:PSS/TAPC/mCP/20 wt% **emitter**:DPEPO/TSPO1/TPBI/LiF/Al) with an EQE of 17.9% at CIE coordinates of (0.29, 0.52) was reported with **33TCzPN**, while the OLEDs with **34TCzPN** and **44TCzPN** are sky-blue with impressive EQEs of 21.8% at CIE coordinates of (0.17, 0.29) (ITO/PEDOT:PSS/TAPC/TCTA/mCP/10 wt% **emitter**:DPEPO/TSPO1/TPBi/LiF/Al) and 19.5% at CIE coordinates of (0.16, 0.23) (ITO/PEDOT:PSS/TAPC/mCP/10 wt% **emitter**:DPEPO/TSPO1/TPBI/LiF/Al), respectively.

Chen et al.[92] prepared two TADF emitters **oPTC** (λ_{max}: 511 nm; PLQY: 46.6%; τ_d: 57.9 μs in 6.5 wt% mCP; ΔE_{ST}: 0.02 eV) and **mPTC** (λ_{max}: 498 nm; PLQY: 54.9%; τ_d: 12.9 μs in 6.5 wt% mCP; ΔE_{ST}: 0.01 eV) (Figure 20) and found that, although the two emitters had very similar photophysical and electrochemical properties, the more sterically restricted conformation in **mPTC** resulted in a slightly improved color purity (FWHM: 86 nm compared with 97 nm for **oPTC**) in the device. However, the most efficient device (ITO/TAPC/TCTA/6.5 wt% **emitter**:mCP/TmPyPb/LiF/Al) was fabricated using **oPTC**, which gave an EQE of 19.9% with CIE coordinates of (0.22, 0.40).

Cyano-based green TADF emitters can essentially be divided into three classes: i). a monomeric series with *ortho* steric hindrance to realize HOMO and LUMO separation (**4CzIPN**,

Table 4. Summary of device structures and performances of green to yellow TADF emitters (500 nm < EL_{max} < 580 nm).

Emitter	Device structure	EL_{max} [nm]	CIE	V_{on} [V]	EQE/PE/CE[a] [%/lm W^{-1}/cd A^{-1}]	Ref.
oPTC	ITO/TAPC/TCTA/6.5 wt% **emitter**:mCP/TmPyPb/LiF/Al	500	(0.22, 0.40)	3.3	19.9/46.0/52.8	[92]
BOX	ITO/α-NPD/6 wt% **emitter**:mCBP/TPBi/LiF/Al	≈500	–	–	9.1/–/–	[117]
PIC-TRZ	ITO/α-NPD/m-CP/6 wt% **emitter**:m-CP/ BP4mPy/LiF/Al	≈500	–	–	5.3/–/–	[13]
TmCzTrz	ITO/PEDOT:PSS /TAPC/mCP/30 wt% **emitter**:DPEPO/TSPO1/TPBI/LiF/Al	500	(0.25, 0.50)	–	25.5/52.1/–	[55]
ACRFLCN	ITO/TAPC/mCP/6 wt% **emitter**:TPSi-F/TmPyPB/LiF/Al	≈500	–	–	10.1/–/–	[103]
PTSOPO	ITO/PEDOT:PSS/TAPC/mCP/30 wt% **emitter**:DPEPO/TSPO1/TPBI/LiF/Al	≈500	–	–	17.7/–/–	[47]
G2TAZ[b]	ITO/PEDOT:PSS/neat **emitter**/TPBI/Ca/Al	≈500	(0.25, 0.49)	3.3	2.4/–/–	[69]
G3TAZ[b]		≈500	(0.27, 0.49)	3.5	3.4/–/–	[69]
G4TAZ[b]		≈500	(0.23, 0.37)	3.5	1.5/–/–	[69]
pCzBP[b]	ITO/PEDOT:PSS/10 wt% **polymer**:TCTA:TAPC/TmPyPB/LiF/Al	500	(0.28, 0.43)	6.0	8.1/9.0/24.9	[124]
26IPNDCz	ITO/α-NPD/mCP/10 wt% **emitter**:DPEPO/TPBi/LiF/Al	501	–	–	9.6/–/–	[72]
PXZ-Mes_3B	ITO/TAPC/16 wt% **emitter**:CBP/BAlq/Liq/Al	502	(0.22, 0.55)	–	22.8/–/–	[78]
PXZ-PXB	ITO/PEDOT:PSS/α-NPD/mCP /6 wt% **emitter**:mCP/PPT/TPBi/LiF/Al	503	–	–	22.1/–/–	[77]
AcPmBPX	ITO/α-NPD/mCP/6 wt% **emitter**:mCBP/PPF/TPBi/LiF/Al	504	–	5.2	10.0/–/23.4	[119]
***t*-BuCz-DBPHZ**	ITO/NPB/10 wt% **emitter**:CBP/TPBi/BCP/LiF/Al	≈505	–	3.7	≈7/–/–	[125]
P12[b]	ITO/PEDOT:PSS/poly-TPD/neat **polymer**/TmPyPB/Ba/Al	506	(0.24, 0.43)	3.1	4.3/11.2/10.7	[89]
2PXZ-OXD	ITO/α-NPD/mCP/6 wt% **emitter**:DPEPO/DPEPO/TPBi/LiF/Al	508	(0.25, 0.45)	–	14.9/–/–	[86]
DMAC-BP	ITO/MoO_3/mCP/neat **emitter**/TPBI/LiF/Al	510	(0.26, 0.55)	2.6	18.9/59/–	[46]
TB-3PXZ	ITO/PEDOT:PSS/10 wt% **emitter**:CzSi/TmPyPB/Liq/Al	510	(0.23, 0.54)	5.2	13.9/32.6/41.5	[91]
TXO-PhCz	ITO/PEDOT/TAPC/5 wt% **emitter**:mCP/TmPyPB/LiF/Al	≈510	(0.31, 0.56)	4.7	21.5/70.0/76.0	[113]
4CzIPN	ITO/α-NPD/5 wt% **emitter**:CBP/TPBi/LiF/Al	≈510	–	–	19.3/–/–	[15a]
33TCzPN	ITO/PEDOT:PSS/TAPC/mCP/20 wt% **emitter**:DPEPO/TSPO1/TPBI/LiF/Al	510	(0.29, 0.52)	–	17.9/38.0/51.7	[88]
BT	ITO/α-NPD/6 wt% **emitter**:mCBP/TPBi/LiF/Al	≈510	–	–	12.1/–/–	[117]
cis-BOX2		≈510	–	–	16.6/–/–	[117]
DTCBPy	ITO/NPB/TAPC/5 wt% **emitter**:CBP/PPT/TmPyPb/LiF/Al	514	(0.30, 0.64)	3.1	27.2/84.5/94.6	[50]
m-ATP-PXZ	ITO/α-NPD/mCP/6 wt% **emitter**:mCP/TPBi/LiF/Al	516	–	3.4	12.6/24.3/34.0	[93]
HAP-3MF	ITO/α-NPD/mCP/6 wt% **emitter**:DPEPO/DPEPO/TPBI/LiF/Al	≈520	–	–	6.0/–/–	[121]
3ACR-TRZ[b]	ITO/PEDOT:PSS/16 wt% **emitter**:CBP/BmPyPhB/Liq/Al	≈520	–	–	18.6/–/–	[110]
CzT	ITO/α-NPD/TCTA/CzSi/3 wt% **emitter**:DPEPO/DPEPO/TPBi/LiF/Al	520	(0.23, 0.40)	–	6/9.7/–	[51]
DACT-II	ITO/TAPC/9 wt% **emitter**:CBP/BAlq/Liq/Al	≈520	–	–	29.6/–/–	[37]
PXZ-DPS	ITO/α-NPD/10 wt% **emitter**:CBP/TPBI/LiF/Al	≈520	–	2.7	17.5/–/–	[15b]
m4CzIPN	ITO/PEDOT:PSS/PVK/1 wt% **emitter**:SiCz/TSPO1/LiF/Al	≈520	(0.29, 0.57)	–	19.6/57.1/–	[100]
4CzCNPy[b]	ITO/PEDOT:PSS/8 wt% **emitter**:mCP/TmPyPB/LiF/Al	524	(0.34, 0.59)	6.2	11.3/14.8/38.9	[105]
PXZ-POB	ITO/HAT-CN/TBBD/TCTA/20 wt% **emitter**:**2c**/TPBI/LiF/Al	528	–	4.6	15.2/36.0/52.8	[120]
PXZ-TRZ	ITO/α-NPD/6 wt% **emitter**:CBP/TPBi/LiF/Al	529	–	–	12.5/–/–	[106]
ATP-PXZ	ITO/α-NPD/mCP/6 wt% **emitter**:CPB/TPBi/LiF/Al	529	–	3.2	11.7/24.8/37.9	[63,93]
PXZPM	ITO/TAPC/TCTA/6 wt% **emitter**:CBP/Tm3PyPB/LiF/Al	≈530	(0.33, 0.57)	3.4	19.9/60.1/65.4	[122]
PXZMePM		≈530	(0.30, 0.56)	3.4	22.2/68.4/71.3	[122]
PXZPhPM		≈530	(0.32, 0.57)	3.4	24.6/73.7/80.0	[122]
trans-BOX2	ITO/α-NPD/6 wt% **emitter**:mCBP/TPBi/LiF/Al	≈530	–	–	14.4/–/–	[117]
PPZ-3TPT	ITO/α-NPD/10 wt% **emitter**:CBP/TPBI/LiF/Al	≈530	–	–	≈8/–/–	[15b]
t4CzIPN[b]	ITO/PEDOT:PSS/PVK/1 wt% **emitter**:SiCz/TSPO1/LiF/Al	≈530	(0.31, 0.59)	–	18.3/42.7/–	[100]
PTZ-TRZ	ITO/α-NPD/2 wt% **emitter**:mCBP/TPBi/LiF/Al	532	–	–	10.8/–/–	[107]

Table 4. Continued.

Emitter	Device structure	EL_{max} [nm]	CIE	V_{on} [V]	EQE/PE/CE[a] [%/lm W^{-1}/cd A^{-1}]	Ref.
ACRDSO2	ITO/HAT-CN6/TAPC/6 wt% **emitter**:CBP/TmPyPB/LiF/Al	534	(0.34, 0.57)	3.5	19.2/54.0/61.8	[115]
Bis-PXZ-TDZ	ITO/α-NPD/mCP/6 wt% **emitter**:DPEPO/DPEPO/TPBi/LiF/Al	537	–	–	10.0/–/–	[116]
Px2BP	ITO/α-NPD/6 wt% **emitter**:mCP/TPBi/LiF/Al	539	(0.37, 0.58)	3.2	10.7/–/35.9	[49]
3DPA3CN	ITO/α-NPD/mCBP/6 wt% **emitter**:DPEPO/TPBI/LiF/Al	≈540	–	–	21.4/–/–	[101]
DTC-DBT	ITO/NPB/38 wt% **emitter**:TAPC/TPBi/BCP/LiF/Al	≈540	–	2.7	14.0/20.3/26.3	[111]
TP-AEN[b]	ITO/PEDOT:PSS/interlayer/neat **polymer**/NaF/Al/Ag	≈540	(0.32, 0.58)	–	10.0/–/–	[126]
BT2	ITO/α-NPD/6 wt% **emitter**:mCBP/TPBi/LiF/Al	≈540	–	–	14.0/–/–	[117]
PxPmBPX	ITO/α-NPD/mCP/6 wt% **emitter**:mCBP/PPF/TPBi/LiF/Al	541	–	3.2	11.3/–/35.3	[119]
TPA-PRZ(CN)2	ITO/MoO_3/TCTA/10 wt% **emitter**:mCP/TmPyPb/LiF/Al	542	(0.43, 0.55)	–	4.0/–/–	[104]
DHPZ-2BI	ITO/α-NPD/6 wt% **emitter**:mCBP/TPBi/LiF/Al	542	–	–	12/–/–	[16a]
DHPZ-2BN		546	–	–	6/–/–	[16a]
DPA-TRZ	ITO/α-NPD/6 wt% **emitter**:mCBP/TPBI/LiF/Al	548	–	–	13.8/–/–	[108]
p-Px2BBP	ITO/α-NPD/6 wt% **emitter**:mCBP/TPBi/LiF/Al	548	(0.49, 0.51)	3.6	6.9/–/20.1	[49]
pAcBP[b]	ITO/PEDOT:PSS/10 wt% **polymer**:TCTA:TAPC/TmPyPB/LiF/Al	548	(0.38, 0.57)	4.3	9.3/20.3/31.8	[124]
Spiro-CN	ITO/α-NPD/6 wt% **emitter**:mCP/Bphen/MgAg/Ag	≈550	–	–	4.4/13.0/13.5	[102]
TXO-TPA	ITO/PEDOT/TAPC/5 wt% **emitter**:mCP/TmPyPB/LiF/Al	552	(0.45, 0.53)	5.3	18.5/47.4/43.3	[113]
bis-PXZ-TRZ	ITO/α-NPD/6 wt% **emitter**:mCBP/TPBi/LiF/Al	552	–	–	9.1/–/–	[109]
tri-PXZ-TRZ		553	–	–	13.3/–/–	[109]
PPZ-DPO	ITO/α-NPD/10 wt% **emitter**:CBP/TPBI/LiF/Al	≈560	–	–	≈9/–/–	[15b]
PXZDSO2	ITO/HAT-CN6/TAPC/6 wt% **emitter**:CBP/TmPyPB/LiF/Al	560	(0.44, 0.54)	3.7	16.7/38.5/49.3	[115]
DPXZ-*as*-TAZ	ITO/TAPC/TCTA/1.5 wt% emitter:CBP/TmPyPB/LiF/Al	≈570	(0.44, 0.52)	3.3	9.6/22.3/25.6	[123]
TPXZ-*as*-TAZ		≈570	(0.45, 0.52)	3.3	13.0/31.2/34.8	[123]
TPA-QNX(CN)2	ITO/MoO_3/TCTA/10 wt% **emitter**:mCP/TmPyPb/LiF/Al	573	(0.45, 0.54)	–	9.4/–/–	[104]
b3	ITO/HAT-CN/Tris-PCz/10 wt% **emitter**:CBP/T2T/Bpy-TP2/LiF/Al	574	–	3	9.0/–/–	[127]

[a]Maximum EQE, power efficiency (PE), and current efficiency (CE); [b]Solution-processed device.

t4CzIPN, **3DPA3CN**, and **4CzCNPy**); ii) a homoconjugation series that relies on through-space interactions to realize HOMO and LUMO separation (**Spiro-CN**, **ACRFLCN**, **TPA-PRZ(CN)2**, and **TPA-QNX(CN)2**; and iii) dimeric emitters (**TCzPN** series).

Monomeric emitters are already very potent green TADF emitters with small ΔE_{ST} (<0.1 eV) and high solid-state PLQYs (81.8–100%). In particular, **4CzIPN** is frequently employed to evaluate new bespoke host materials and is arguably the most widely studied TADF emitter and the highest recorded EQE using this emitter is 31.2%. On the other hand, HOMO and LUMO separation can be elegantly achieved by homoconjugation, but those emitters in general suffer from lower PLQYs compared with monomeric and the dimeric emitters. This reflects that homoconjugation limits orbital overlap too substantially, such that the transition dipole moment is significantly weakened, negatively impacting emission efficiency. This is especially true for **Spiro-CN**, whose solid-state PLQY is only 26%, which seriously limits the device performance. The dimeric emitters show significantly higher ΔE_{ST} (0.11–0.21 eV) than emitters from the other two classes. It is worth noting that PLQYs in toluene solution (61–87%) of these dimeric emitters are lower than the monomeric analogs (e.g., 93% for **4CzIPN**), which actually runs contradictory to the design paradigm of these emitters (i.e., an increase in molar absorptivity to boost the PLQY).

Numerous green TADF emitters contain a 1,3,5-triazine acceptor. **PXZ-TRZ** is a green TADF emitter (λ_{max}: ≈540 nm; PLQY: 66%; τ_d: 0.68 µs in 6 wt% CBP; ΔE_{ST}: 0.07 eV) (**Figure 21**) built upon a phenoxazine donor.[106] Although the molecule may seem largely planar at first sight, the dihedral angle between the donor and acceptor is indeed as high as 74.9°, based on the crystal structure, which effectively localizes the HOMO and LUMO. The device (ITO/α-NPD/6 wt% **emitter**:CBP/TPBi/LiF/Al) using **PXZ-TRZ** has an EQE of 12.5% with EL_{max} at 529 nm. Changing the phenoxazine (PXZ) to phenothiazine (PTZ) results in an interesting TADF emitter, **PTZ-TRZ** (λ_{max}: 562 nm; PLQY: 66%; τ_d: 0.3–0.5 µs in 2 wt% mCBP; ΔE_{ST}: 0.18 eV), which exhibits a dual intramolecular charge-transfer (ICT) emission due to two different conformations of the phenothiazine in the ground state: quasi-axial and quasi-equatorial.[107] The former has a large ΔE_{ST} of 1.14 eV while the latter has a much smaller ΔE_{ST} of 0.18 eV, and, therefore, only the latter conformation produces TADF. The device (ITO/α-NPD/2 wt% **emitter**:mCBP/TPBi/LiF/Al) with this emitter provides a green emission with an EQE of 10.8% and EL_{max} at 532 nm.

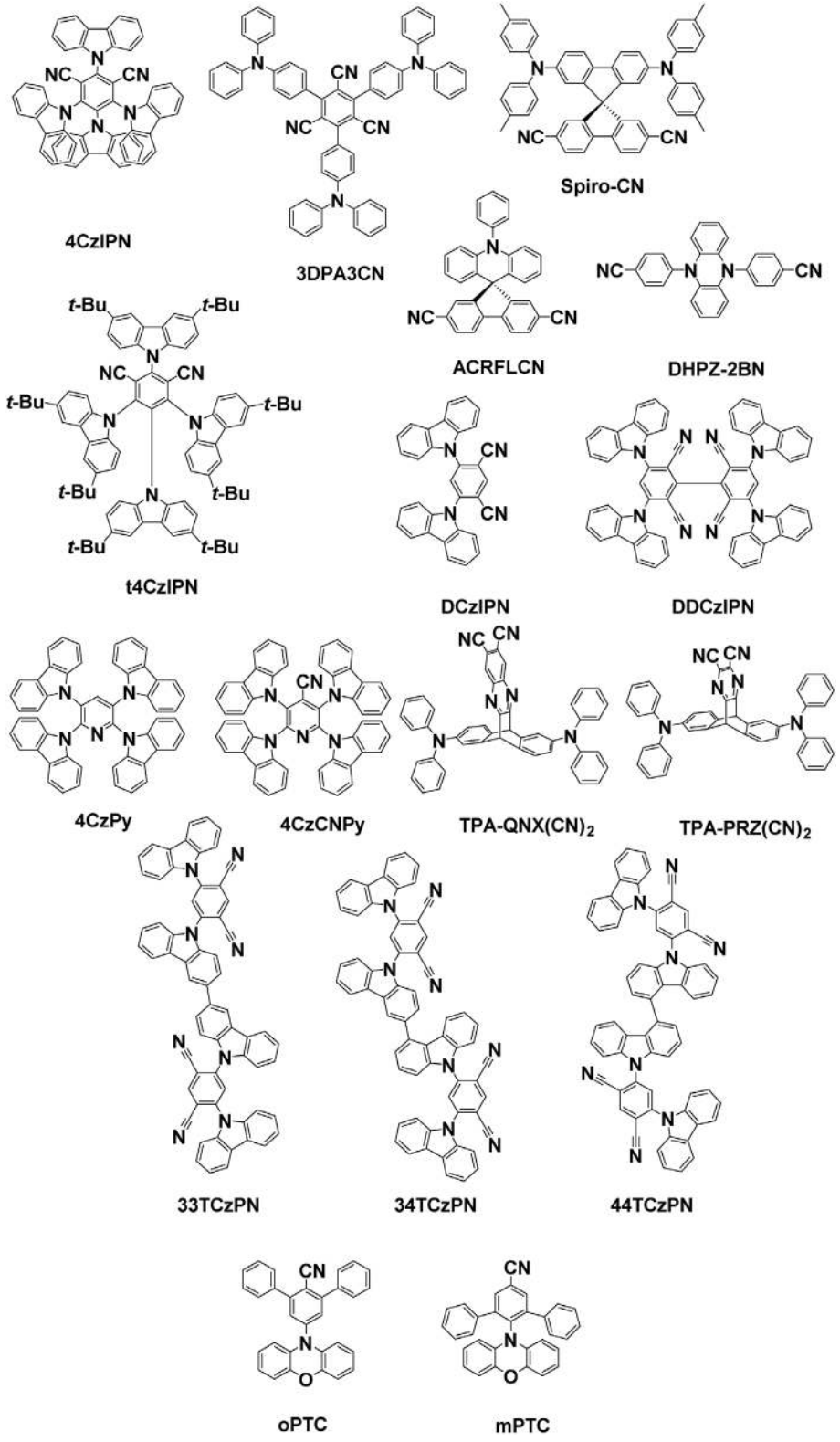

Figure 20. Chemical structures of cyano-based green TADF OLEDs.

Replacing phenoxazine with 4,4′-bis(diphenylamino)phenylamine group leads to the emitter **DPA-TRZ** (λ_{max}: 540 nm; PLQY: 100%; τ_d: 160 µs in 6 wt% mCBP; ΔE_{ST}: 0.11 eV) (Figure 21), whose nonradiative decay is completely suppressed in doped film (6 wt% in **mCBP**), resulting in 100% PLQY.[108] The enhanced PLQY of **DPA-TRZ** compared with **PXZ-TRZ** stems

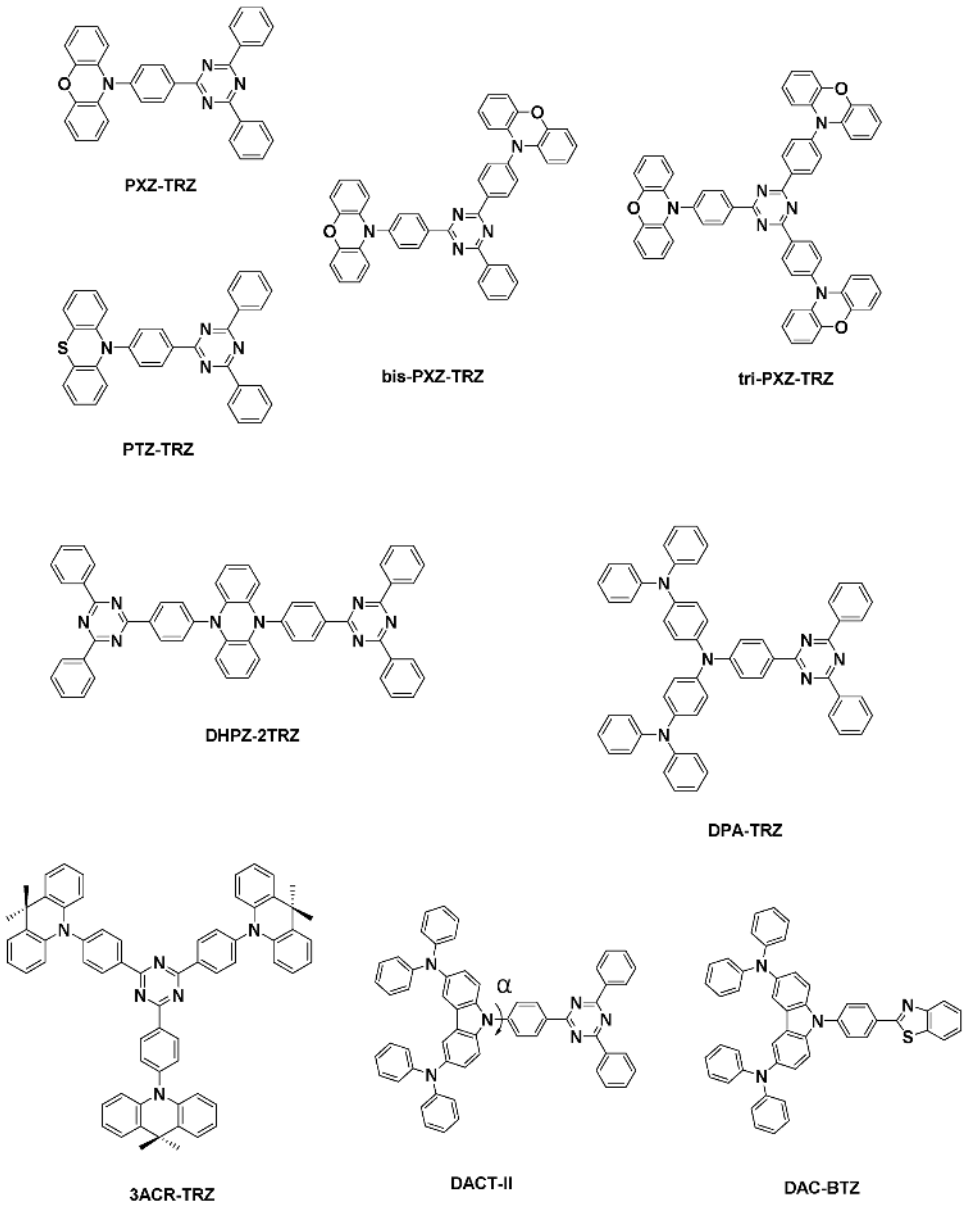

Figure 21. Chemical structures of 1,3,5-triazine-based green TADF OLEDs and **DAC-BTZ**, which is a close analogue of **DACT-II**.

from the better orbital overlap between the donor and acceptor moieties, and thus a stronger transition dipole moment that thereby enhances the k_r. The device (ITO/α-NPD/6 wt% **emitter**:mCBP/TPBI/LiF/Al) with **DPA-TRZ** gives a green emission with an EQE of 13.8% and EL_{max} at 548 nm. A close analog, **DACT-II** (λ_{max}: ≈520 nm; PLQY: 100% in 10 wt% DPEPO; ΔE_{ST}: 0.01 eV) (Figure 21), realizes a simultaneous 100% emission and RISC efficiency, thus giving a state-of-art green device (EL_{max} ≈ 520 nm) (ITO/TAPC/9 wt% **emitter**:CBP/BAlq/Liq/Al) (BAlq = bis(8-hydroxy-2-methylquinolinato)-(4-phenylphenoxy)aluminum; Liq = 8-quinolinolato lithium) with an impressive EQE of 29.6%.[37] The excellent photophysical properties of **DACT-II** are a consequence of the fine tuning of the dihedral angle (α) between the central carbazole and the bridging phenyl ring so that the oscillator strength (f) and the ΔE_{ST} can be both optimized (f and ΔE_{ST} both increase with increasing conjugation). The former is responsible for the large radiative decay rate (k_r), and hence boosts the PLQY, while the latter is linked to the efficiency of the RISC process. Therefore, while **PXZ-TRZ**, with a large dihedral angle of 74.9° between the donor and the bridge, shows a PLQY of 66%, the PLQY of **DACT-II** reaches unity. However, **DAC-BTZ** (λ_{max}: 496 nm; PLQY: 82%; τ_d: 52 µs in 6 wt% DPEPO; ΔE_{ST}: 0.18–0.22 eV), a close analog of **DACT-II** in which the triazine acceptor is changed to benzothiazole, gives a blue device (EL_{max} at 493 nm) with a much lower EQE of 10.3% (ITO/α-NPD/m-CBP/6 wt% **emitter**:DPEPO/DPEPO/TPBi/LiF/Al) due to its larger ΔE_{ST} compared with that of **DACT-II** (0.009 eV).[94] This suggests that the acceptor choice is very important in the design of high-efficiency TADF emitters. Tanaka et al.[109]

reported the disubstituted and trisubstituted analogs **bis-PXZ-TRZ** (λ_{max}: 560 nm; PLQY: 64%; τ_d: 1.3 µs in 6 wt% mCP; ΔE_{ST}: 0.05 eV) and **tri-PXZ-TRZ** (λ_{max}: 568 nm; PLQY: 58%; τ_d: 1.1 µs in 6 wt% mCP; ΔE_{ST}: 0.07 eV) (Figure 21) using this scaffold in order to color-tune the emission. Despite the evident redshift in their emission energies compared with the parent **PXZ-TRZ**, **bis-PXZ-TRZ** and **tri-PXZ-TRZ** show almost identical emissions in both their PL and EL spectra. This observation can be attributed to the fact that the additional PXZ arms are *meta*-disposed where the conjugation length is not strongly affected. Nevertheless, the device (ITO/α-NPD/6 wt% **emitter**:mCBP/TPBi/LiF/Al) using **tri-PXZ-TRZ** shows a green emission with an EQE of 13.3% and EL_{max} at 553 nm. A solution-processable green emitter, **3ACR-TRZ** (λ_{max}: 504 nm; PLQY: 98%; τ_d: 6.7 µs in 16 wt% CBP; ΔE_{ST}: 0.02 eV), was reported by Adachi et al. (Figure 20),[110] which shows a very efficient triplet utilization of 96% together with a PLQY close to unity in doped **CBP**. It is worth noting that although the dihedral angle between the acridan donor and the phenyl bridge is nearly 90°, the PLQY of the emitter remains exceptionally high. This result may seem to contradict the design paradigm illustrated in **PXZ-TRZ** and **DACT-II**, where the torsional angle between the donor and the phenyl bridge plays a crucial role in the balance between PLQY and ΔE_{ST}. The solution-processed device (ITO/PEDOT:PSS/16 wt% **emitter**:CBP/BmPyPhB/Liq/Al) (BmPyPhB = 1,3-bis[3,5-di(pyridin-3-yl)phenyl]benzene) shows a very high EQE of 18.6% with a EL_{max} at ≈520 nm.

Sulfone-based acceptors can also be used for green-TADF-emitter design but the key difference compared with blue TADF analogs is that diphenyl sulfone is no longer useful because of its very weak acceptor strength (LUMO: ≈2.5–2.6 eV). Jankus et al.[111] applied a TADF emitter, **DTC-DBT** (λ_{max}: 540 nm; PLQY: 53%; τ_d: 18, 44 µs in 30 wt% TAPC; ΔE_{ST}: 0.35 eV) (Figure 7), in the fabrication of a green device (ITO/NPB/38 wt% **emitter**:TAPC/TPBi/BCP/LiF/Al) (BCP = bathocuproine) with a maximum EQE of 14.0% at an EL_{max} at ≈540 nm using notably very high doping concentrations. Given that the PLQYs of **DTC-DBT**:**TAPC** (**TAPC** = 4,4′-cyclohexylidenebis[*N*,*N*-bis(4-methylphenyl)benzenamine]) films are around 50%, nearly full triplet utilization is achieved in the device. Within the film, emission from both **DTC-DBT** (ICT in nature) and the exciplex (typically, a bimolecular electronically excited complex formed of two non-bonded monomers where one monomer acts as the donor and the other acts as the acceptor; the formation of the excited state is the result of electron transfer from the donor to the acceptor) between **DTC-DBT** and **TAPC** is active in the device. The ICT emission is favoured under low (7 wt%) doping concentrations while exciplex emission dominates at high (30 wt%) doping concentrations. Notably, delayed fluorescence from the ICT state has a lifetime of 1–2 µs, whereas the lifetimes for exciplex emission are significantly longer, up to 100 µs. Kim et al.[112] reported a similar green emitter **DTAO** (ΔE_{ST}: 0.19 eV, Figure 7) in which di-*tert*-butylcarbazole was replaced with a dimethylacridan donor. The device shows an EQE of 14.3% and CIE coordinates of (0.32, 0.56) (ITO/PEDOT:PSS/TAPC/mCP/10 wt% **emitter**:mCP:TPBi/TSP01/TPBi/LiF/Al). Wang et al.[113] designed two green TADF emitters, **TXO-PhCz** (λ_{max}: 520 nm; PLQY: 90% in 5 wt% mCP; ΔE_{ST}: 0.07 eV) and **TXO-TPA** (λ_{max}: 580 nm; PLQY: 83% in 5 wt% mCP; ΔE_{ST}: 0.05 eV) (Figure 7) based on thioxanthone acceptors, whose device (ITO/PEDOT/TAPC/5 wt% **emitter**:mCP/TmPyPB/LiF/Al) EQEs are 21.5% and 18.5% with CIE coordinates of (0.31, 0.56) and (0.45, 0.53), respectively. The **TPA** derivative shows a markedly redshifted emission by 60 nm (1990 cm^{-1}) compared with the **PhCz** analog due to the much stronger donor in the former (HOMO: −5.37 eV) than the latter (HOMO: −5.78 eV). Nevertheless, other photophysical parameters, such as PLQY and ΔE_{ST}, seem little affected by the donor choice. The group later developed an emitting layer with a multi-quantum-well structure consisting of alternating nanolayers of **mCP** and **TXO-PhCz** designed for improved charge and exciton confinement. The OLED device (ITO/PEDOT:PSS/TAPC/**TXO-PhCz**:mCP (multi-quantum-well)/TmPyPB/LiF/Al) employing this enhanced architecture gave a slightly improved EQE of 22.6% compared with the 21.5% EQE of the original device (ITO/PEDOT/TAPC/5 wt% **emitter**:mCP/TmPyPB/LiF/Al).[114] Xie et al.[115] reported two emitters **ACRDSO2** (λ_{max}: 575 nm; PLQY: 71%; τ_d: 8.3 µs in 6 wt% CBP; ΔE_{ST}: 0.06 eV) and **PXZDSO2** (λ_{max}: 540 nm; PLQY: 62%; τ_d: 5.0 µs in 6 wt% CBP; ΔE_{ST}: 0.05 eV) (Figure 7) based on a thianthrene-9,9′,10,10′-tetraoxide acceptor. Similar to aforementioned examples of **TXO-PhCz** and **TXO-TPA**, the choice of donor mainly affects the emission energy but leaves other photophysical parameters essentially unchanged. According to the authors, the phenyl bridge between the donor and acceptor decreases nonradiative internal conversion channels to increase the radiative rate constant (k_r) resulting in high PLQY. Interestingly, these two molecules can be either vacuum-deposited or solution-processed during device fabrication (ITO/HAT-CN6/TAPC/6 wt% **emitter**:CBP/TmPyPB/LiF/Al) to give comparable device performance regardless of fabrication method (EQEs: 15.2–19.2%). **ACRDSO2** and **PXZDSO2** emit green (CIE coordinates of (0.34, 0.57)) and yellow (CIE coordinates of (0.44, 0.54)) light, respectively.

1,3,4-Oxadiazole and its derivatives are also commonly found in green TADF emitters. Lee et al.[86] prepared a series of emitters (**PXZ-OXD**, **PXZ-TAZ**, **2PXZ-OXD**, and **2PXZ-TAZ**) (**Figure 22**) based on phenoxazine as the donor and 1,3,4-oxadiazole and 1,2,4-triazole as the acceptor. In their study, the D–A–D type molecules (**2PXZ-OXD** and **2PXZ-TAZ**) were found to show higher PLQYs along with a more efficient RISC process compared to D–A-type analogs (**PXZ-OXD** and **PXZ-TAZ**). The best device was fabricated using **2PXZ-OXD** as a green emitter (λ_{max}: 517 nm; PLQY: 87%; τ_d: 520 µs in 6 wt% DPEPO; ΔE_{ST}: 0.15 eV), which shows an EQE of 14.9% with CIE coordinates of (0.25, 0.45) (ITO/α-NPD/mCP/6 wt% **emitter**:DPEPO/DPEPO/TPBi/LiF/Al). Tanaka et al.[116] studied the effect of atom substitution on TADF by contrasting **2PXZ-OXD** (a.k.a. **bis-PXZ-OXD**) and **bis-PXZ-TDZ** (λ_{max}: ≈540 nm; PLQY: 69%; τ_d: 7, 56, 311 µs in 6 wt% DPEPO; ΔE_{ST}: 0.11 eV) (Figure 22), where the only difference between the two emitters is the nature of the chalcogen in the acceptor. It was found that the substitution of sulfur results in an enhanced acceptor strength and stronger intersystem crossing due to the presence of vacant 3d orbitals on the sulfur atom, resulting in a smaller ΔE_{ST} and higher k_{RISC}. Thus, **bis-PXZ-TDZ** gives a higher fraction of EQE contributed from the delayed component ($\eta_{delayed}$: 78.0%) than **2PXZ-OXD** ($\eta_{delayed}$: 65.1%). Nevertheless, it is important to note that a high $\eta_{delayed}$ does not necessarily

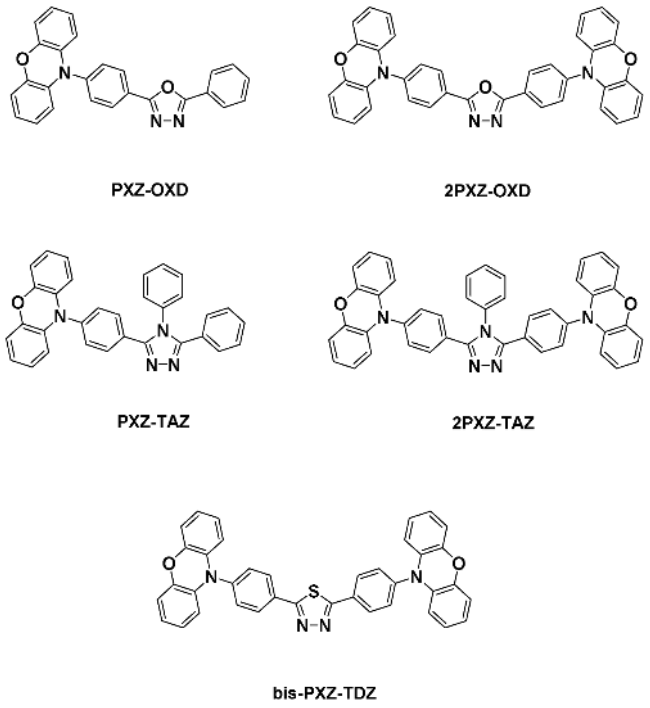

Figure 22. Chemical structures of 1,3,4-oxadiazole-, 1,2,4-triazole-, and 1,3,4-thiadiazole-based green TADF emitters.

translate into an improved TADF emitter because the emission efficiency from the singlet state is of prime importance. The device (ITO/α-NPD/mCP/6 wt% **emitter**:DPEPO/DPEPO/TPBi/LiF/Al) EQEs and EL_{max} of **2PXZ-OXD** and **bis-PXZ-TDZ** are 14.9% and 10.0% and 508 nm and 537 nm, respectively.

Sagara et al.[117] prepared a series of green emitters (**BT**, **BT2**, **BOX**, ***cis*-BOX2**, and ***trans*-BOX2**) (**Figure 23**) based on phenoxazine donors and benzoxazole or benzothiazole accepters in order to contrast the properties and device performance between D–A and D–A–D molecular design. They found that D–A–D molecules have faster radiative rate constants (k_r), better PLQYs, and smaller ΔE_{ST}. All emitters gave reasonably good device performance (EQEs of 9.1% to 16.6%) with the best OLED (ITO/α-NPD/6 wt% **emitter**:mCBP/TPBi/LiF/Al) using ***cis*-BOX2** as the emitter (λ_{max}: ≈510 nm; PLQY: 98% in 6 wt% mCBP; ΔE_{ST}: 0.03 eV). The study concluded that D–A–D molecules clearly outperform their D–A analogs as emitters in OLEDs. Very recently, ***cis*-BOX2** was found to exhibit a completely horizontal orientation when doped into a **CBP** matrix at 200 K. It was important to keep the deposition temperature below the glass-transition temperature of the **CBP** matrix; otherwise, the preferred horizontal orientation was no longer present. Thanks to the greatly enhanced light-out-coupling, the device (ITO/TAPC/15 wt% ***cis*-BOX2**:CBP/6 wt% ***cis*-BOX2**:CBP)/PPT/LiF/Al) gave an EQE of 33.4%.[118] Though not explicitly discussed by the authors, ***trans*-BOX2** should possess a very similar molecular length, planarity, and shape compared with ***cis*-BOX2**, and thus it would be expected that ***trans*-BOX2** should also give a preferential horizontal arrangement, as was observed for ***cis*-BOX2**.

Two emitters **AcPmBPX** (λ_{max}: 492 nm; PLQY: 46%; τ_d: 925 µs in 6 wt% mCP; ΔE_{ST}: 0.05 eV) and **PxPmBPX** (λ_{max}: 530 nm; PLQY: 57%; τ_d: 314 µs in 6 wt% mCP; ΔE_{ST}: 0.02 eV)

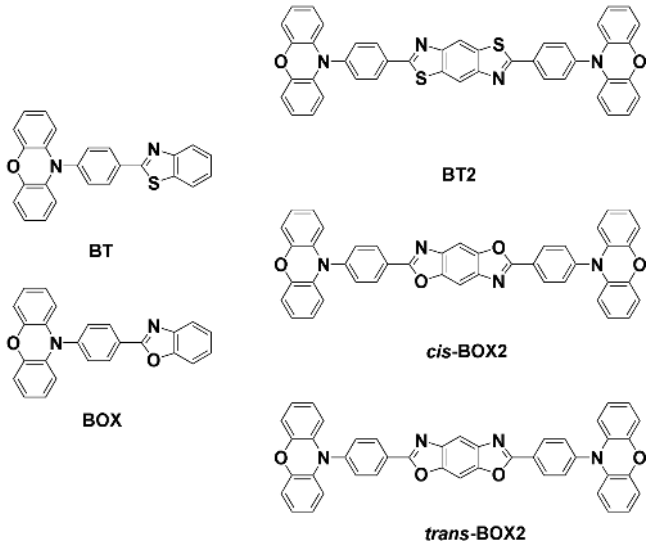

Figure 23. Chemical structures of **BT**, **BT2**, **BOX**, ***cis*-BOX2**, and ***trans*-BOX2**.

(**Figure 24**) based on an X-shaped benzoylbenzophenone scaffold were recently reported by Adachi et al.[119] Within this molecular design a large dihedral angle between the peripheral donor and the central benzoylbenzophenone acceptor exists, leading to a well-separated HOMO and LUMO. In particular, **PxPmBPX** achieves a very small ΔE_{ST} of 0.02 eV. Devices (ITO/α-NPD/mCP/6 wt% **emitter**:mCBP/PPF/TPBi/LiF/Al) using **AcPmBPX** and **PxPmBPX** gave green (EL_{max} at 504 nm) and yellow (EL_{max} at 541 nm) emission with EQEs of 10.0% and 11.3%, respectively.

Lee et al.[16a] prepared a series of emitters (**DHPZ-2BI**, **DHPZ-2BN**, **DHPZ-2BTZ**, and **DHPZ-2TRZ**) (**Figure 25**) based on a dihydrophenazine donor and a variety of acceptors including benzonitrile, triazine, benzimidazole, and benzothiazole. Emission, along with ΔE_{ST}, can be tuned from green to orange through the choice of acceptor. The most efficient device employed **DHPZ-2BI** as the emitter (λ_{max}: 537 nm; PLQY: 68%; τ_d: 50 µs in 6 wt% mCP; ΔE_{ST}: 0.19 eV) and gave a green emission with an EQE of 12% with EL_{max} at 542 nm (ITO/α-NPD/6 wt% **emitter**:mCBP/TPBi/LiF/Al).

Hirai et al.[120] reported a green emitter **PXZ-POB** (λ_{max}: 492 nm; PLQY: 92%; τ_d: 2.69 µs in 1 wt% poly(methyl methacrylate) (PMMA); ΔE_{ST}: 0.06 eV) (**Figure 26**) based on a phenoxazine donor and a 1,3-diaryloxybenzene borane acceptor.

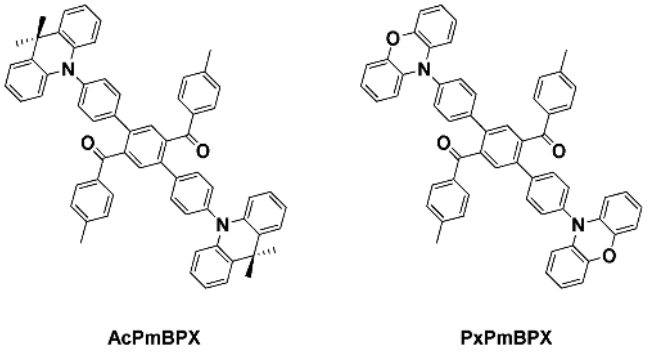

Figure 24. Chemical structures of **AcPmBPX** and **PxPmBPX**.

Due to strong localization of the HOMO and LUMO on the donor and acceptor, respectively, a small ΔE_{ST} of 0.06 eV is achieved. As a result of its high PLQY of 92%, the device achieves a high EQE of 15.2% with EL_{max} at 528 nm (ITO/HAT-CN/TBBD/TCTA/20 wt% **emitter**:**2c**/TPBI/LiF/Al) (TBBD = $N^4,N^4,N^{4'},N^{4'}$-tetra([1,1′-biphenyl]-4-yl)-[1,1′-bipheny l]-4,4′-diamine). However, the operational stability of the device is poor with an LT_{80} of less than 1 h. Liu et al.[91] also prepared a series of TADF emitters (**TB-1PXZ**, **TB-2PXZ**, and **TB-3PXZ**) based on a phenoxazine donor and tridurylborane acceptor design (Figure 26). Interestingly, advantageous merits such as smaller ΔE_{ST} (0.12 eV, 0.05 eV, and 0.01 eV) and higher PLQY (12%, 47%, and 95%) are realized through increased phenoxazine substitution across the series, a similar observed behavior to the analogous phosphine oxides systems (**PXZPOs**) (Figure 16). The best solution-processed device (ITO/PEDOT:PSS/10 wt% **emitter**:CzSi/TmPyPB/Liq/Al) was obtained using **TB-3PXZ** (λ_{max}: 509 nm; PLQY: 95%; τ_d: 1.3 µs in 10 wt% CzSi; ΔE_{ST}: 0.01 eV) as the emitter with an EQE of 13.9%.

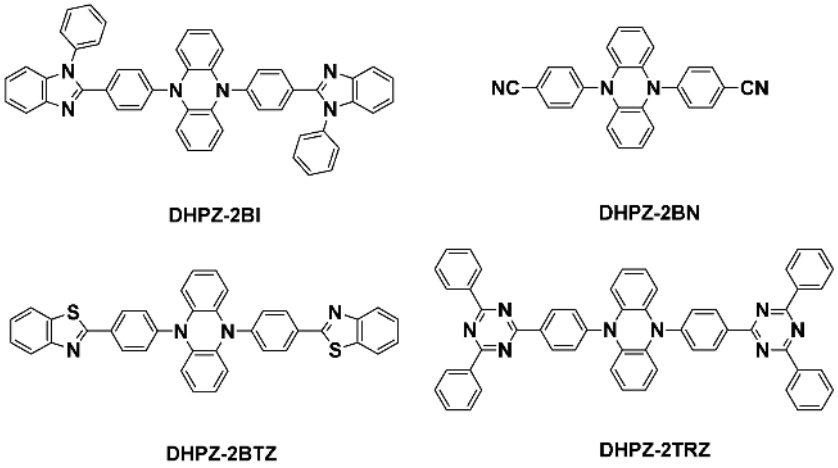

Figure 25. Chemical structures of **DHPZ-2BI, DHPZ-2BN, DHPZ-2BTZ**, and **DHPZ-2TRZ**.

The emitter **HAP-3MF** (λ_{max}: 520 nm; PLQY: 26% in 6 wt% DPEPO; ΔE_{ST}: 0.17 eV) (**Figure 27**), employing an interesting heptaazaphenalene, was reported by Adachi et al.[121] Among all the TADF emitters reported so far, this molecule is special for two reasons: Firstly, the lowest singlet (S_1) and triplet (T_1) involved in the RISC process are all highly n–π^* excited states, which is highly unusual. Secondly, to the best of our knowledge, **HAP-3MF** is arguably the only TADF emitter for OLED applications that does not involve a nitrogen-based donor (the heptaazaphenalene here acts as the acceptor). However, because emission results from an n–π^* excited state, k_r is small (on the order of 10^{-6} s^{-1}), resulting in a relatively low PLQY of 26% in degassed toluene for the molecule. The OLED (ITO/α-NPD/mCP/6 wt% **emitter**:DPEPO/DPEPO/TPBI/LiF/Al) using this emitter gave a green emission with an EQE of 6.0% with EL_{max} at ≈520 nm.

Wu et al.[122] prepared a series of three pyrimidine-based green TADF emitters (**Figure 28**). As expected, having only two nitrogen atoms in the pyrimidine renders it a weaker acceptor than the three-nitrogen-atom-containing triazine analog (**bis-PXZ-TRZ**).[109] The λ_{EL} of these pyrimidine emitters are therefore blueshifted by ≈20 nm. The two classes of emitters share very similar ΔE_{ST} (≈0.05 eV), while the triazine emitter has significantly lower PLQY (64%) than the pyrimidine emitters (88–91%). Each of the OLEDs (ITO/TAPC/TCTA/6 wt% **emitter**:CBP/Tm3PyPB/LiF/Al) showed the same turn-on voltage (3.4 V) and very similar EL_{max} (527–531 nm). Their EQEs were likewise similar (19.9–24.6%), with the most efficient device (EQE = 24.6%) fabricated using **PXZPhPM** (λ_{max}: ≈530 nm; PLQY: 91%; τ_d: 1.82 µs in 6 wt% CBP; ΔE_{ST}: 0.03 eV) as the emitter.

Xiang et al.[123] employed an asymmetric 1,2,4-triazine acceptor, a regioisomeric analog of the commonly used 1,3,5-triazine acceptor in the construction of TADF emitters. With phenoxazine as the donor, the authors fabricated yellow emitters **TPXZ-*as*-TAZ** (λ_{max}: 555 nm; PLQY: 53%; τ_d: 1.10 µs in 1.5 wt% CBP; ΔE_{ST}: 0.03 eV) and **DPXZ-*as*-TAZ** (λ_{max}: 553 nm; PLQY: 43%; τ_d: 0.98 µs in 1.5 wt% CBP; ΔE_{ST}: 0.08 eV) (**Figure 29**). The most efficient device (ITO/TAPC/TCTA/1.5 wt% **emitter**:CBP/TmPyPB/LiF/Al) employed **TPXZ-*as*-TAZ** as the emitter with an EQE of 13.0% and yellow emission at CIE coordinates of

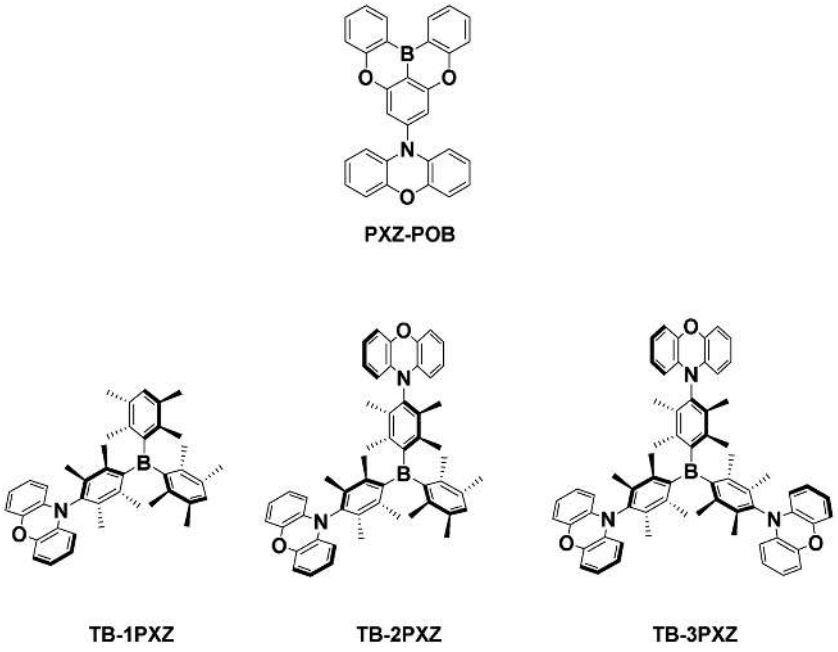

Figure 26. Chemical structures of **PXZ-POB**, **TB-1PXZ**, **TB-2PXZ**, and **TB-3PXZ**.

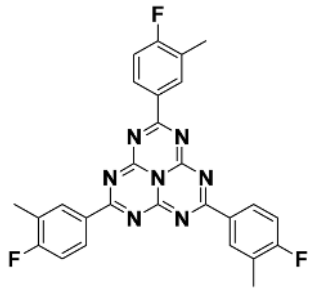

HAP-3MF

Figure 27. Chemical structure of **HAP-3MF**.

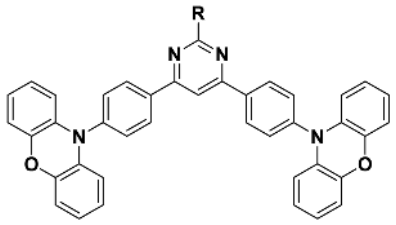

R= H PXZPM
R=Me PXZMePM
R=Ph PXZPhPM

Figure 28. Chemical structures of pyrimidine-based green TADF emitters.

(0.45, 0.52). Remarkably, the device underwent a small efficiency roll-off of 11.5% at high luminance of 1000 cd m^{-2}, thanks to a short decay lifetime of the delayed component (1.10 µs) that contributes to minimizing triplet quenching processes.

2.3. Orange–Red TADF Emitters

In this section, we define orange-to-red emitters as those whose electroluminescence peak wavelength (EL_{max}) is longer than 580 nm. Compared with the number of reported blue and green counterparts, red TADF emitters are underexplored. The distribution of CIE coordinates for the OLEDs reported in this section is shown in **Figure 30** (vide infra). **Table 5** summarizes the photophysical properties of emitters in this section while **Table 6** summarizes the OLED device performance metrics. An early orange TADF emitter, **4CzTPN-Ph** (λ_{max}: 577 nm; PLQY: 26%; τ_d: 1.1 µs in toluene), reported by Adachi et al. (**Figure 31**),[15a] achieved a remarkable EQE of 11.2% with EL_{max} at ≈590 nm (ITO/α-NPD/5 wt% **emitter**:CBP/TPBi/LiF/Al).

The research team then compared two series of anthraquinone-based orange-to-red TADF emitters based on D–A–D (**a1–a4**) and D–Ph–A–Ph–D (**b1–b4**) molecular scaffolds (**Figure 32**), with the key difference being the presence of an additional phenyl bridge separating the donor and the acceptor.[127] It was found that increased separation between the donor and the acceptor conferred by the phenyl bridge in the **b** series results in a higher transition dipole moment and thus an enhanced radiative rate constant, k_r. This was verified by their higher PLQYs; the phenyl bridge has a negligible effect on ΔE_{ST}. On the other hand, the N–C stretching and twisting observed in D–A–D molecules helps to lower the ΔE_{ST} but at the same time reduces k_r and enhances k_{nr} due to increased vibronic coupling between the excited and ground states. The best red OLED (ITO/HAT-CN/Tris-PCz/10 wt% **emitter**:CBP/T2T/Bpy-TP2/LiF/Al) (Tris-PCz = 9,9′-diphenyl-6-(9-phenyl-9*H*-carbazol-3-yl)-9*H*,9′*H*-3,39′*H*-bicarbazole; T2T = 2,4,6-tris(biphenyl-3-yl)-1,3,5-triazine; Bpy-TP2 = 2,7-di(2,2′-bipyridin-5-yl)triphenylene) was fabricated using **b1** as the emitter (λ_{max}: 594 nm; PLQY: 80%; τ_d: 416 µs in 1 wt% CBP; ΔE_{ST}: 0.24 eV), which showed an impressive EQE of 12.5% with CIE coordinates of (0.61, 0.39).

Wang et al.[128] reported the first near-infrared (NIR) TADF emitter, **TPA-DCPP** (λ_{max}: 645 nm; PLQY: 50%; τ_d: 86.2 µs in 10 wt% TPBI; ΔE_{ST}: 0.13 eV) (**Figure 33**), which was based on a dicyanodiazatriphenylene acceptor moiety. The best device performance was achieved for a doped device (ITO/NPB/TCTA/20 wt% **emitter**:TPBi/TPBi/LiF/Al), which exhibited an EQE of 9.8% with CIE coordinates of (0.68, 0.32). It is important to note that the DPA groups are not significantly twisted compared to the 2,3-dicyanopyrazinophenanthrene (DCPP) plane, with a dihedral angle between the phenyl and the DCPP of only 35°. Nevertheless, RISC is efficient in this molecule, most likely due to the extended distance between the donor and the acceptor. This is in line with the conclusions from Adachi et al.[74] about the requirements for TADF molecular design, where the twist angle between the donor and acceptor can be reduced if the distance between donor and acceptor units is increased. A smaller twist angle results in better orbital overlap, which is important for increasing the radiative rate constant, k_r. Indeed, **TPA-DCPP** in degassed toluene shows an excellent PLQY of 84%.

Li et al.[129] prepared an orange–red emitter, **HAP-3TPA** (λ_{max}: 610 nm; PLQY: 91%; τ_d: 100 µs in 6 wt% 26mCPy; ΔE_{ST}: 0.17 eV) (**Figure 34**), based on a heptaazaphenalene acceptor. Interestingly, the emitter shows very weak TADF behavior in the photophysical study ($\Phi_d/\Phi_f = 0.07$, where Φ_d and Φ_f are the contributions from the delayed and prompt components to the total PLQY, respectively) while the singlet-harvesting process is turned on in the device ($\Phi_d/\Phi_f = 1.58$). The EQE of the OLED

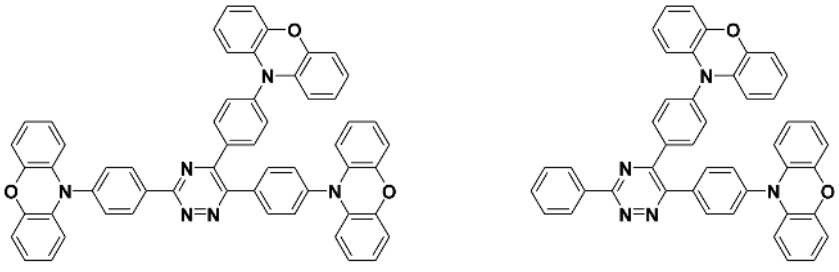

TPXZ-*as*-TAZ DPXZ-*as*-TAZ

Figure 29. Chemical structures of **TPXZ-*as*-TAZ** and **DPXZ-*as*-TAZ**.

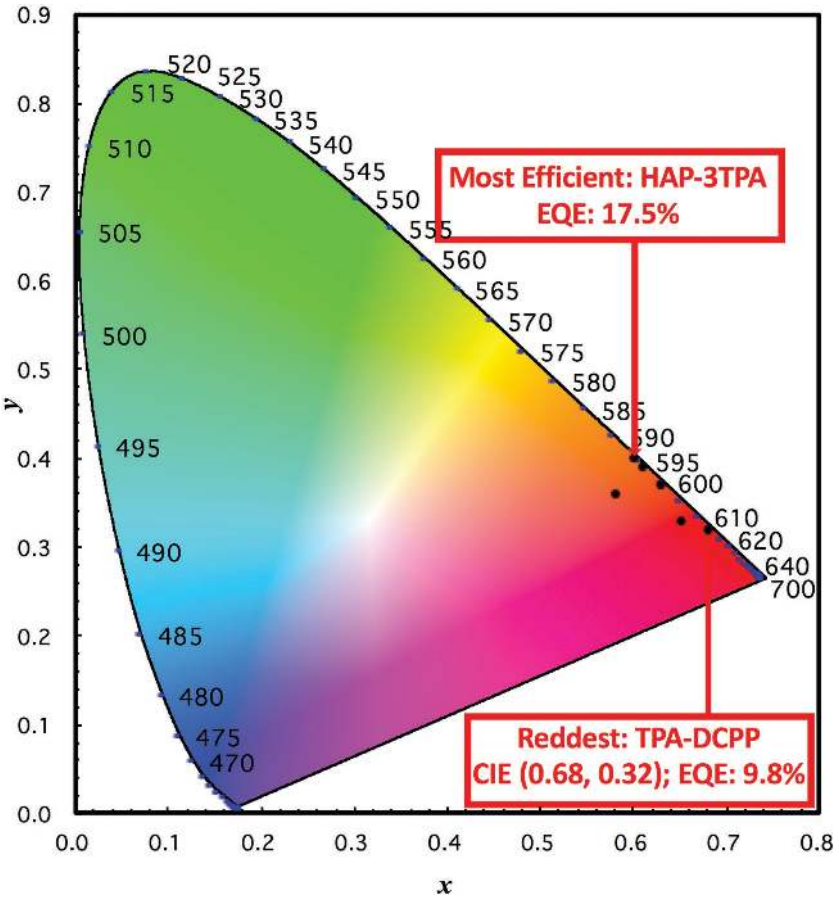

Figure 30. Summary of CIEs of red TADF OLED.

(ITO/α-NPD/6 wt% **emitter**:26mCPy/Bphen/Mg:Ag/Ag) is 17.5% with CIE coordinates of (0.60, 0.40).

Chen et al.[68] prepared a solution-processed nondoped red TADF OLED using **red-1b** (λ_{max}: 622 nm; PLQY: 28%; τ_d: 82.8 µs as neat; ΔE_{ST}: 0.40 eV) (**Figure 35**). Magneto-electroluminescence studies suggest that the material can undergo both TADF and triplet–triplet annihilation (TTA) processes, depending on the current density in the device. The EQE achieved was 1.75% (ITO/PEDOT:PSS/PVK/emitter/TPBi/CsF/Al) with CIE coordinates of (0.65, 0.33).

Data et al.[125] reported a series of three TADF emitters based on dibenzo-[*a*,*j*]-phenazine acceptors, ***t*-BuCz-DBPHZ** (λ_{max}: 509 nm; PLQY: 31%; τ_d not observed in 10 wt% CBP; ΔE_{ST}: 0.33 eV), **MeODP-DBPHZ** (λ_{max}: 592 nm; PLQY: 58%; τ_d: 16, 6440 µs in 10 wt% CBP; ΔE_{ST}: 0.19 eV), and **POZ-DBPHZ** (λ_{max}: 595 nm; PLQY: 79%; τ_d: 1.84, 26.4 µs in 10 wt% CBP; ΔE_{ST}: 0.02 eV) (**Figure 36**). Due to the much reduced donating ability of the *tert*-butyl carbazole, ***t*-BuCz-DBPHZ** showed both much bluer emission than **MeODP-DBPHZ** and **POZ-DBPHZ** and the largest ΔE_{ST} due to weakened ICT character. While the OLED (ITO/NPB/10 wt% **emitter**:CBP/TPBi/BCP/LiF/Al) based on ***t*-BuCz-DBPHZ** (EQE: ≈7%) was green-emitting, those using **MeODP-DBPHZ** (EQE: ≈10%) and **POZ-DBPHZ** (EQE: ≈16%) emitted red light owing to the use of stronger donors. Interestingly, when 10 wt% **POZ-DBPHZ** was doped in the ***m*-MTDATA** host (*m*-MTDATA = 4,4′,4″-tris[(3-methylphenyl)-phenylamino]triphenylamine) (see Section 6, **Figure 37**) as the emitting layer, strongly exciplex-driven NIR emission at 741 nm was observed with an excellent EQE of about 5%. No corroborating evidence was provided to support the TADF mechanism of this exciplex system.

Table 5. Summary of photophysical and electrochemical properties of orange to red TADF emitters (EL_{max} > 580 nm).

Emitter	Solution PL_{max}/PLQY/τ[a)] (medium) [nm/%/µs]	Solid State PL_{max}/PLQY/τ[a)] (medium) [nm/%/µs]	ΔE_{ST} [eV]	HOMO [eV]	LUMO [eV]	Ref.
b4	609/17/3.5 (PhMe)	564/50/6.5 (1 wt% in CBP)	0.07	5.9	3.4	[127]
m-Px2BBP	566/36/– (PhMe)	541/71/13 (6 wt% in mCP)	0.10	5.64	3.03	[49]
4CzTPN-Ph	577/26.3/1.1 (PhMe)	–/–/–	–	–	–	[15a]
MeODP-DBPHZ	509/49/– (cyclohexane)	592/58/16, 6440 (10 wt% in CBP)	0.19	5.30	3.20	[125]
PPZ-DPS	577/3/0.28 (PhMe)	580/20/1.0 (10 wt% in mCP)	0.08	5.10	2.69	[15b]
DHPZ-2BTZ	605/9.7/0.24 (PhMe)	577/33/1 (6 wt% in mCBP)	≈0	5.30	2.92	[16a]
HAP-3TPA	560/95/48 (PhMe)	610/91/100 (6 wt% in 26mCPy)	0.17	5.6	3.4	[129]
POZ-DBPHZ	521/33/– (cyclohexane)	595/79/1.84, 26.4 (10 wt% in CBP)	0.08	5.36	3.38	[125]
DHPZ-2TRZ	648/2.2/– (PhMe)	598/6.6/0.1 (6 wt% in mCBP)	–	5.28	3.18	[16a]
b1	597/59/102 (PhMe)	594/80/416 (1 wt% in CBP)	0.24	–	–	[127]
b2	608/62/85 (PhMe)	601/76/185 (1 wt% in CBP)	0.22	5.7	3.4	
red-1b	≈610/–/– (PhMe)	622/28/0.83 (neat)	≈0.40	5.4	3.2	[68]
TPA-DCPP	588/84/– (PhMe)	708/14/0.76 (neat)	0.13	5.30	3.52	[128]

[a)] Lifetime of delayed component.

Table 6. Summary of device structures and performances of orange to red TADF emitters (EL_{max} > 580 nm).

Emitter	Device Structure	EL_{max} [nm]	CIE	V_{on} [V]	EQE/PE/CE[a] [%/lm W^{-1}/cd A^{-1}]	Ref.
b4	ITO/HAT-CN/Tris-PCz/10 wt% **emitter**:CBP/T2T/Bpy-TP2/LiF/Al	584	–	3	6.9/–/–	[127]
m-Px2BBP	ITO/α-NPD/neat **emitter**/TPBi/LiF/Al	586	(0.58, 0.36)	2.8	4.2/–/11.1	[49]
4CzTPN-Ph	ITO/α-NPD/5 wt% **emitter**:CBP/TPBi/LiF/Al	≈590	–	–	11.2/–/–	[15a]
MeODP-DBPHZ	ITO/NPB/10 wt% **emitter**:CBP/TPBi/BCP/LiF/Al	≈600	–	3.7	≈10/–/–	[125]
PPZ-DPS	ITO/α-NPD/10 wt% **emitter**:CBP/TPBI/LiF/Al	≈600	–	–	≈5/–/–	[15b]
DHPZ-2BTZ	ITO/α-NPD/6 wt% **emitter**:mCBP/TPBi/LiF/Al	601	–	–	5/–/–	[16a]
HAP-3TPA	ITO/α-NPD/6 wt% **emitter**:26mCPy/Bphen/Mg:Ag/Ag	610	(0.60, 0.40)	4.4	17.5/22.1/25.9	[129]
POZ-DBPHZ	ITO/NPB/10 wt% **emitter**:CBP/TPBi/BCP/LiF/Al	≈610	–	3.7	≈16/–/–	[125]
DHPZ-2TRZ	ITO/α-NPD/6 wt% **emitter**:mCBP/TPBi/LiF/Al	617	–	–	1/–/–	[16a]
b1	ITO/HAT-CN/Tris-PCz/10 wt% **emitter**:CBP/T2T/Bpy-TP2/LiF/Al	624	(0.61, 0.39)	3	12.5/–/–	[127]
b2		637	(0.63, 0.37)	3	9.0/–/–	[127]
red-1b[b]	ITO/PEDOT:PSS/PVK/**emitter**/TPBi/CsF/Al	644	(0.65, 0.33)	–	1.75/–/1.22	[68]
TPA-DCPP	ITO/NPB/TCTA/20 wt% **emitter**:TPBi/TPBi/LiF/Al	668	(0.68, 0.32)	3.1	9.8/–/4.0	[128]

[a]Maximum EQE, power efficiency (PE), and current efficiency (CE); [b]Solution-processed device.

2.4. Application of TADF in Light-Emitting Electrochemical Cells

Light-emitting electrochemical cells (LEECs) are an alternative type of EL device, which possesses a much simpler device architecture compared to multilayered OLEDs. In LEECs, the emitter also serves as a charge transporter, facilitated by the presence of charged groups. These groups also facilitate charge injection from the electrodes, resulting in charge injection being insensitive to electrode work function, and thus an air-stable cathode (e.g., Al) can be used. LEECs are fabricated via spin-coating techniques, and the device performance is relatively insensitive to the emitting layer thickness.[130]

We recently reported the first charged organic TADF emitters (**TL-1** and **TL-2**, **Figure 38**) for use in LEECs.[67] Emission in MeCN is uniquely fluorescence due to preferential stabilization of the triplet excited state with respect to the singlet excited state, which increases ΔE_{ST} and turns off TADF. Photophysical studies in both neat and 10 wt%-doped PMMA film on the other hand confirm TADF, with dramatically enhanced PLQY that is O_2-sensitive. The emitter **TL-2** (λ_{max}: 536 nm; PLQY: 21%; τ_d: 2.73 µs in neat film) in the LEEC (ITO/PEDOT:PSS/**emitter**/Al) gave an EQE of 0.39%, significantly lower than when the same emitter was used in an OLED device configuration (EQE of 5.1%, vide supra).

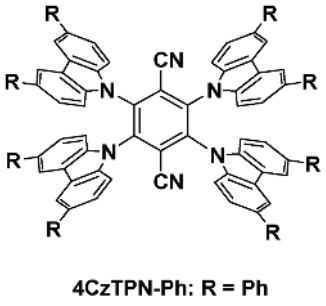

Figure 31. Chemical structure of **4CzTPN-Ph**.

2.5. TADF Macromolecules for OLED Applications

Macromolecules have a profound place in OLED history, and they form an important class of emitters.[131] The chief merits for the use of macromolecules are the capability of solution-processing the materials and their supreme morphological stability (i.e., high T_g). Given these important benefits, it is surprising that there are so few reports of TADF macromolecules (e.g., dendrimers and polymers).

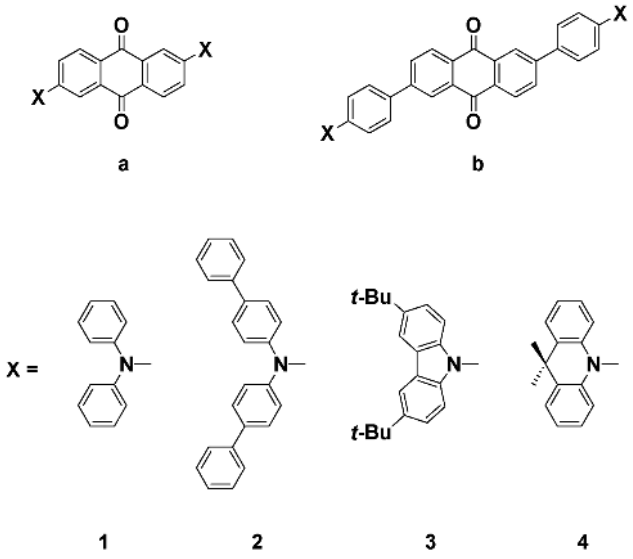

Figure 32. Chemical structure of anthraquinone-based orange-to-red TADF emitters.

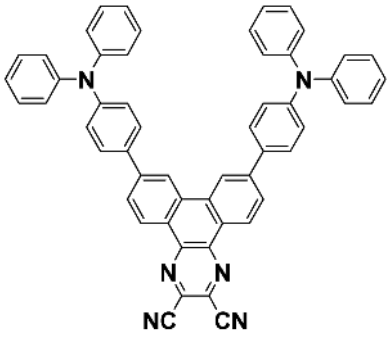

TPA-DCPP

Figure 33. Chemical structure of **TPA-DCPP**.

The first TADF macromolecule was reported by Albrecht et al.[69] who prepared a series of TADF dendrimers (**G2-4TAZ**, **Figure 39**) possessing a triazine acceptor core and carbazole donor dendrons, up to four generations. Neat films of **G2-4TAZ** show essentially the same emission profile (λ_{max}: ≈500 nm) and (ΔE_{ST}: 0.03–0.06 eV). However, the major difference among them is the emission efficiency of the neat film, where the PLQYs of **G2TAZ**, **G3TAZ** and **G4TAZ** are 52%, 31%, and 8.5%, respectively. The best nondoped and solution-processed device was obtained using **G3TAZ** (λ_{max}: ≈500 nm; PLQY: 31%; τ_d: 1.1, 4.7 µs neat film; ΔE_{ST}: 0.06 eV), which gave a green device with an EQE of 3.4% at CIE coordinates of (0.27, 0.49) (ITO/PEDOT:PSS/neat **emitter**/TPBI/Ca/Al). The device EQEs using these dendrimers can be explained by the trade-off between film-forming properties and PLQYs of their neat films. Higher-molecular-weight materials generally afford better spin-coated thin films, which is one of the main reasons for pursuing polymeric and dendritic materials. Thus, **G3TAZ** should possess better film-forming properties compared with **G2TAZ**, despite its lower PLQY. On the other hand, **G3TAZ** has a higher PLQY than **G4TAZ**, albeit with ostensibly poorer relative film-forming properties. Therefore, **G3TAZ** shows the best balance between

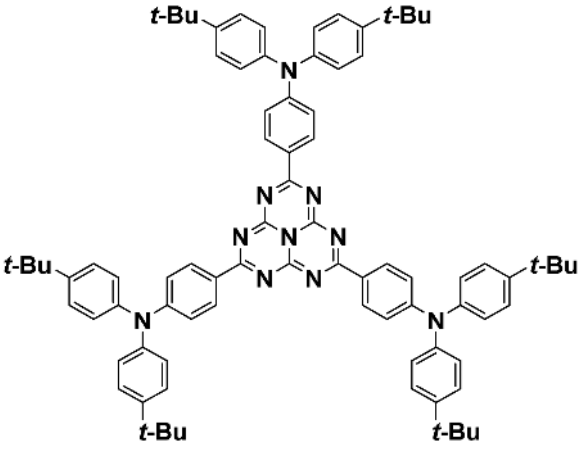

HAP-3TPA

Figure 34. Chemical structure of **HAP-3TPA**.

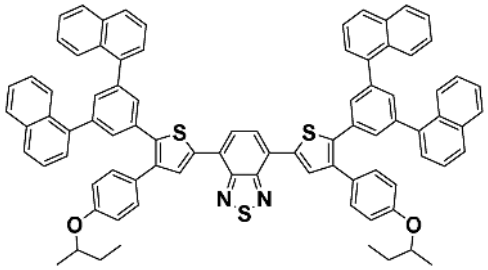

red-1b

Figure 35. Chemical structure of **red-1b**.

PLQY and film-forming properties and hence the highest device EQE among the series.

Nikolaenko et al.[126] reported the first TADF polymer **TP-AEN** (λ_{max}: ≈540 nm; PLQY: 44% in neat film; ΔE_{ST}: 0.22 eV) (**Figure 40**) for OLED applications. **TP-AEN** is made of 5 mol% triphenylamine donor, 50 mol% triazine acceptor, and 45 mol% backbone unit. Low doping of the donor helps to prevent its concentration quenching. Together with 50% high doping of the acceptor, the electron mobility of the polymer is preferentially enhanced to drive the recombination zone away from the cathode. The backbone unit, which consists of electronically insulating alkyl groups, limits an increase in conjugation length and thus avoids generating triplet traps in the polymer. The polymer was applied neat by solution-processing, and the device (ITO/PEDOT:PSS/interlayer/neat **polymer**/NaF/Al/Ag) achieved an EQE of 10.0% at CIE coordinates of (0.32, 0.58). However, it is worth noting that no physical characterization (e.g., NMR, IR, gel-permeation chromatography (GPC), etc.) was included in the report.

Luo et al.[89] then prepared a series of copolymers (**P0–P12**, **Figure 41**) by grafting a known TADF chromophore (**PXZ-OXD**, Figure 22)[86] unit onto the copolymer backbone. The best device employed **P12** (λ_{max}: 494 nm; PLQY: 34%; τ_d: 2.36 µs in neat film). The polymer was solution-processed as a neat emitting layer, which gave a device with an EQE of 4.3% at CIE coordinates of (0.24, 0.43) (ITO/PEDOT:PSS/poly-TPD/neat **polymer**/TmPyPB/Ba/Al) (poly-TPD = poly[*N*,*N*′-bis(4-butylphenyl)-*N*,*N*′-bisphenylbenzidine]).

Lee et al.[124] also reported a series of π-conjugated TADF polymers **pCzBP** (λ_{max}: 508 nm; PLQY: 23%; τ_d: 74 µs in 10 wt% TCTA:TAPC; ΔE_{ST}: 0.18 eV) and **pAcBP** (λ_{max}: 540 nm; PLQY: 46%; τ_d: 10 µs 10 wt% TCTA:TAPC; ΔE_{ST}: 0.10 eV) (**Figure 42**) based on benzophenone as the acceptor. Solution-processed devices (ITO/PEDOT:PSS/10 wt% **polymer**:TCTA:TAPC/TmPyPB/LiF/Al) using **pCzBP** and **pAcBP**, using TCTA and TAPC as host materials, afforded green and yellow devices with EQEs of 8.1% and 9.3% with CIE coordinates of (0.28, 0.43) and (0.38, 0.57) respectively.

Sun et al.[132] reported a solution-processed TADF device based on a crosslinked polymer design employing **DV-CDBP** (CDBP = 4,4′-bis(9-carbazolyl)-2,2′-dimethylbiphenyl) as a host-type monomer and **DV-MOS-DPS** as the emitter monomer, which is based on a well-known carbazole-diphenylsulfone architecture (**Figure 43**).[15c] Different mass ratios (6%, 9%, and 12%) of **DV-MOC-DPS** were included into the crosslinked polymer, and it was found that **P9** exhibited the highest PLQY

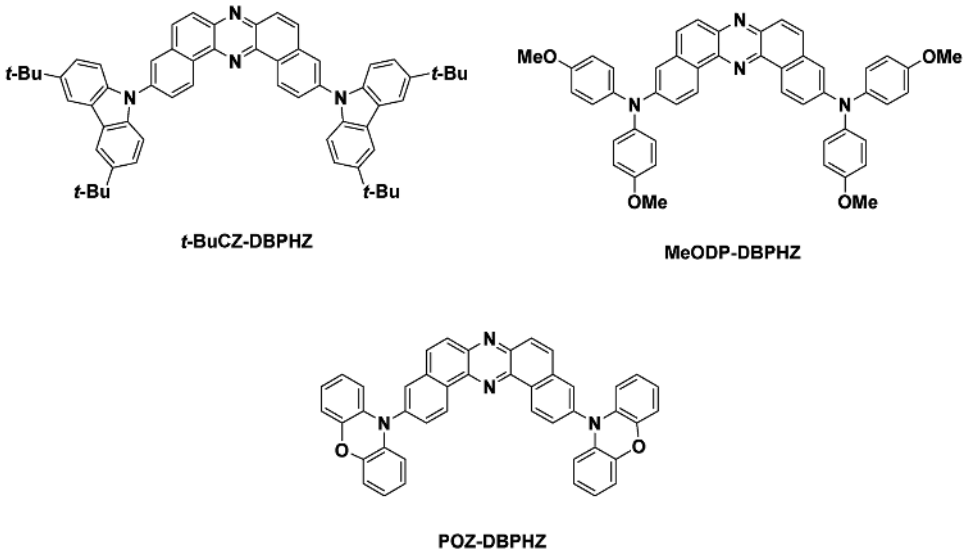

Figure 36. Chemical structures of dibenzo-[*a*,*j*]phenazine-based TADF emitters.

of 71%. The OLED device using **P9** (ITO/PEDOT:PSS/**emitter** neat/TPBi/$CsCO_3$/Al) gave an EQE of 2.0%.

2.6. TADF Emitters Exhibiting Aggregation-Induced Emission

Xu et al.[133] reported an asymmetric 4-carbazol-10-phenothiazine diphenyl sulfone, **CZSOPT** (λ_{max}: 518 nm; PLQY: 93%; τ_d: 1230 µs in neat film) (**Figure 44**) that exhibits simultaneously TADF, aggregation-induced emission (AIE), and mechanoluminescence (ML). The PLQY of the emitter is very high at 93.3%, but no device performance is reported. Lee et al.[47] reported a related asymmetric molecule, **PTSOPO** (λ_{max}: 418 nm; PLQY: 80%; τ_d: 6.2 µs as neat; ΔE_{ST}: 0.09 eV) (Figure 44), which shows both AIE and TADF. Both doped and nondoped devices (ITO/PEDOT:PSS/TAPC/mCP/30 wt% **emitter**:DPEPO or neat **emitter**/TSPO1/TPBI/LiF/Al) (TSPO1 = diphenyl-4-triphenylsilylphenyl-phosphine oxide) of **PTSOPO** gave high EQEs of 17.7% and 17.0%, respectively, with EL_{max} at ≈500 nm. The asymmetric structure is believed to suppress emission quenching caused by intermolecular stacking.[134] On the other hand, the symmetric analog, **PTSOPT** (Figure 44), has a much larger ΔE_{ST} of 0.41 eV and shows weak TADF. However, devices with **PTSOPT** also gave a similar EQE of ≈13%, which was ascribed to non-adiabatic coupling observed in D–A–D TADF molecular scaffolds.[43] The authors claimed that the nondoped device performance of **PTSOPT** is much poorer than that of **PTSOPO**.

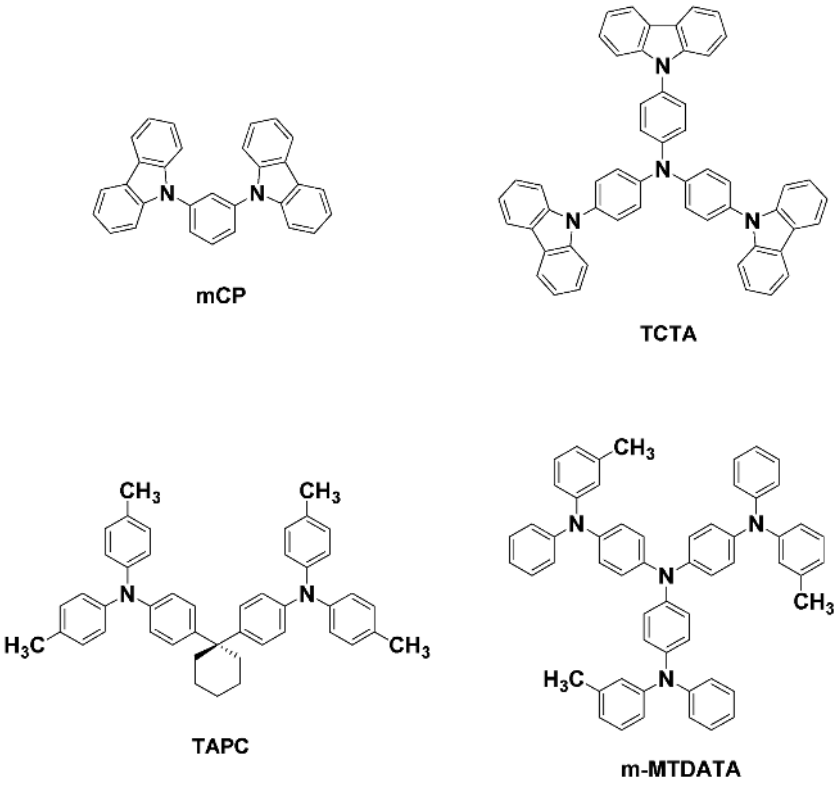

Figure 37. Chemical structures of donor materials used in TADF exciplexes.

3. White Organic Light-Emitting Diodes using TADF Emitters

White OLEDs (WOLEDs) can be fabricated by stacking multicomponent emitters of red, green, and blue colors. One common way of achieving this is to employ a high-energy fluorophore used together with low-energy phosphor, the so-called hybrid WOLED.[135] A single emitter with a broad emission spectrum can also be utilized for WOLEDs.[136]

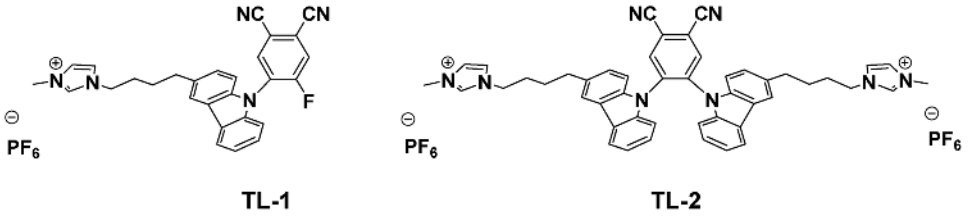

Figure 38. Chemical structure of **TL-1** and **TL-2** (cf. Figure 13).

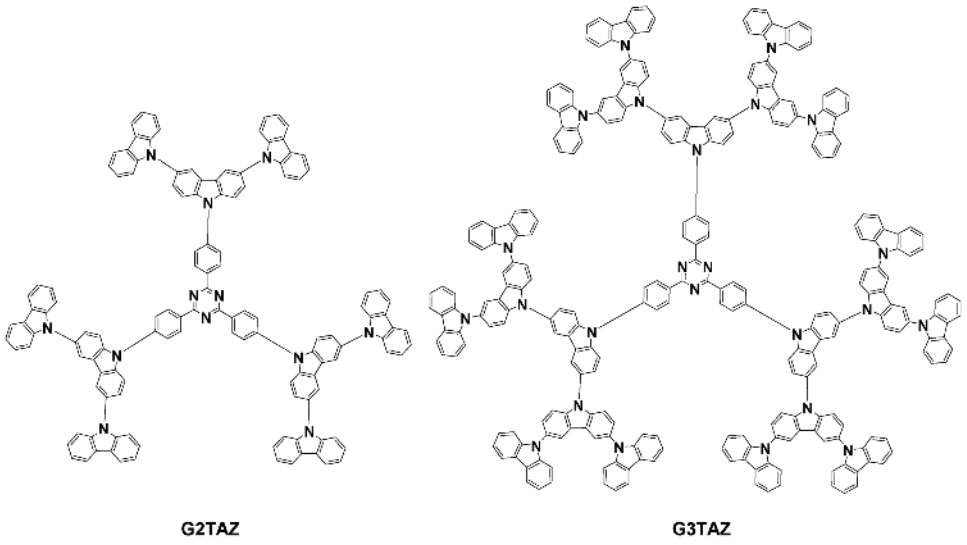

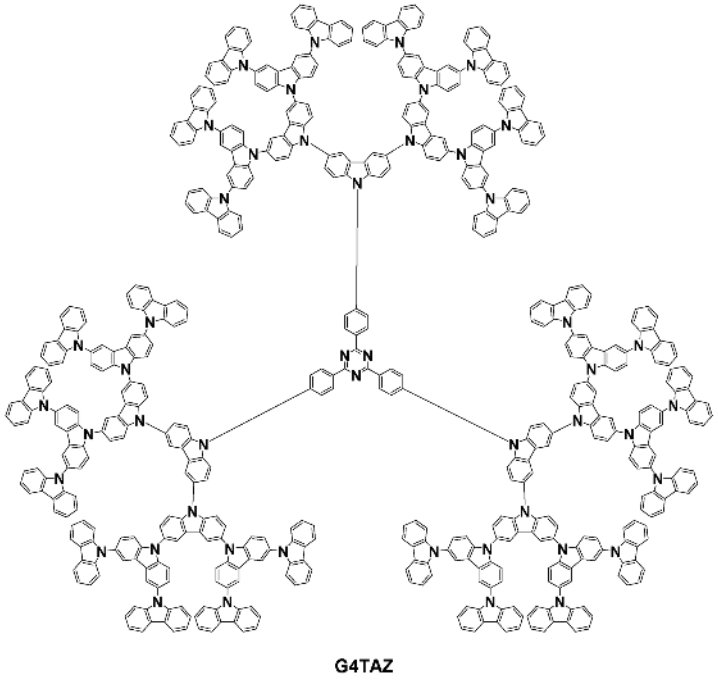

Figure 39. Chemical structure of **G2TAZ**, **G3TAZ**, and **G4TAZ**.

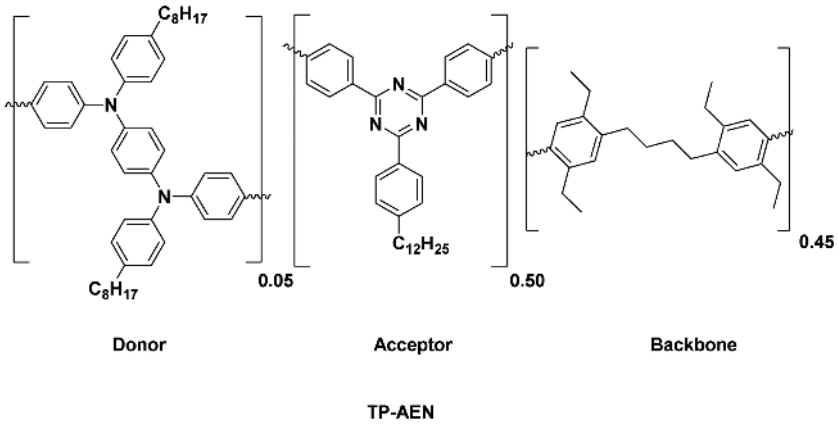

Figure 40. Chemical structure of TADF polymer **TP-AEN** reported by Nikolaenko et al.

When used as a lighting source, WOLEDs are more energy-efficient than compact fluorescent lighting technologies, and for this reason, much research effort has been devoted in this area.[135b,137] The following section will review the contribution of TADF in the area of WOLED development.

Adachi et al.[138] prepared an all-TADF WOLED that achieved an EQE of 17.1% with CIE coordinates of (0.30, 0.38) operating at 3.6 V. The emitters **3CzTRZ**, **4CzPN**, and **4CzTPN-Ph** were used as blue, green, and red TADF emitters, respectively, which form three adjacent stacked layers in the device. So far, this is the only all-TADF WOLED. However, it was discovered that each layer would be subjected to different degrees of exciton annihilation (e.g., singlet–triplet annihilation) because each TADF emitter has its own characteristic triplet exciton lifetime, mainly due to different k_{RISC} values based on their intrinsic ΔE_{ST}. As a result, a gradual EL spectral shift was observed upon increasing current density. More recently, the same group proposed the use of a blue TADF emitter (**DMAC-DPS**) stacked with an emitting layer of green and red conventional fluorescent emitters (**TTPA** and **DBP**, **Figure 45**) to fabricate a WOLED whose EQE reached 12.1% with CIE coordinates of (0.24, 0.31). The device unfortunately suffers from low operational stability (LT_{50} < 1 h) because of the poor electrochemical stability of the **DMAC-DPS** emitter.[139]

Zhang et al.[140] studied the quenching effect in mCP of the heavy-metal phosphors such as **Ir(ppz)$_3$**, **FIrpic**, **PO-01**, and **Pt(COD)Cl$_2$**, ranging from 0–25 wt% concentration on the emission of TADF fluorophores (**2CzPN** and ***t*-Bu$_4$CzTPN**) in WOLEDs (**Figure 46**). It was found that, while the conventional fluorophore (bis(10-hydroxybenzo[h] quinolinato)beryllium ($Bebq_2$)) emission was strongly suppressed due to enhanced ISC induced by the external heavy-atom effect, TADF emission was barely affected due to its unchanged k_{ISC} and enhanced k_{RISC}. Given the intrinsically high triplet energy of blue TADF fluorophores, phosphor emission is likewise not quenched by the blue TADF fluorophore. Therefore, mutual quenching between fluorophore and phosphor in TADF-based WOLEDs is effectively blocked. The authors used **2CzPN** and **PO-01** as a blue TADF fluorophore and a yellow phosphor (Figure 46), respectively, and achieved a WOLED of maximum forward EQE of 19.6% with CIE coordinates of (0.42, 0.48), far from pure white of (0.33, 0.33). The authors also prepared a single-emitting-layer hybrid WOLED in which the blue-emitting **DMAC-DPS** was used as a host for the **PO-01** phosphor dopant.[141] According to the authors, the rationale of this design was to minimize the short-range Dexter energy transfer from the host to the dopant, which requires triplet diffusion, a process associated with significant triplet loss. Instead, triplets on the TADF host can be upconverted to singlets via RISC followed by long-range Förster energy transfer to the dopant. Conventional fluorophore hosts are not able to fulfil this simply because they are unable to carry out RISC. The WOLED thus fabricated achieved a forward EQE of 20.8% with CIE coordinates of (0.40, 0.46). The efficiency roll-off of the device was small as well. Song and Lee[142] co-doped the same combination of emitters (**DMAC-DPS** and **PO-01**) into a **DPEPO** host, which formed the emitting layer in a WOLED device that achieved an EQE of 22.4% with CIE coordinates of (0.30, 0.37). The EL spectrum of the device was stable up to 5000 cd m^{-2}, which was

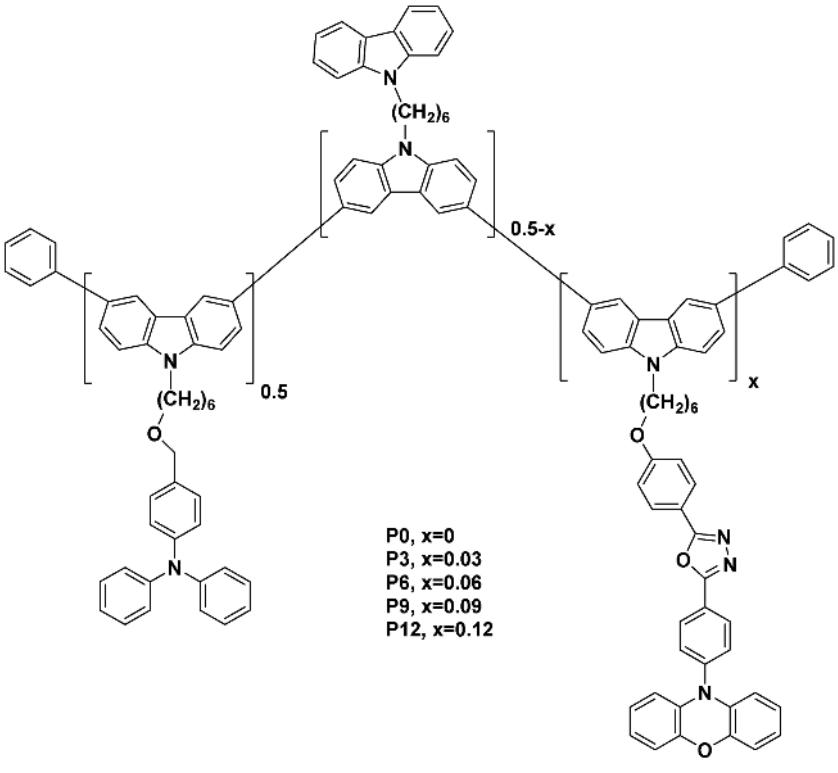

Figure 41. Chemical structure of TADF polymer **P0–P12**.

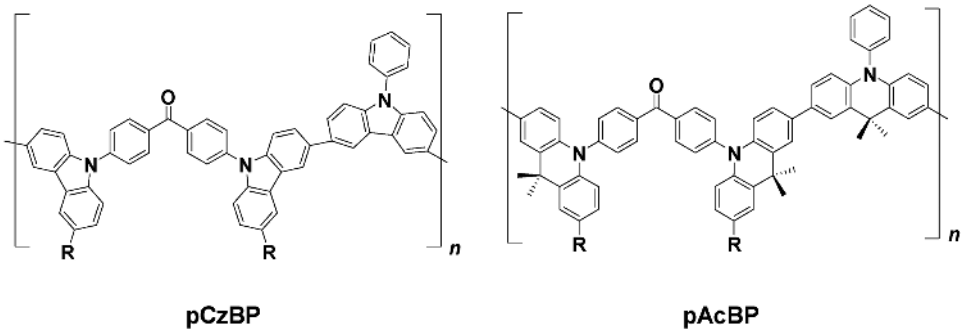

Figure 42. Chemical structure of TADF polymer **pCzBP** and **pAcBP**.

attributed to the energy transfer from **DMAC-DPS** to **PO-01** being implicated in the dominant emission mechanism. The group also prepared another WOLED by replacing the **PO-01** phosphor with a yellow **TBRb** fluorophore (Figure 46).[143] The device showed an EQE of 15.5% with CIE coordinates of (0.28, 0.35). It was important to maintain **TBRb** at very low doping concentration (0.05%) in order to minimize both its charge-trapping effect and Dexter energy transfer from the **DMAC-DPS** to **TBRb** as triplet excitons on **TBRb** cannot be upconverted to singlets for light emission. Efficient Förster energy transfer between **DMAC-DPS** and **TBRb** is an important condition for the operation of this device. Song et al.[134] prepared a single-emitting-layer WOLED in which a blue TADF emitter **CzAcSF** was used as the host for conventional blue (**TBPe**) and yellow (**TBRb**) fluorophores (Figure 46). Efficient energy transfer from the host to the dopant resulted in a WOLED with an EQE of 14.0% with CIE coordinates of (0.31, 0.37). Zhao et al. applied the blue TADF emitter **DMAC-DPS** as both emitter and host for the orange fluorophore **rubrene** to achieve a two-component WOLED (Figure 46).[144] The device showed an EQE of 7.48% with CIE coordinates of (0.36, 0.44).

Zhang et al.[145] prepared a WOLED by stacking blue (**2CzPN**:**mCP**) and yellow (**PO-01**:**TAZ**) emitting layers. Given that the exciton formation region lies at the interface between the two emitting layers, the TADF emitter **2CzPN** solves the traditional problem that the low triplet energy of the blue fluorophore (large ΔE_{ST} in conventional fluorophores) can quench the emission of the **PO-01** phosphor. The device demonstrated a forward EQE of 22.6% with CIE coordinates of (0.45, 0.48). Similarly, Meng et al.[146] fabricated a WOLED by stacking a yellow TADF emitting layer (**TXO-TPA**:**mCP**)[113] and blue fluorescent emitting layer (**4P-NPB**:**mCP**) to afford a WOLED with an EQE of 4.7% at (0.34, 0.34), very close to pure white emission. Cho et al.[87] reported an interesting device structure to achieve white light. They prepared a bespoke blue TADF emitter **DCzIPN** (Figure 20), which was used as both emitter and host for the yellow phosphor **PO-01** in their study. The blue-emitting layer (**DCzIPN**:**mCP**) and yellow-emitting layer (**PO-01**:**DCzIPN**) were stacked in the fashion of blue–yellow–blue, absent of any interlayer between them for white-light generation. By controlling the thickness of the central yellow-emitting layer, warm and cool white-light devices could be fabricated. The former displayed an EQE of 22.9% with CIE coordinates of (0.39, 0.43) and the latter showed an EQE of 21.0% with CIE coordinates of (0.31, 0.33). Kim and Lee[147] fabricated a WOLED using a green TADF emitter (**4CzIPN**) together with blue **FIrpic** and red **[Ir(pq)$_2$(acac)]** phosphors (**Figure 47**). They demonstrated that there are two possible device architectures to achieve white light. In one design, **4CzIPN** and **[Ir(pq)$_2$(acac)]** form an emitting layer, which is stacked with an **FIrpic** layer, whereas in another device architecture, a **4CzIPN** layer is stacked on a layer of **FIrpic** and an **[Ir(pq)$_2$acac]** layer, where their doping ratio is 5%:1% or 15%:1%. No interlayer was inserted between the two layers in both devices. EQE and CIE coordinates of 16.2% and (0.45, 0.47) and 18.0% and (0.37, 0.47) were achieved for the first and second device,

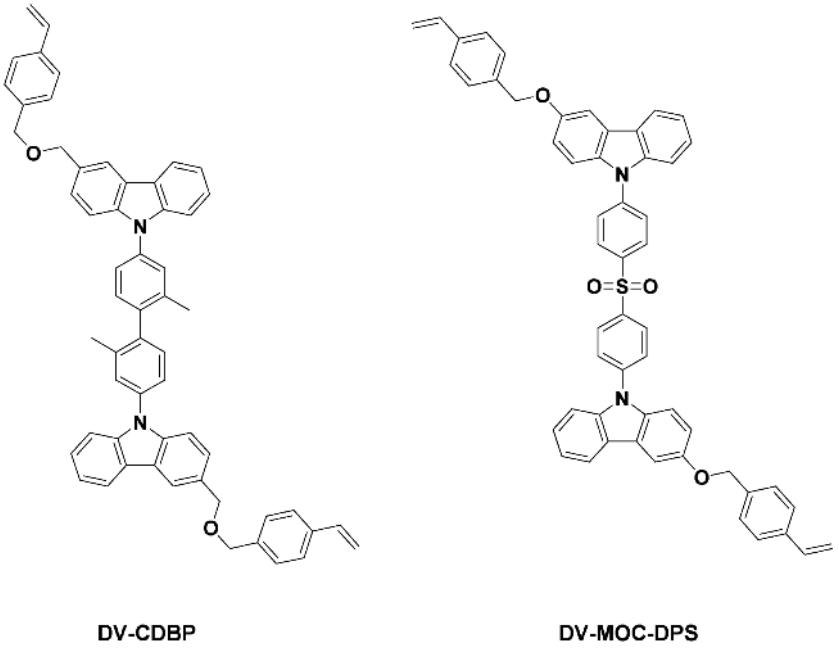

Figure 43. Chemical structure of thermally crosslinkable monomers **DV-CDBP** (as host) and **DV-MOS-DPS** (as TADF chromophore).

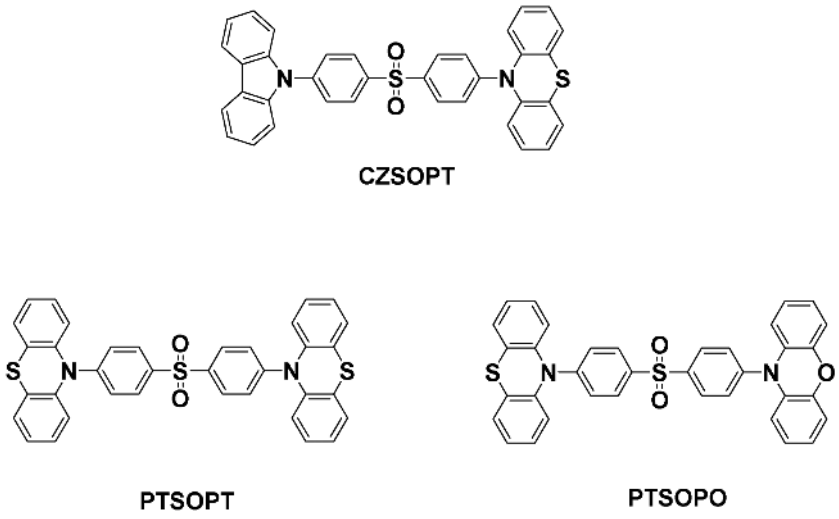

Figure 44. Chemical structures of **CZSOPT**, **PTSOPT**, and **PTSOPO**.

respectively. In another report by the same group, **4CzIPN** and **FIrpic** constituted one emitting layer stacked on a **[Ir(pq)$_2$acac]** layer.[148] The hybrid WOLED showed an EQE of 20.2% with CIE coordinates of (0.49, 0.41).

TADF exciplexes can also play an important role in WOLED development, where the donors and acceptors used are shown in **Figure 48** (see Section 6 for discussion of TADF exciplexes). In 2014, Hung et al.[149] reported the first all-exciplex TADF WOLED. With **mCP**:**PO-T2T** and **DTAF**:**PO-T2T** (PO-T2T = 2,4,6-tris[3-(diphenylphosphinyl)phenyl]-1,3,5-triazine; DTAF = 9,9-di[4-(di-*p*-tolyl)aminophenyl]fluorene) as blue- and yellow-emitting layers, respectively, stacked against each other in the device, white light was achieved with an EQE of 11.6% with CIE coordinates of (0.29, 0.35) and a color rendering index (CRI) of 70.6, device metrics of which are nearly independent of EL intensity. Zhao et al.[150] fabricated a WOLED based on blue (**TCTA**:**Bphen**) and orange (**TAPC**:**3P-T2T**) TADF exciplexes (3P-T2T = 2,4,6-tris(3-(1*H*-pyrazol-1-yl)phenyl)-1,3,5-triazine). The device showed an EQE of 9.17% with CIE coordinates of (0.41, 0.44) with only negligible shifting of the EL spectrum upon increasing voltage from 6 V to 14 V, which was attributed to balanced charge injection and transport of the exciplex layers. Liu et al.[151] employed a TADF exciplex formed between **CDBP** and **PO-T2T** as both blue emitter and host for green **[Ir(ppy)$_2$(acac)]** and red **[Ir(MDQ)$_2$(acac)]** phosphors to achieve a WOLED operating at 2.5 V that exhibited a forward-viewing EQE of 25.5% with CIE coordinates of (0.41, 0.45). The exciplex host again was shown to be beneficial in terms of balanced charge injection and transport.

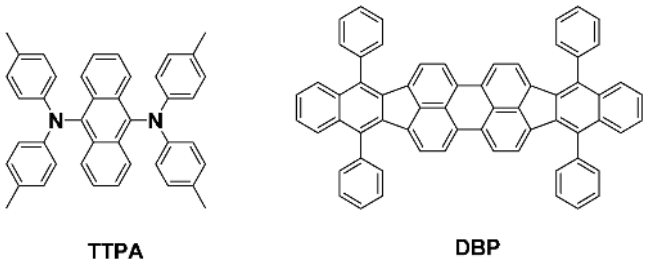

Figure 45. Chemical structures of **TTPA** and **DBP**.

4. Development of Host Materials for TADF Devices

In addition to the emitters for light emission, the development of host materials is also of prime importance.[152] In general, emitters are doped in a host material in the device to avoid self-quenching. There are a number of requirements for an effective host material. Firstly, the host should have a high triplet energy level to avoid back energy transfer from the dopant to the host so that the triplet excitons can be confined on the dopant for light emission. Secondly, the host should be chemically and thermally robust. Host molecules must show a large degree of electrochemical reversibility. They must not degrade when they are vacuum deposited during device fabrication. They should have a high glass-transition temperature (T_g) so that they stay amorphous during device operation when Joule heat is produced. Thirdly, the energy levels of the frontier molecular orbitals of the host should be in close alignment with the adjacent layers to ease charge injection. Fourthly, the charge mobility of the host materials has to be high and balanced so that the recombination zone can be widely dispersed within the emitting layer.[153] Finally, a host material of enhanced solubility can be exploited for solution-processed devices.[154] Therefore, the design of host materials for highly efficient OLED devices is, in many ways, as challenging as the TADF emitters themselves. In this section, we summarize the most commonly used host materials and review the recent developments of bespoke host materials for TADF OLEDs.

Currently, in the vast majority of cases, the OLEDs fabricated with a TADF dopant utilize traditional host materials. **Figure 49** shows the acronyms and structures of hosts material most commonly employed in the fabrication of TADF OLEDs while **Table 7** summarizes their electronic properties. The preference for these host materials is certainly based on their low cost, availability, and well-documented physical properties, with many precedents of the fabrication of high-performance phosphorescent and fluorescent OLEDs.

For blue TADF OLEDs, one of the most commonly used host materials is DPEPO.[15c,45,48,49,86,159] DPEPO benefits from a high triplet level (E_T: 2.995 eV),[156] which prevents undesirable energy transfer from the dopant to the host and, as asserted by Monkman and co-workers,[159] has high polarity, which contributes to a lowering of the energy of the ^{1}CT state so as to minimize the ΔE_{ST} (ΔE_{ST} in this compound is the gap between the ^{1}CT state and the lowest local ^{3}LE state). Representative examples of other hosts used for blue TADF OLEDs include mCP,[84,87] PPT,[15a,73] and SiCz.[76] For green TADF OLEDs, the most commonly used hosts are mCP[63,77,113] and mCBP.[107,117,119] CBP[15a,110] has also been used, suggesting back energy transfer from the dopant to the host is less prominent in green TADF devices, given that the triplet level of CBP (T_1: 2.6 eV) is significantly lower than mCP (T_1: 2.9 eV) and mCBP (T_1: 2.8 eV).[160] DPEPO has also been used in some green TADF devices.[72,86] CBP[15b,127] seems to be the most

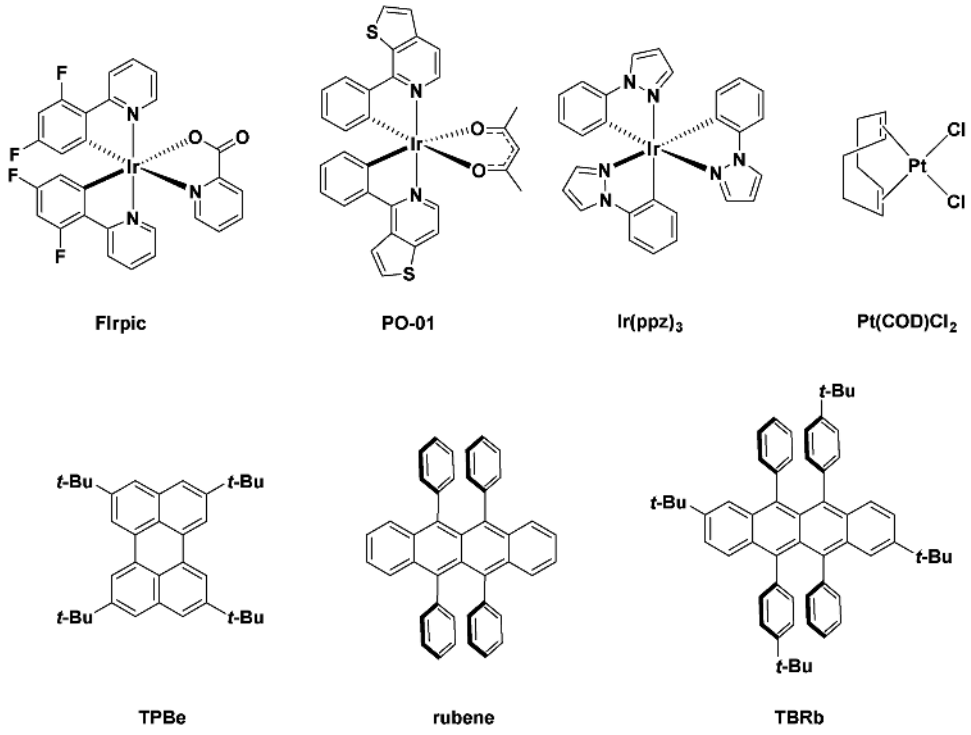

Figure 46. Chemical structures of **PO-01**, **Ir(ppz)$_3$**, **FIrpic**, **Pt(COD)Cl$_2$**, **TPBe**, **rubene**, and **TBRb**.

commonly used host for red TADF devices, while TPBI[128] and mCBP[16a] have also been employed as host materials.

The electronic properties of bespoke TADF compounds used as host materials in OLEDs are summarized in **Table 8**. Kim et al.[98c] employed 2,7-bis(diphenylphosphoryl)-9-phenyl-9*H*-carbazole (**PPO27**) as a bipolar host for **4CzIPN**, where the device achieved a maximum EQE of 24.2% (**Figure 50**). The TADF emitter interacted strongly with the **PPO27** host due to the latter's strong polarity. As a result, at high doping concentrations, a significant redshift in the EL spectrum was observed. Due to the poor stability of the **PPO27** host, the device lifetime was poor. Im et al.[98d] reported two bipolar hosts, **3TPAPFP** and **4TPAPFP**, which are based on a triphenylamine donor and a furodipyridine acceptor for balanced charge mobility. These functional groups have high triplet energy levels, which mitigates back energy transfer from the dopant to the host. However, **4TPAPFP** showed more pronounced intermolecular interactions with the **4CzIPN** dopant, which was attributed to the elongated shape of the host as a result of the *para* configuration of the ambipolar functional groups.[161] Energy transfer to **4CzIPN** was poor as a result. Thus, while a maximum EQE of 21.2% was achieved using **3TPAPFP** as the host, a much lower EQE of 6.6% was achieved in the case of **4TPAPFP** as the host. The same group prepared a carbazole analog, **3CzPFP**, as the host and achieved a significant enhancement in EQE up to 31.2% (Figure 50).[162] The enhancement in performance is due to the absence of exciplex formation in the emitting layer **3CzPFP**:**4CzIPN**, which is probably due to the deeper HOMO of the carbazole moiety in **3CzPFP** compared with triphenylamine in **3TPAPFP**. Gaj et al.[98e] employed an ambipolar host based on carbazole and diphenyl sulfone (**mCPSOB**) with **4CzIPN** as the emitter, and achieved an excellent EQE of 26.5% (Figure 50). The T_g of **mCPSOB** is 110 °C and the host forms a morphologically stable thin film to give high operational stability. Nishimoto et al. prepared an ambipolar **PzCz** host with a cyclophosphazene core decorated with six carbazole moieties (Figure 50).[160b] **PzCz** has a high triplet energy of 3.00 eV and thanks to its rigid, planar core it demonstrates excellent chemical and thermal stability. The 5% weight-loss decomposition temperature (T_d) is as high as 474 °C. No signal is observed for the glass transition, crystallization, or melting points by differential scanning calorimetry (DSC) measurements, yet the authors claimed the host material to be intrinsically amorphous. Devices using emitter layers (**PzCz**:**CzTPN**, blue–green) and (**PzCN**:**4CzIPN**, green) gave EQEs of 15.0% and 18.2%, respectively. Cho et al.[163] reported a universal ambipolar host **DCzDCN** for both TADF and phosphorescent devices. Using **4CzIPN** as the TADF dopant, they achieved a maximum EQE of 26.7% with much longer device lifetime (LT_{90} up to 200 h) compared with

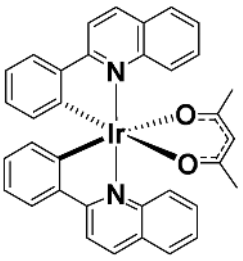

Figure 47. Chemical structure of complexe[**Ir(pq)$_2$(acac)**].

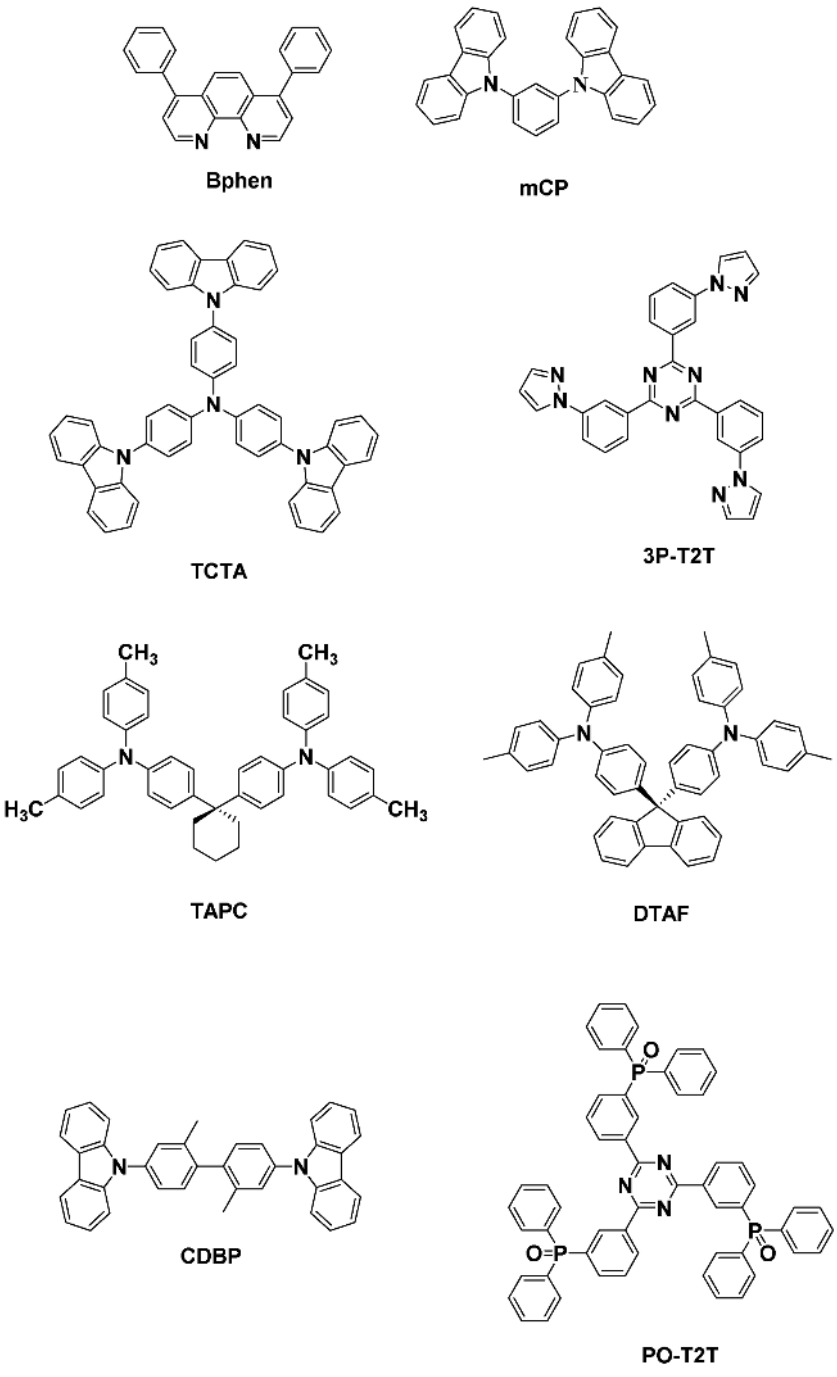

Figure 48. Chemical structures of commonly used donors and acceptors used in TADF exciplexes for WOLEDs.

that using **CBP** as the host (LT_{90}: 10.2 h). The enhanced stability was attributed to improved charge confinement, morphological stability, low singlet energy, and little charge accumulation at the interface. Suzuki et al.[164] prepared a solution-processable host **CPCB** and used it in conjunction with **4CzIPN** as the emitter. The device achieved a maximum EQE of 9.9%. **CPCB** solution-processed devices showed longer device half-lives (LT_{50} up to 184 h) compared with that using **CBP** as the host (LT_{50}: 56 h). This was attributed to the poor morphological stability of **CBP**, which crystallizes easily during device operation. Indeed, the glass-transition temperature (T_g) of **CPCB** (165 °C) is much higher than that of **CBP** (62 °C),[165] justifying the longer device lifetime. Cui et al.[98a] reported the first pure hydrocarbon (PHC) hosts, **SF33** and **SF34**, for TADF devices (Figure 50). PHC hosts are believed to have higher chemical stability than heteroatom-based analogs. By tuning the interconnection pattern, a greater twisting of the two spirofluorenes is obtained in **SF34**, resulting in greater ambipolar charge transport. An EQE of 22.3% was achieved when **SF34** was used as the host for **4CzIPN**. The efficiency roll-off is remarkably small, that the EQE drops only to 20.8% at 5000 cd m^{-2}, which is attributed to a short delayed component emission lifetime of **4CzIPN** in the **SF34** host. The device lifetime using **SF34** as the host (LT_{80}: 252.4 h) is approximately four times longer than that using **CBP** (LT_{80}: 61.5 h). Im et al.[98f] contrasted two hosts (**DBTTP1** and **DBTTP2**) for devices using **4CzIPN** as the TADF dopant (Figure 50). It was found that **DBTTP1** conferred higher device stability (LT_{80}: 250 h) than **DBTTP2** (LT_{80}: 100 h), and the authors attributed this to higher chemical stability of the host in which the planar triphenylene moiety has a great conjugation compared with the terphenyl group in the **DBTTP2** host. Li et al.[166] reported a highly twisted spirocyclic phosphine oxide host, **SFXSPO** (Figure 50), which prevents intermolecular interaction between host molecules and allows uniform dispersion of TADF dopants. Notably, **SFXSPO** could be used as a host for blue to red full-color TADF dopants, including a white device made of blue and yellow TADF dopants. The EQEs obtained using this host ranged from 13.9% to 22.5%. Notably, using **4CzPNPh**[15a] as the yellow TADF dopant, a record high EQE of 22.5% was obtained, much higher than the 9.9% EQE obtained using mCP as the host. Cui et al.[167] reported two benzimidazobenzothiazole-based hosts, **29Cz-BID-BT** and **39Cz-BID-BT**, (Figure 50). These hosts possessed high triplet energies (>3.0 eV) and favor ambipolar charge transport. Using **DMAC-TPZ** as a blue TADF dopant (10 wt%), the two hosts gave practically the same device EQEs (20.2–20.4%) (ITO/HAT-CN/TAPC/10 wt% **DMAC-TRZ**: **host**/TSPO1/TPBi/LiF/Al).

Lee et al.[98b] prepared a series of three novel ambipolar hosts (***o*CzB-2CN**, ***m*CzB-2CN**, and ***p*CzB-2CN**) based on carbazole and isophthalonitrile in order to probe the relationship between the donor-group regiochemistry and the device performance (**Figure 51**). Importantly, the triplet energies (E_T) are strongly affected by the regiochemistry. The E_T of *ortho*, *meta*, and *para* isomers were found to be 2.99 eV, 2.73 eV, and

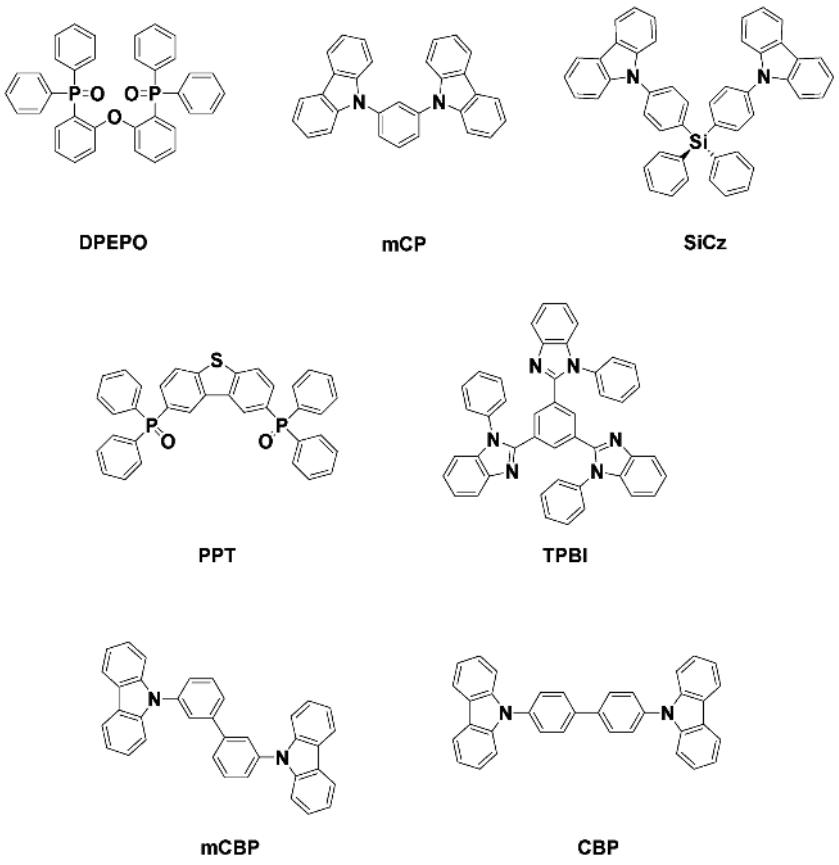

Figure 49. Chemical structures of traditional hosts used in TADF studies.

2.58 eV, respectively, which is due to: i) the steric hindrance between the carbazole and isophthalonitrile moieties for the *o*-isomer, and ii) the relative degree of conjugation in the hosts. The maximal current density was found in the device based on the *para* analog due to its better intermolecular orbital overlap with the dopant. However, the highest EQE of 26.0% in the study was obtained using **mCzB-2CN** because the PLQY of the **4CzIPN**:**mCzP-2CN** film is the highest. A similar study was carried out by Kim et al.[168] who studied the effect of interconnection pattern on the device performance by comparing two hosts, **3CN34BCz** and **4CN34BCz**.[169] The latter, in which the cyano group is installed *para* to the carbazole, is more capable of accommodating electron density than the *meta* analog. Thus, the charge transport is more balanced in the **4CN34BCz**:**4CzIPN** device, which achieved a maximum EQE of 20.8% compared with only 13.8% using **3CN34BCz** as the host. Li et al.[170] prepared four novel ambipolar hosts based on carbazole and pyrazole (***o*-CzDPz**, ***m*-CzDPz**, **3-CzDPz**, and ***m*CPDPz**) (Figure 51). The different interconnection patterns result in varying degrees of twisting of the conformations of the hosts, which thereby affect important properties such as triplet energies and charge mobility. In addition, the increase in n-type pyrazole to p-type carbazole ratio in **mCPDPz** enhances the host electron density in the device, resulting in improved charge balance. The best device performance in this study was achieved using **2CzPN**:**3-CzDPz** and **4CzIPN**:***o*-CPDPz** as the emitting layers, demonstrating EQEs of 15.8% and 13.7% respectively. Zhang et al.[171] reported an impressive true-blue TADF device by doping **DMAC-DPS** into a bespoke host **DPETPO** as the emitting layer, which showed excellent color purity at EL_{max} of 464 nm and CIE coordinates of (0.16, 0.21) (Figure 51). The EQE and power efficiency were 23.0% and 44.4 lm W^{-1}, respectively, with a small efficiency roll-off of 15% at 1000 cd m^{-2} and a small onset voltage of 2.8 V. Indeed, **DPETPO** is sophisticatedly designed such that the asymmetry of the molecule reduces the intermolecular packing. The central p-type diphenyl ether (DPE) core is partially exposed to achieve the best hole and electron mobility compared with analogs **DPEPO** and **DPEQPO**, which show maximal and minimal DPE exposure, respectively.

Table 7. Summary of electronic properties of traditional hosts designated for TADF emitters.

Host	HOMO [eV]	LUMO [eV]	E_T [eV]	T_d[a)] [°C]	Ref.
CBP	5.9	2.7	2.6	–	[153c]
TPBI	6.30	2.80	2.65	–	[155]
mCBP	5.60	2.13	2.8	–	[153c]
mCP	5.9	2.4	2.9	–	[153c]
DPEPO	6.53	2.48	3.00	322	[156]
PPT	6.6	2.9	3.0	–	[157]
SiCz	5.58	1.95	3.02	–	[158]

[a)]Temperature at 5 wt% loss.

The primary merit of the mixed host approach is balanced charge mobility due to the presence of both *p*-type and *n*-type components. Kim and Lee[172] used a mixed host **mCP**:**BmPyPb** for **4CzIPN** and achieved an excellent EQE_{max} of 28.6% (**Figure 52**). The authors pointed out the importance of a deep HOMO of the p-type component to prevent exciplex formation in the mixed host. Efficient mixed host systems require that the singlet energy of the mixed host should be high and emission should strongly overlap with the absorption spectrum of the TADF dopant to realize efficient Förster energy transfer. Later, the same group doped **4CzIPN** emitter in mixed hosts of **mCP**:**TSPO1** and **mCP**:**SPPO1** and achieved an EQE_{max} of 27.5% (Figure 52).[173] The latter host system gave a slightly more red-shifted emission spectrum because of stronger intermolecular interaction between the emitter in the excited state and the host molecules.

Table 9 summarizes the device performances using **4CzIPN** as the emitter in different hosts. The highest EQE reported is 31.2% using the bespoke host **3CzPFP**. Indeed, due to different device architectures and doping concentrations, a precise ranking of the hosts is not possible. However, there are some clear conclusions that can be drawn.

Table 8. Summary of electronic properties of bespoke hosts designated for TADF emitters.

Host	HOMO [eV]	LUMO [eV]	E_T [eV]	T_d[a)] [°C]	Ref.
pCzB-2CN	6.09	3.21	2.58	–	[98b]
4TPAPFP	5.88	2.98	2.63	–	[98d]
DBTTP1	5.84	2.21	2.64	–	[98f]
SF33	5.59	2.06	2.68	433	[98a]
DCzDCN	6.14	3.26	2.71	–	[163]
DBTTP2	6.33	2.72	2.71	–	[98f]
mCzB-2CN	6.07	3.18	2.73	–	[98b]
SF34	5.76	2.11	2.76	407	[98a]
mCPDPz	5.67	2.15	2.76	434	[170]
3-CzDPz	5.61	2.21	2.78	378	[170]
CPCB	6.2	2.9	2.79	500	[164]
PPO27	6.25	3.00	2.81	–	[98c]
3TPAPFP	5.90	3.02	2.82	–	[98d]
3CzPFP	6.08	3.06	2.82	–	[162]
m-CzDPz	5.63	2.13	2.83	350	[170]
DBTDPO	6.05	2.50	2.91	–	[175]
4CN34BCz	6.11	3.05	2.94	–	[169]
28DBSODPO	6.56	3.46	2.97	456	[175]
37DBSODPO	6.56	3.54	2.97	481	[175]
46DBSODPO	6.56	3.22	2.97	459	[175]
SFXSPO	6.52	2.61	2.97	>300	[166]
3CN34BCz	6.11	2.98	2.98	–	[168]
oCzB-2CN	6.15	3.13	2.99	–	[98b]
PzCz	6.4	2.5	3.00	474	[160b]
9CzFSPO	6.07	2.49	3.0	449	[178]
9CzFDPEPO	6.07	2.52	3.0	474	[178]
9CzFDPESPO	6.07	2.39	3.0	511	[178]
mCPSOB	5.8	2.5	3.02	–	[98e]
o-CzDPz	5.69	2.16	3.02	333	[170]
29Cz-BID-BT	6.01	6.07	3.02	–	[167]
39Cz-BID-BT	2.55	2.62	3.04	–	[167]
DPETPO	6.43	2.68	3.10	–	[171]
DPEQPO	6.50	2.83	3.10	–	[171]

[a)]Temperature at 5 wt% loss.

Firstly, a mixed host approach gives excellent device EQEs (27.5% and 28.6%), which are comparable to that of the device employing **3CzPFP**.[172,173] Secondly, in most cases, devices using bespoke hosts with tailored energy levels or mixed hosts display improved performance than devices that use a single traditional host (e.g., **CBP**).[15a] Finally, **CPCB** is the only solution-processed host among all those listed that contributes to a device with a decent EQE of 14.5%. Thus, solution-processable bespoke hosts for TADF emitters are currently still underexplored and deserve greater attention.

Cho et al.[174] carried out a study with the goal of designing the ideal combination of hosts and dopants in order to maximize device efficiency. They classified hosts and dopants each into two groups: common ones and TADF ones. They fabricated four types of devices: a common host with a common dopant; a common host with a TADF dopant; a TADF host and a common dopant; and a TADF host and a TADF dopant. It was found that the combination of a common host with a TADF dopant resulted in devices with the highest EQE, which was attributed to efficient energy transfer from the host to the dopant. In particular, singlet and triplet energies on the common host can be transferred to the TADF dopant by Förster and Dexter mechanisms, respectively. Together with efficient RISC occurring in the TADF dopant, very efficient emission was realized using this approach. It was also determined that, for all combinations, the best doping concentration was 1%, with significant drop in EQE even when the concentration was increased to 5%. On the other hand, Fan et al.[175] revealed the importance of compatible molecular configuration and polarity between the host and dopant. Both the blue TADF emitter **DMAC-DPS** and the host **DBTDPO** have similar V-shape molecular configurations and polarities (**Figure 53**). As a result, the thin film of the emitting layer (**DMAC-DPS**:**DBTDPO**) has a small root-mean-square (RMS) surface roughness of 0.25 nm. The authors found that device performance was improved by matching the molecular configuration and polarity of the electron-transporting layer with those of the host material in the emitting layer. Thus, **46DBSODPO** performs better than the **28DBSODPO** and **37DBSODPO** analogs for its similar shape compared to **DMTDPO** (Figure 53). The best blue TADF device reported in this work showed an EQE of 16.1%.

Komino et al.[176] studied the relationship between efficiency roll-off and the molecular orientation of the host. Deposition of the **CBP** host at high temperature (350 K) results in a random orientation of molecules with a corresponding 1.8-fold-lower hole mobility compared with the film deposited at 200 K where the **CBP** molecules are more ordered. Due to the lower hole mobility, the recombination zone of the emitting layer **CBP**:**4CzIPN** is shifted away from its interface with the electron-transporting layer, resulting in a decrease in the efficiency roll-off of 30%. The authors then reported the preferential horizontal orientation of a linearly shaped **PXZ-TRZ** (Figure 21) TADF emitter in an **mCBP** host by lowering the deposition temperature ($T_{deposition}$) at which the anisotropic molecular configuration is slower than the deposition rate.[177] The device using the more horizontally orientated **PXZ-TRZ** in **mCBP** ($T_{deposition}$ = 200 K) achieved an EQE of 11.9%, higher than that using a more vertically oriented **PXZ-TRZ** ($T_{deposition}$ = 300 K), where the EQE was 9.6%, this the result of an enhancement in the outcoupling efficiency.

Ding et al.[178] studied the effect of intergroup distance in host molecules (**9CzFSPO**, **9CzFDPEPO**, and **9CzFDPESPO**) on device performance (**Figure 54**). Despite their identical optical and charge-injection properties, the authors showed that a larger distance between the phosphine oxide and the carbazole moieties (**9CzFDPESPO**) results in a higher hole mobility. The device with the blue TADF **DMAC-DPS** in **9CzFDPESPO** gave the best EQE of 16.7%, compared with 13.2% and 12.2% using **9CzFDPEPO** and **9CzFSPO**, respectively.

Méhes et al.[179] carried out photophysical studies of the TADF emitter **ACRFLCN** (see Section 2.2) doped in a variety of traditional hosts such as **DPEPO** and **CzSi**, as well as **T2T**, and found that the choice of host can have a dramatic effect on the

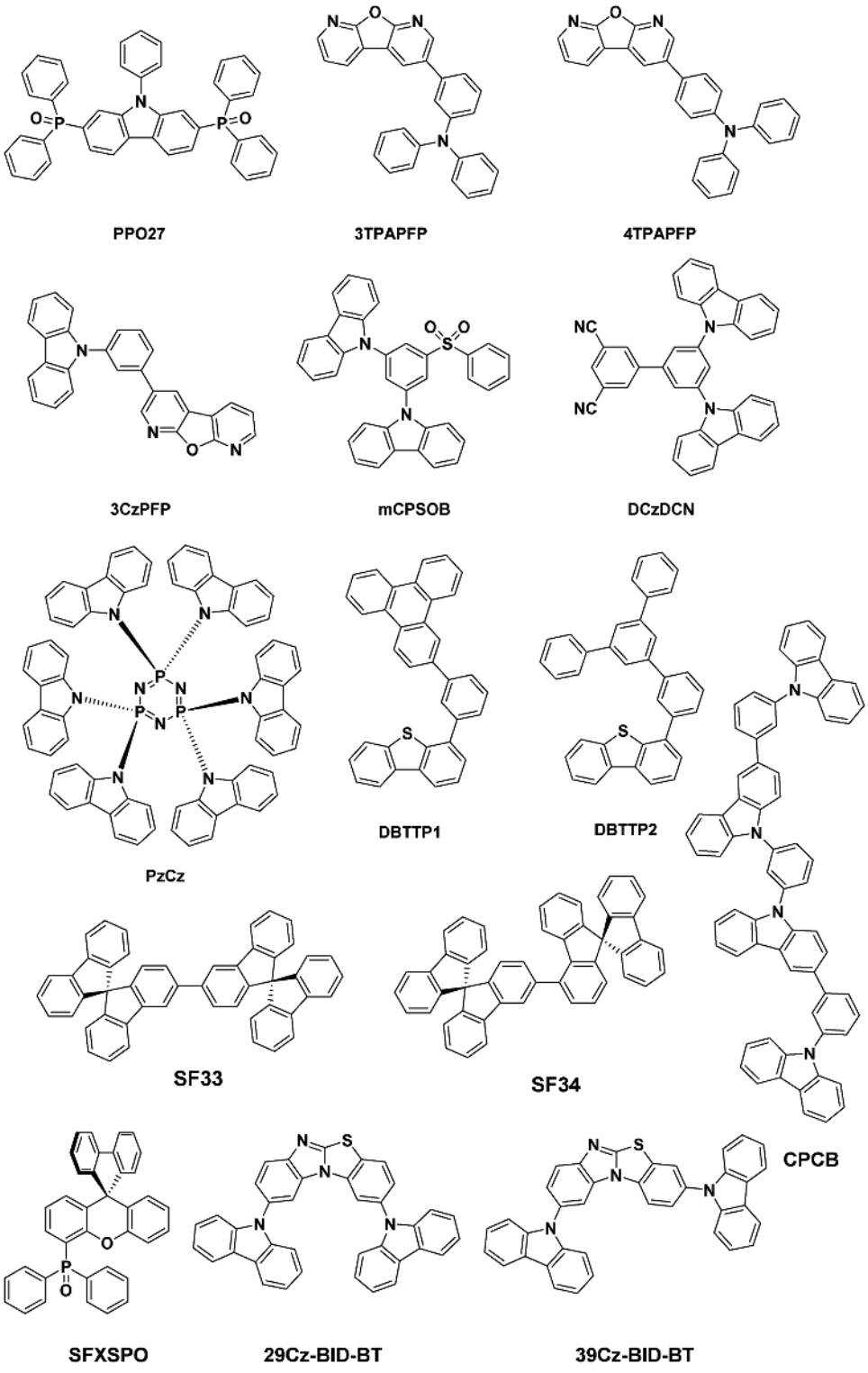

Figure 50. Chemical structures of bespoke hosts for TADF emitters.

PLQY (15% to 70%) and the magnitude of the delayed component of the emission lifetime (2–70 ms) of the TADF emitter **ACRFLCN**. The authors suggested avoiding exciplex formation between the host and dopant due to its more pronounced nonradiative decay. Interestingly, the study demonstrated that ΔE_{ST} is a time-dependent parameter after excitation, which is due to the dipole interaction between the host and the **ACRFLCN** emitter in the excited state. According to the authors, when

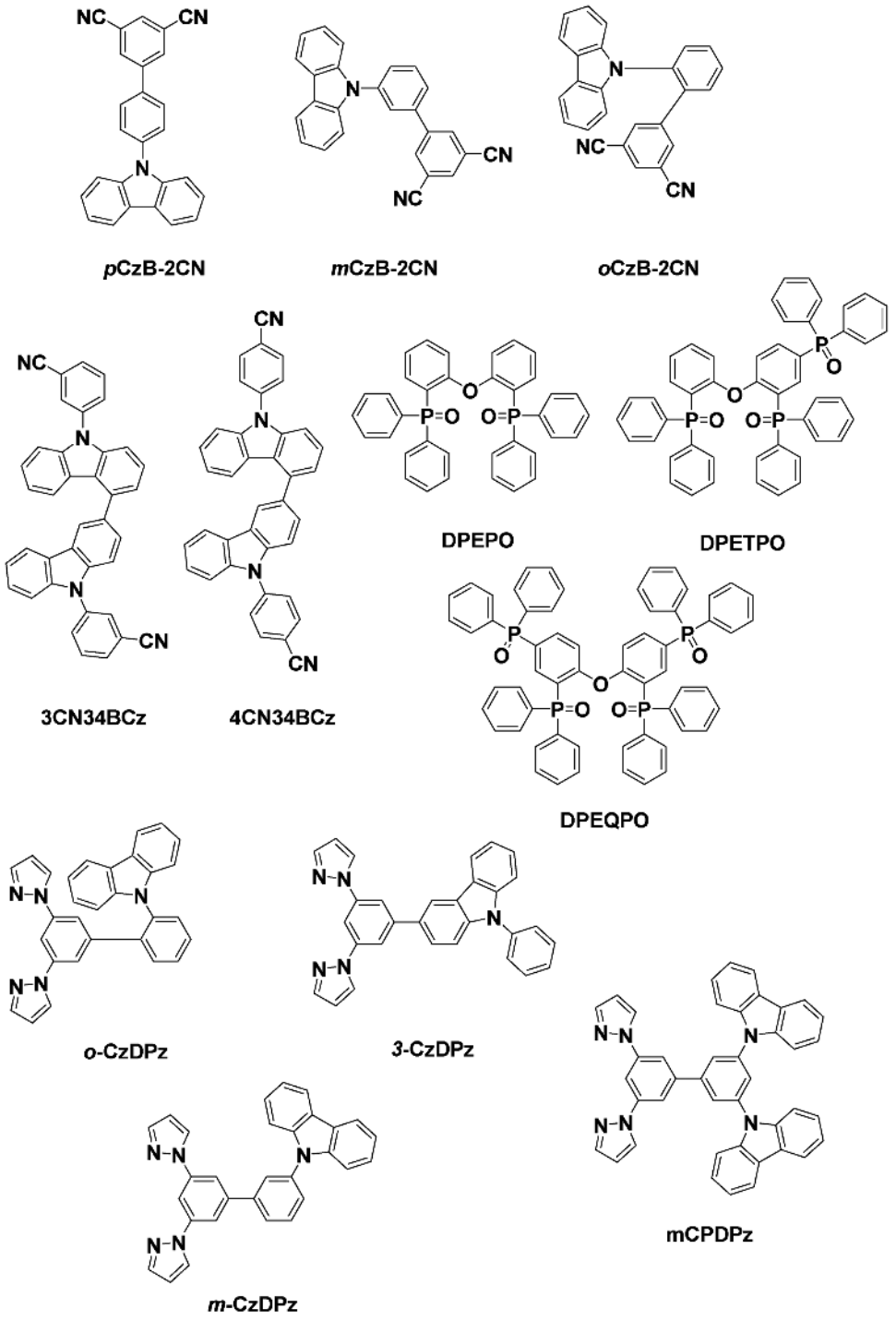

Figure 51. Chemical structures of bespoke hosts for TADF emitters.

ACRFLCN is excited, the population of ^{3}CT states increases such that the polar host molecules will orient to stabilize both highly polar ^{1}CT and ^{3}CT states: the former, being more polar, is stabilized to a greater extent. This results in an initial decrease in ΔE_{ST}, which is, by definition, the energy gap between the lowest singlet state (e.g., ^{1}CT state) and the lowest triplet state (e.g., ^{3}LE state that is a π–π^* state in nature). As the T_1 state is not a charge-transfer state, its energy will not be affected to the same degree as the CT states. As radiative decays occurs, the populations of both the ^{1}CT and ^{3}CT states will decrease, followed by a loss of host molecule orientation. Thus, the energy of both the ^{1}CT and ^{3}CT states will increase again, resulting in a subsequent blueshift in the emission spectrum and an increase in ΔE_{ST}.

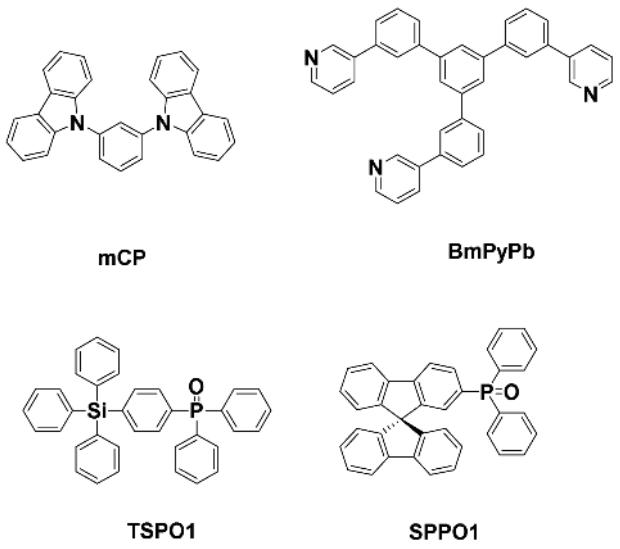

Figure 52. Chemical structures of materials used in a mixed host approach for TADF emitters.

5. TADF Emitters employed as Host Materials

Qiu et al.[180] employed a TADF material, **PIC-TRZ** (a.k.a. **PBICT**),[181] as the host for the well-known phosphor, ***fac*-[Ir(ppy)$_3$]**, and contrasted its device performances with those using the traditional host **CBP**. It was found that the TADF host permits a much lower doping concentration (3 wt%) of phosphor while achieving excellent device efficiency (EQE: 23.9%). Triplet excitons on the TADF host can be up-converted to singlets, which can then be transferred to **[Ir(ppy)$_3$]** by long-range Förster energy transfer, and thus, a low doping concentration (i.e., longer separation between host and dopant) can be tolerated. On the other hand, triplets on **CBP** cannot carry out RISC and can only transfer to the dopant via short-range Dexter energy transfer, and, therefore, under low doping concentration, the energy transfer is incomplete and loss occurs in the form of triplet–triplet annihilation. The device lifetime using **PBICT** as the host also showed less dependence on doping concentration, whereas the **CBP** device becomes less stable at low doping concentration because of the more pronounced interactions between **CBP** excitons and its positive polarons, given the incomplete energy transfer to the dopant. The same group also used this TADF-sensitized phosphorescence strategy to address the commonly observed problem of efficiency roll-off in TADF devices.[182] They noted that the roll-off is mainly caused by singlet–triplet annihilation (STA) and triplet–triplet annihilation (TTA), and therefore, the key to reducing the roll-off is to minimize the triplet density in the emitting layer. In devices where TADF dopants are used as the end-emitters, the triplet density is inevitably high due to the intrinsically low k_r of the singlet states (i.e., cycling between S_1 and T_1 occurs as k_{isc} competes with k_r). Their strategy involved making use of a high Förster resonance energy transfer rate (k_{FRET}) and efficient emission from the triplet state of the phosphor dopant to effectively remove the singlet excitons of the TADF host. The elegance of their design is that while k_r of the TADF emitter is an intrinsic parameter (i.e., cannot be altered), k_{FRET} can be easily tuned by varying the doping concentration. Zhang et al.[181] attempted to construct a fluorescent OLED using a TADF material as the host. They noted that while triplet excitons can be upconverted to singlets via RISC, the small exchange integral present in the TADF materials intrinsically results in a low k_r and thus a low PLQY. They used both **PIC-TRZ** and **DIC-TRZ** as the TADF host, which acted as a sensitizer for the fluorescent dopant **DDAF** (**Figure 55**). In these devices, the host is responsible for singlet harvesting via RISC, while the dopant is responsible for light emission. The host transfers its energy to the dopant via Förster energy transfer; Dexter energy transfer should be avoided because triplets on **DDAF** cannot undergo RISC. Thus, a doping concentration as low as 1 wt% was used in these devices. Interestingly, the device efficiencies achieved using **PIC-TRZ** and **DIC-TRZ** are very different (EQE: 4.5% and 11.7%,

Table 9. Comparison of OLED performances using 4CzIPN as TADF dopant using various host materials

Device Structure	V_{on} [V]	EQE/PE/CE[a)] [%/lm W^{-1}/cd A^{-1}]	Ref.
ITO/PEDOT:PSS/TAPC/mCP/1 wt% **4CzIPN**:**3CzPFP**/TSPO1/LiF/Al	–	31.2/–/–	[162]
ITO/PEDOT:PSS/TAPC/mCP/3 wt% **4CzIPN**:**mCP**:**BmPyPb**/TSPO1/LiF/Al	–	28.6/56.6/–	[172]
ITO/PEDOT:PSS/TAPC/mCP/3 wt% **4CzIPN**:**mCP**:**TSPO1**/TSPO1/LiF/Al	3.5	27.5/51.6/–	[173]
ITO/PEDOT:PSS/TAPC/mCP/3 wt% **4CzIPN**:**DCzDCN**/TSPO1/LiF/Al	–	26.7/–/–	[163]
ITO/MoO_3/Poly-TriCZ/5 wt% **4CzIPN**:**mCPSOB**/TPBi/LiF/Al	3.2	26.5/79/81	[98e]
ITO/PEDOT:PSS/TAPC/mCP/5 wt% **4CzIPN**:**mCzB-2CN**/TSPO1/LiF/Al	–	26.0/71.7/–	[98b]
ITO/PEDOT:PSS/TAPC/mCP/2 wt% **4CzIPN**:**PPO27**/TSPO1/LiF/Al	–	24.2/52.0/–	[98c]
ITO/HAT-CN/TAPC/8 wt% **4CzIPN**:**SF34**/TmPyPB/Liq/Al	2.8	22.3/51.5/69.0	[98a]
ITO/PEDOT:PSS/TAPC/1 wt% **4CzIPN**:**4CN34BCz**/TSPO1/LiF/Al	–	21.8/–/–	[169]
ITO/PEDOT:PSS/TAPC/mCP/1 wt% **4CzIPN**:**3TPAPFP**/TSPO1/LiF/Al	5.5	21.2/–/–	[98d]
ITO/PEDOT:PSS/TAPC/mCP/3 wt% **4CzIPN**:**DBTTP2**/TSPO1/TPBi/LiF/Al	4.0	20.0/–/–	[98f]
ITO/α-NPD/5 wt% **4CzIPN**:**CBP**/TPBi/LiF/Al	–	19.3/–/–	[15a]
ITO/PEDOT:PSS/6 wt% **4CzIPN**:**CPCB**/T2T/Bpy-TP2/LiF/Al	6.0	14.5/–/–	[164]
ITO/PEDOT:PSS/TAPC/5 wt% **4CzIPN**:***o*-CzDPz**/TmPyPB/LiF/Al	4.8	13.7/23.7/39.6	[170]

[a)]PE = power efficiency; CE = current efficiency.

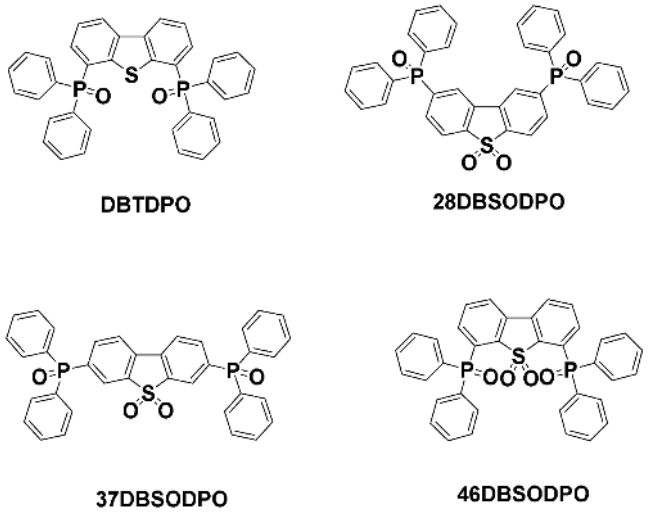

Figure 53. Chemical structures of **DBTDPO**, **28DBSODPO**, **37DBSODPO**, and **46DBSODPO**.

respectively). This is, in part, due to the smaller ΔE_{ST} of **DIC-TRZ** (0.06 eV). More importantly, as a result of the energy levels of the frontier molecular orbitals and charge-transporting abilities of the TADF hosts, charges are trapped on **DDAF** in the case of the device with **PIC-TRZ** as the host, whereas they reside on the host in the case of **DIC-TRZ**. Wang et al.[183] employed **4CzIPN** as the host for **C_4-DFQA** and **C_4-TCF$_3$QA** fluorophores and achieved a maximum EQE of 14.6%. Lee et al. (**Figure 56**).[90] used a co-host system consisting of a TADF emitter (**CzAcSF**) and **DPEPO** and combined it with the fluorophore **TBPe**: a maximum EQE of 18.1% was obtained.

Pertegás et al.[184] demonstrated an excellent host–guest system application in an LEEC using the TADF emitter **TL-2** (Figure 38) as an ambipolar host for a cyanine dye **S2108**

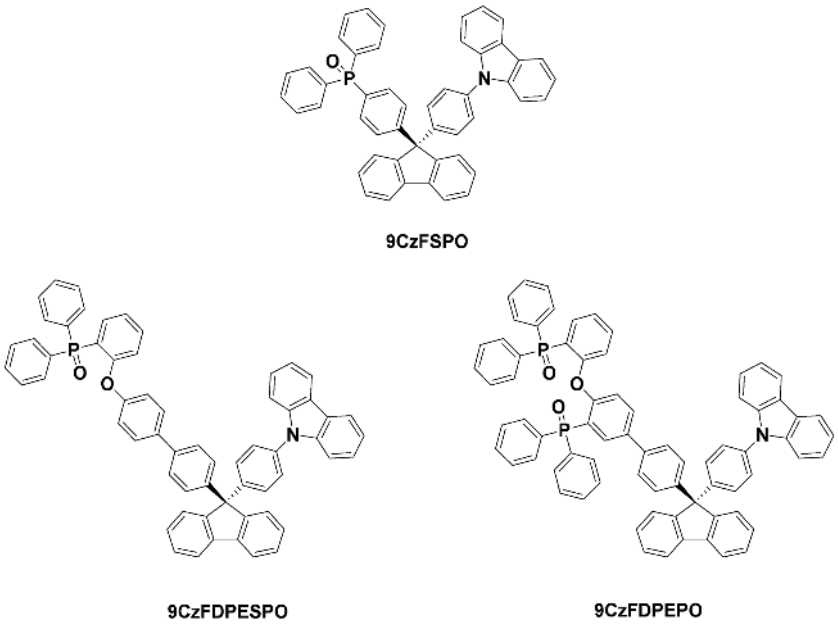

Figure 54. Chemical structures of **9CzFSPO**, **9CzFDPEPO**, and **9CzFDPESPO**.

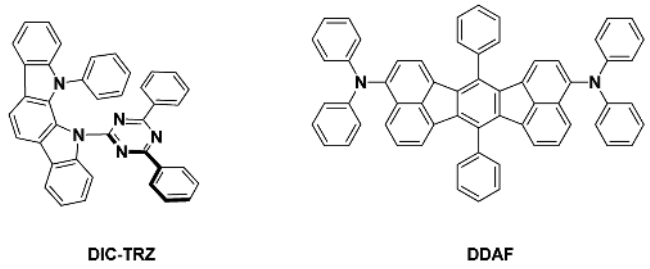

Figure 55. Chemical structures of **DDAF** and **DCI-TRZ**.

(**Figure 57**). By doping 0.1 wt% **S2108** in **TL-2** (which functions as the host) as the emitting layer in the LEEC, only emission from **S2108** was observed with a device EQE of 1.90%, which was nearly the maximum achievable value (2.20%) considering doped-thin-film PLQY (43.0%), singlet-exciton-generation yield (25%), and outcoupling efficiency (assumed to be 20%).

TADF materials can also be used as pseudo-hosts, a strategy that Adachi et al. coined as "hyperfluorescence", in which a combination of a host matrix (an ordinary host material) containing TADF materials (termed an "assistant dopant") and ordinary fluorescent materials (termed an "emitter dopant") are used as the emitting layer.[185] The assistant dopant is responsible for upconverting electrically generated triplets into singlets by RISC and then transferring this energy to the emitter dopant via an FRET mechanism. For example, an OLED device of structure ITO/α-NPD/1 wt% **TBRb**: 25 wt% **PXZ-TRZ**: mCBP/T2T/Alq_3/LiF/Al demonstrated an EQE of 18.0%, with emission originating from **TBRb** (Figure 46), which undoubtedly surpasses the theoretical limit of traditional fluorescent devices. Obviously, one important merit of a "hyperfluorescence" device is the emission color purity, as it is not of charge-transfer in nature. Apart from the high device efficiency and improved color purity, hyperfluorescent devices have also been demonstrated to have improved operational lifetimes, which is attributed to a more optimized position of the recombination zone within the device.

Liu et al.[186] developed the TADF compound **PrDPhAc** (ΔE_{ST}: 0.07 eV) and applied it as a host for red phosphors such as [**Ir(MDQ)$_2$(acac)**] (**Figure 58**). The OLED achieved an EQE of 25.8% with CIE coordinates of (0.61, 0.39), much higher than the 12.4% EQE reported[187] when using CBP as host. Unfortunately, the use of **PrDPhAc** as the TADF emitter in an OLED was not investigated.

6. TADF Exciplexes

While emitters of a single chemical entity are the "norm" for light generation, exciplexes, which are based on the electronic coupling of two distinct donor and acceptor molecules, can also be an important class of emitting materials employed in OLED devices.

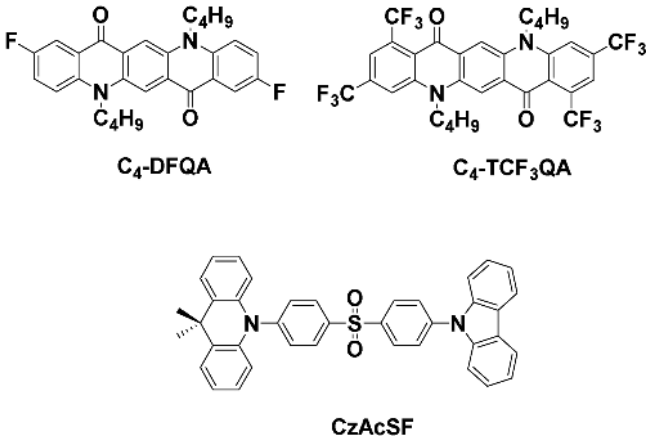

Figure 56. Chemical structures of **C_4-DFQA**, **C_4-TCF_3QA**, and **CzAcSF**.

Holes and electrons reside on the donor and acceptor, respectively, followed by radiative relaxation, which involves the two molecules. The advantages of using exciplexes for light emission include: i) facile control of emission colors based on the energy levels of the frontier molecular orbitals of the donor and acceptor,[188] and ii) the intrinsic ambipolar charge-transporting characteristics, which can contribute to a simplified device architecture.[135c,188b] In this section, the recent developments of exciplex systems that demonstrate upconversion of triplet states by TADF is reviewed.

The first TADF exciplex was reported by Adachi et al. in 2012.[189] They compared two types of TADF exciplexes **m-MTDATA**:***t*Bu-PBD** (*t*Bu-PBD = 2-(4-*tert*-butylphenyl)-5-(4-biphenylyl)-1,3,4-oxadiazole) and **m-MTDATA**:**3TPYMB** (Figure 37 and **Figure 59**). The latter showed a higher device EQE of 5.4% with a EL_{max} at ≈550 nm in the green region, although the PLQY of the **m-MTDATA**:**3TPYMB** film was only 26%. The same group studied a green TADF exciplex consisting of **m-MTDATA** and **PPT** and achieved an EQE of 10.0% with EL_{max} at ≈520 nm.[190] The authors demonstrated that, when the concentration of the donor (**m-MTDATA**) is sufficiently high (70 mol%), the triplet excitons on the exciplex can be lost to the donor, resulting in lower device efficiency. The device, based on an **mCP**:**HAP-3MF** exciplex, showed green emission with an EQE of 11.3%, with EL_{max} at ≈540 nm.[191] This work is the first report of an exciplex based on a heptaazaphenalene-derived acceptor for OLED devices. Zhang et al.[192] studied TADF exciplex systems between **m-MTDATA** and **BPhen** or **TPBi**. The best result was obtained using the **m-MTDATA**:**BPhen** exciplex system, where the green device

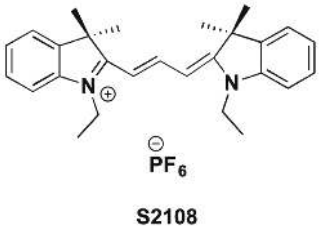

Figure 57. Chemical structure of cyanine dye **S2108**.

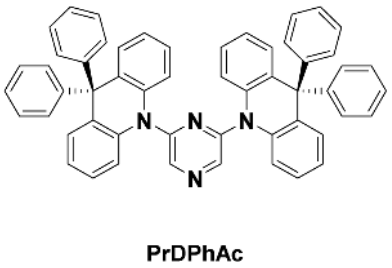

Figure 58. Chemical structure of **PrDPhAc**.

showed an EQE of 7.79% with EL_{max} at ≈550 nm. Such a high efficiency is due to the near-zero ΔE_{ST} of the exciplex system, where there is very efficient RISC. However, the efficiency roll-off was found to be as high as 41% at 100 mA cm^{-2}, which was attributed to imbalanced charge in the exciplex-emitting layer leading to singlet and triplet excitons in the exciplex being quenched by polarons. The group then compared a series of three TADF exciplexes between **mCP** as the donor and three different acceptors (**TBPi**, **BPhen**, and **3PT2T**).[193] However, the efficiencies of these violet-to-sky-blue devices are poor (EQEs: 0.57–2.23%). The authors proposed, based on theoretical calculations, that the HOMO of **mCP** is mainly located on the peripheral carbazole moiety whose planar structure inhibits the spin flip required for RISC to occur. When the blue exciplex **mCP**:**3PT2T** was used as a host for yellow phosphor **[$Ir(bt)_2$(acac)]** with a high doping concentration (4.0 wt%), enhanced charge trapping by the dopant occurred and no emission from the exciplex was observed. Zhang et al.[194] employed a TADF exciplex, **TCTA**:**Tm3PyBPZ** (Tm3PyBPZ = 2,4,6-tris(3′-(pyridin-3-yl)biphenyl-3-yl)-1,3,5-triazine), as the emitting layer to fabricate a green device with EL_{max} at 528 nm and EQE of 13.1% with a very low operating voltage of 2.4 V. Park et al.[195] employed a related TADF exciplex **TCTA**:**B3PYMPM** in a bluish-green device (EL_{max} at ≈500 nm) whose EQE increased from 3.1% to 10% when the temperature decreased from room temperature to 35 K. This is because the PLQY of the exciplex is maximized (99%) at 35 K. Interestingly, the delayed emission becomes more dominant at 35 K compared with room temperature, due to the exceedingly low nonradiative losses of exciplex singlets and triplets at this lower temperature, while maintaining efficient RISC. Liu et al.[196] fabricated a TADF OLED based on the exciplex **TAPC**:**DPTPCz**, which has a very low ΔE_{ST} of 47 meV and a high PLQY of 68%. The green device showed an EQE of 15.4% with CIE coordinates of (0.27, 0.52). The authors pointed out that the emission energy of the exciplex can be conveniently estimated from solution electrochemical measurements. For efficient RISC to occur, it is also of prime importance that the E_T of individual components be higher than the exciplex emission energy.

The same group also reported the first example of using a TADF exciplex (**TAPC**:**DPTPCz**) as a host for sensitizing a conventional fluorescent emitter (**C545T**).[197] Given that RISC is not prevalent in **C545T**, the HOMO and LUMO of the **TAPC**:**DPTPCz** exciplex system must be comparable to those of **C545T** in order to avoid charge trapping by the dopant. In the study, the doping concentration was kept at very low level (1 wt%) to avoid undesirable Dexter energy transfer to **C545T**

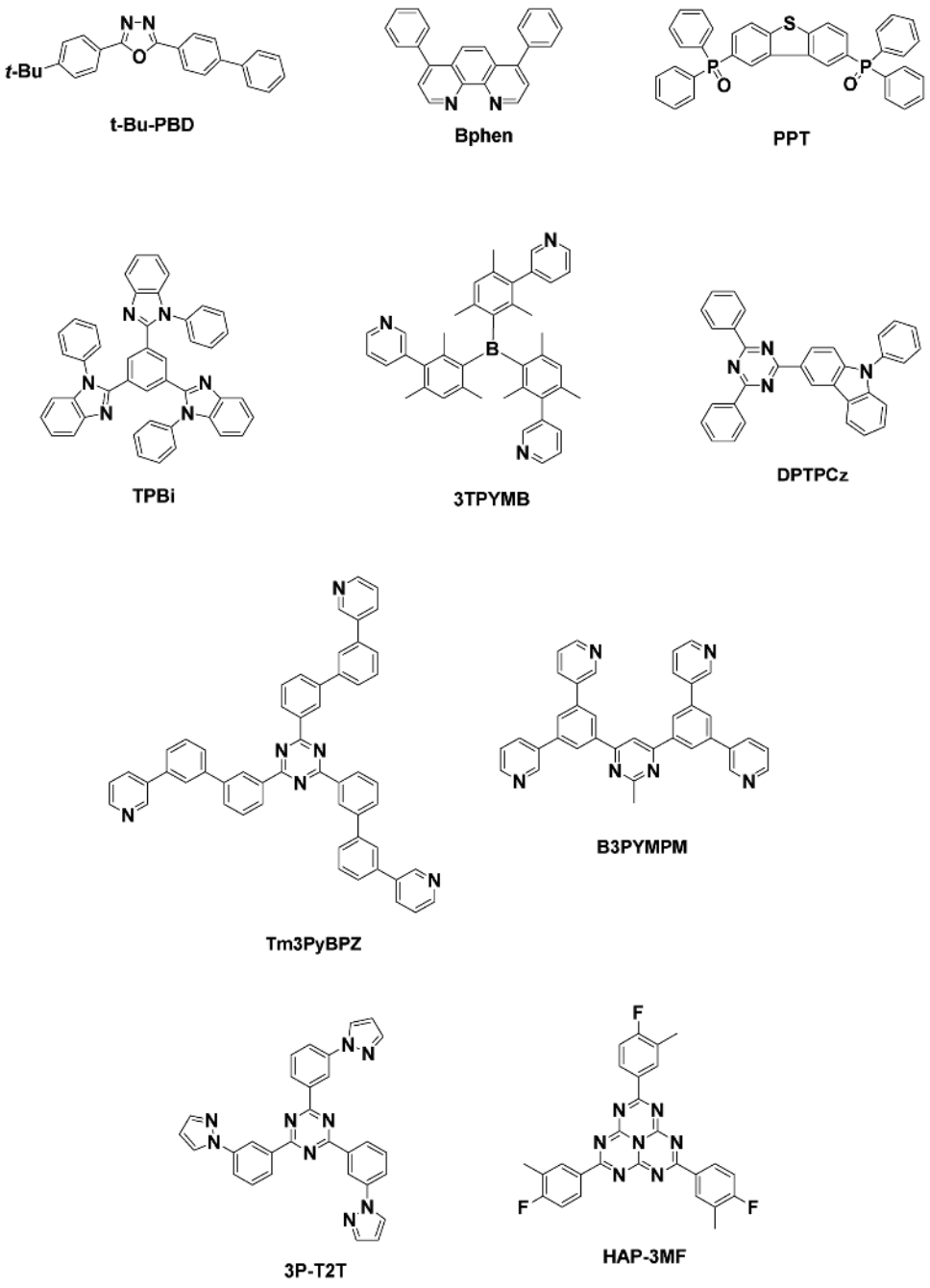

Figure 59. Chemical structures of acceptor materials used in TADF exciplexes.

from the exciplex, where it would then only nonradiatively decay. Thanks to nearly 100% triplet recruitment, the EQE of the device was 14.5% with an operating voltage at 2.8 V. A similar approach was reported by Zhao et al.[198] who used the TADF exciplex **TCTA**:**3P-T2T** as a host for a red conventional fluorescent emitter **DCJTB**. The device showed an EQE of 10.2%, which is, to date, the highest among devices based on the use of TADF exciplex host and one of conventional red emitters or phosphors **[Ir(piq)$_3$]** in a **CBP** host.

Graves et al.[199] carried out a photophysical study on a 50:50 blend exciplex between **m-MTDATA** and **PBD** (a.k.a. "***t*Bu-PBD**"). From the PL transient decay curve, the lifetime of the TADF component is on the order of 100 ns, which corresponds to a ΔE_{ST} as small as 5 meV, a value that is far smaller than 50 meV obtained from the initial study by Adachi et al.[189] The authors explained that **m-MTDATA** excimer emission was overlooked in the prior study, which exhibits emission at room temperature 1–30 µs after excitation (τ_e = 5800 ns), which contributes to a convolution of the emission processes. Because the **m-MTDATA**:**PBD** exciplex is not an efficient emitting system, whose PL_{max} is at 550 nm, no device was fabricated in their work. Hontz et al.[200] discovered an interesting finding from a

photophysics study on a 1:1 blend of **m-MTDATA** and photoluminescence of the exciplex, they observed there was no MFE on a short time-scale (<100 ns), while there was a strong MFE observed at longer time scales (positive for 100 ns to 1 µs and negative for 5–30 µs). By establishing a quantum-mechanical rate model, the authors concluded that the TADF process observed in this exciplex system is dynamic in nature. While, initially, the ΔE_{ST} is so large that MFE is unable to influence the rate of singlet-triplet interconversion, the hole and electron on the exciplex soon separate beyond the exchange radius (≈1 nm), resulting in a decrease in ΔE_{ST} and efficient RISC by hyperfine coupling. The hole and electron finally recombine to form an emissive singlet. It was estimated that about 30% of RISC is carried out by this "indirect" path.

Hung et al.[201] reported a bilayer interfacial TADF exciplex employed in an OLED device. Yellow emission was generated between two adjacent layers of **TCTA** and **3P-T2T**. Thanks to the excellent and balanced charge mobility of the exciplex components, together with the large energy-level offset (0.8 eV) of the **TCTA/3P-T2T** interface, the device showed an EQE of 7.7% with CIE coordinates of (0.40, 0.55). There have been no other reports of interfacial TADF exciplex applications in OLED devices apart from this work.

7. Conclusions and Outlook

It is exciting and gratifying to witness OLED devices based on purely organic TADF emitters that show performance metrics comparable, and in some cases improved upon, compared to the current state-of-the-art organometallic complexes. What is particularly surprising is the rate of development of and increased interest in TADF emitters since Adachi's seminal *Nature* paper in 2012. However, we believe that there is still much to learn with respect to understanding the intricacies of the TADF mechanism and to developing TADF materials that exhibit improved performance in EL devices, particularly in the following areas:

i) Mechanism of TADF

While it is generally agreed that ΔE_{ST} is an important factor that governs the efficiency of TADF, it presupposes that the singlet-harvesting process is the result of a RISC from T_1 to S_1. Other pathways have been proposed in the literature. For example, the presence of "hidden" $^3n\pi^*$ states[42] and non-adiabatic effects between excited states[43] have been proposed by different research groups to explain the efficient RISC process in diphenylsulfone-based blue TADF emitters with rather large ΔE_{ST} (>0.3 eV). The TADF process has been proposed to be induced by spin–orbit coupling (SOC) or hyperfine coupling (HFC) in certain cases.[24] Some researchers have suggested that ΔE_{ST} is a dynamic property, which can change during the timeframe of the emission decay.[179] Access to higher energy triplet states through reverse internal conversion (RIC) followed by RISC renders ΔE_{ST} a less accurate indicator of singlet-harvesting efficiency as access to the singlet excited state does not occur directly through a T_1–S_1 RISC pathway. In each of these frameworks, the photophysics of the emitter are discussed without taking the conformational flexibility within the molecule into account. Each conformer will possess an associated set of HOMO and LUMO energy levels, as well as different singlet and triplet excited-state energies. The experimental spectroscopic picture produced is an aggregate of the photophysics of each of these conformers, which complicates analysis. Clearly, there is still much research to be done to comprehend the detailed nature of the TADF mechanism.

ii) Lifetime of TADF EL devices

We note that TADF EL device lifetime data are seriously underreported. We can find only six cases out of more than 140 TADF emitters where their device lifetimes have been disclosed.[46,53,99d,120,202] Indeed, it is probably fair to state that the reported device architectures have been designed to optimize efficiency and not stability, despite the fact that device stability is an essential factor for the marketability of this technology. Gratifyingly, a recent report by Tsang and Adachi demonstrated a device lifetime (LT_{95}) of 1315 h under 1000 cd m^{-2} operation, which is comparable to existing green phosphorescent OLEDs.[99d] Designing similarly stable blue and red (and white) TADF OLEDs remains a challenge.

iii) Fabrication cost of TADF OLEDs

The fabrication cost of TADF OLEDs also plays a critical role in their marketability, particularly in the context of their use in lighting. Simplified device architecture and solution-processing are two major approaches to cut fabrication costs. A focus on the development of suitable small-molecule, polymeric, and dendrimeric TADF emitters for solution-processable devices possessing comparable performance metrics is strongly desired.

iv) Emission energy of TADF emitters

There are now ample examples of high performance green and yellow emitters, and a large number of blue emitters. There remains a dearth of deep-red TADF emitters and, for other applications such as telecommunications, a need for near-IR emitters.

v) Consistency in the reporting of the optoelectronic properties of emitters

There needs to be a commonly accepted protocol for determining the optoelectronic properties of TADF emitters. As an example, ΔE_{ST} is determined by a number of different methods that may not necessarily provide the same value. These include: extrapolation from an Arrhenius plot of variable-temperature emission data; estimating the singlet and triplet energies from room and low-temperature measurements (either as their λ_{max} values or by determining their emission onset); and determining the ΔE_{ST} from time-resolved emission spectroscopy (TRES). Likewise, the reporting of methodology for evaluating emission lifetimes, particularly the delayed fluorescence lifetime, is frequently absent. It is mechanistically important to

know, for instance, whether the delayed fluorescence is monoexponential or polyexponential. It is usually the case that a single delayed emission lifetime value is reported, without substantiation for whether this is an average value or whether the delayed emission fits to a monoexponential decay.

Acknowledgements

The authors thank the University of St Andrews for support. E.Z.-C. thanks the Leverhulme Trust (RPG-2016-047) and the EPSRC (EP/P010482/1) for financial support.

Received: October 9, 2016
Revised: November 22, 2016
Published online:

[1] C. W. Tang, S. A. VanSlyke, *Appl. Phys. Lett.* **1987**, *51*, 913.
[2] H. Sasabe, J. Kido, *Eur. J. Org. Chem.* **2013**, *2013*, 7653.
[3] M. Pope, H. P. Kallmann, P. Magnante, *J. Chem. Phys.* **1963**, *38*, 2042.
[4] a) A. C. A. Chen, J. U. Wallace, S. K. H. Wei, L. Zeng, S. H. Chen, T. N. Blanton, *Chem. Mater.* **2006**, *18*, 204; b) Y. Tao, Q. Wang, C. Yang, J. Qin, D. Ma, *ACS Appl. Mater. Interfaces* **2010**, *2*, 2813; c) Q. Wang, H. Aziz, *ACS Appl. Mater. Interfaces* **2013**, *5*, 8733.
[5] a) M. S. Park, J. Y. Lee, *Chem. Mater.* **2011**, *23*, 4338; b) J. Jin, W. Zhang, B. Wang, G. Mu, P. Xu, L. Wang, H. Huang, J. Chen, D. Ma, *Chem. Mater.* **2014**, *26*, 2388.
[6] M. A. Baldo, D. F. O'Brien, Y. You, A. Shoustikov, S. Sibley, M. E. Thompson, S. R. Forrest, *Nature* **1998**, *395*, 151.
[7] D. Y. Kondakov, *J. Soc. Information Display* **2009**, *17*, 137.
[8] B. Minaev, G. Baryshnikov, H. Agren, *Phys. Chem. Chem. Phys.* **2014**, *16*, 1719.
[9] C. Adachi, M. A. Baldo, M. E. Thompson, S. R. Forrest, *J. Appl. Phys.* **2001**, *90*, 5048.
[10] H. Xu, R. Chen, Q. Sun, W. Lai, Q. Su, W. Huang, X. Liu, *Chem. Soc. Rev.* **2014**, *43*, 3259.
[11] Y. Zhang, J. Lee, S. R. Forrest, *Nat. Commun.* **2014**, *5*, 5008.
[12] a) I. R. d. Moraes, S. Scholz, B. Lüssem, K. Leo, *Org. Electron.* **2011**, *12*, 341; b) K. P. Klubek, C. W. Tang, L. J. Rothberg, *Org. Electron.* **2014**, *15*, 1312.
[13] A. Endo, K. Sato, K. Yoshimura, T. Kai, A. Kawada, H. Miyazaki, C. Adachi, *Appl. Phys. Lett.* **2011**, *98*, 083302.
[14] a) Y. Tao, K. Yuan, T. Chen, P. Xu, H. Li, R. Chen, C. Zheng, L. Zhang, W. Huang, *Adv. Mater.* **2014**, *26*, 7931; b) A. Chihaya, *Jpn. J. Appl. Phys.* **2014**, *53*, 060101.
[15] a) H. Uoyama, K. Goushi, K. Shizu, H. Nomura, C. Adachi, *Nature* **2012**, *492*, 234; b) Q. Zhang, B. Li, S. Huang, H. Nomura, H. Tanaka, C. Adachi, *Nat. Photonics* **2014**, *8*, 326; c) Q. Zhang, J. Li, K. Shizu, S. Huang, S. Hirata, H. Miyazaki, C. Adachi, *J. Am. Chem. Soc.* **2012**, *134*, 14706.
[16] a) J. Lee, K. Shizu, H. Tanaka, H. Nakanotani, T. Yasuda, H. Kaji, C. Adachi, *J. Mater. Chem. C* **2015**, *3*, 2175; b) I. S. Park, S. Y. Lee, C. Adachi, T. Yasuda, *Adv. Funct. Mater.* **2016**, *26*, 1813; c) X. Cai, X. Li, G. Xie, Z. He, K. Gao, K. Liu, D. Chen, Y. Cao, S.-J. Su, *Chem. Sci.* **2016**, *7*, 4264.
[17] A. Kretzschmar, C. Patze, S. T. Schwaebel, U. H. Bunz, *J. Org. Chem.* **2015**, *80*, 9126.
[18] S. Y. Lee, T. Yasuda, H. Komiyama, J. Lee, C. Adachi, *Adv. Mater.* **2016**, *28*, 4019.
[19] R. Czerwieniec, M. J. Leitl, H. H. H. Homeier, H. Yersin, *Coord. Chem. Rev.* **2016**, *325*, 2.
[20] K. Shizu, Y. Sakai, H. Tanaka, S. Hirata, C. Adachi, H. Kaji, *ITE Trans. Media Technol. Appl.* **2015**, *3*, 108.
[21] M. Moral, L. Muccioli, W. J. Son, Y. Olivier, J. C. Sancho-García, *J. Chem. Theory Comput.* **2015**, *11*, 168.
[22] M. A. El-Sayed, *Acc. Chem. Res.* **1968**, *1*, 8.
[23] S. Lobsiger, M. Etinski, S. Blaser, H.-M. Frey, C. Marian, S. Leutwyler, *J. Chem. Phys.* **2015**, *143*, 234301.
[24] J. C. Deaton, S. Switalski, D. Y. Kondakov, R. H. Young, T. D. Pawlik, D. J. Giesen, S. B. Harkins, A. J. M. Miller, S. F. Mickenberg, J. C. Peters, *J. Am. Chem. Soc.* **2010**, *132*, 9499.
[25] a) C. A. Parker, T. A. Joyce, *Photochem. Photobiol.* **1967**, *6*, 395; b) R. E. Brown, L. A. Singer, J. H. Parks, *Chem. Phys. Lett.* **1972**, *14*, 193.
[26] P. F. Jones, A. R. Calloway, *Chem. Phys. Lett.* **1971**, *10*, 438.
[27] a) A. Maciejewski, M. Szymanski, R. P. Steer, *J. Phys. Chem.* **1986**, *90*, 6314; b) M. Szymanski, A. Maciejewski, R. P. Steer, *J. Phys. Chem.* **1988**, *92*, 2485.
[28] M. Sikorski, I. V. Khmelinskii, W. Augustyniak, F. Wilkinson, *J. Chem. Soc., Faraday Trans.* **1996**, *92*, 3487.
[29] B. S. Yamanashi, D. M. Hercules, *Appl. Spectrosc.* **1971**, *25*, 457.
[30] It is noted that the involvement of RISC in OLED devices first appeared in 2006 in a patent filed by Kawai et al. However, the operating principle proposed by the inventors is fundamentally different from the TADF emitters presented in this review, which all undergo thermally actived uphill RISC. The inventors' proposed mechanism involves intentionally enlarging the T_1–T_2 gap (e.g., >1.3 eV) so as to decrease the rate of radiationless transition from T_2 to T so that downhill RISC from T_2 to S_1 becomes much more kinetically favourable. See: US patent: T. Kawai, K. Suzuki, H. Tanabe, K. Okinaka, N. Yamada, C. Negishi, A. Saito, M. Okajima, (Canon Kabushiki Kaisha), US7034454 B2, 2016.
[31] H. Yersin, U. Monkowius, DE 10 2008 033 563 A1, **2008**.
[32] A. Endo, M. Ogasawara, A. Takahashi, D. Yokoyama, Y. Kato, C. Adachi, *Adv. Mater.* **2009**, *21*, 4802.
[33] a) R. Czerwieniec, K. Kowalski, H. Yersin, *Dalton Trans* **2013**, *42*, 9826; b) M. J. Leitl, F. R. Kuchle, H. A. Mayer, L. Wesemann, H. Yersin, *J. Phys. Chem. A* **2013**, *117*, 11823; c) M. J. Leitl, V. A. Krylova, P. I. Djurovich, M. E. Thompson, H. Yersin, *J. Am. Chem. Soc.* **2014**, *136*, 16032; d) C. L. Linfoot, M. J. Leitl, P. Richardson, A. F. Rausch, O. Chepelin, F. J. White, H. Yersin, N. Robertson, *Inorg. Chem.* **2014**, *53*, 10854.
[34] a) V. A. Krylova, P. I. Djurovich, B. L. Conley, R. Haiges, M. T. Whited, T. J. Williams, M. E. Thompson, *Chem. Commun.* **2014**, *50*, 7176; b) T. Hofbeck, U. Monkowius, H. Yersin, *J. Am. Chem. Soc.* **2015**, *137*, 399.
[35] a) D. M. Zink, D. Volz, T. Baumann, M. Mydlak, H. Flügge, J. Friedrichs, M. Nieger, S. Bräse, *Chem. Mater.* **2013**, *25*, 4471; b) M. Wallesch, D. Volz, D. M. Zink, U. Schepers, M. Nieger, T. Baumann, S. Brase, *Chemistry* **2014**, *20*, 6578.
[36] a) C. Bizzarri, C. Strabler, J. Prock, B. Trettenbrein, M. Ruggenthaler, C. H. Yang, F. Polo, A. Iordache, P. Bruggeller, L. De Cola, *Inorg. Chem.* **2014**, *53*, 10944; b) D. Liang, X. L. Chen, J. Z. Liao, J. Y. Hu, J. H. Jia, C. Z. Lu, *Inorg. Chem.* **2016**, *55*, 7467; c) Z. Wang, C. Zheng, W. Wang, C. Xu, B. Ji, X. Zhang, *Inorg. Chem.* **2016**, *55*, 2157; d) F. Dumur, *Org. Electron.* **2015**, *21*, 27.
[37] H. Kaji, H. Suzuki, T. Fukushima, K. Shizu, K. Suzuki, S. Kubo, T. Komino, H. Oiwa, F. Suzuki, A. Wakamiya, Y. Murata, C. Adachi, *Nat. Commun.* **2015**, *6*, 8476.
[38] a) J.-H. Jou, S. Kumar, A. Agrawal, T.-H. Li, S. Sahoo, *J. Mater. Chem. C* **2015**, *3*, 2974; b) W.-C. Chen, C.-S. Lee, Q.-X. Tong, *J. Mater. Chem. C* **2015**, *3*, 10957; c) L. Bergmann, D. M. Zink, S. Bräse, T. Baumann, D. Volz, *Top. Curr. Chem.* **2016**, *374*, 1; d) L. Bergmann, D. M. Zink, S. Bräse, T. Baumann, D. Volz, *Top. Curr. Chem.* **2016**, *374*, 22; e) D. Volz, M. Wallesch, C. Fléchon,

M. Danz, A. Verma, J. M. Navarro, D. M. Zink, S. Bräse, T. Baumann, *Green Chem.* **2015**, *17*, 1988; f) D. Volz, *J. Photonics Energy* **2016**, *6*, 020901; g) M. J. Leitl, D. M. Zink, A. Schinabeck, T. Baumann, D. Volz, H. Yersin, *Top. Curr. Chem.* **2016**, *374*, 25.
[39] A. F. Henwood, E. Zysman-Colman, *Top. Curr. Chem.* **2016**, *374*, 36.
[40] S. A. Bagnich, S. Athanasopoulos, A. Rudnick, P. Schroegel, I. Bauer, N. C. Greenham, P. Strohriegl, A. Köhler, *J. Phys. Chem. C* **2015**, *119*, 2380.
[41] a) J. Ritchie, J. A. Crayston, J. P. J. Markham, I. D. W. Samuel, *J. Mater. Chem.* **2006**, *16*, 1651; b) S. Y. Hong, D. Y. Kim, C. Y. Kim, R. Hoffmann, *Macromolecules* **2001**, *34*, 6474.
[42] F. B. Dias, K. N. Bourdakos, V. Jankus, K. C. Moss, K. T. Kamtekar, V. Bhalla, J. Santos, M. R. Bryce, A. P. Monkman, *Adv. Mater.* **2013**, *25*, 3707.
[43] X.-K. Chen, S.-F. Zhang, J.-X. Fan, A.-M. Ren, *J. Phys. Chem. C* **2015**, *119*, 9728.
[44] M. K. Etherington, J. Gibson, H. F. Higginbotham, T. J. Penfold, A. P. Monkman, *Nat. Commun.* **2016**, *7*, 13680.
[45] S. Wu, M. Aonuma, Q. Zhang, S. Huang, T. Nakagawa, K. Kuwabara, C. Adachi, *J. Mater. Chem. C* **2014**, *2*, 421.
[46] Q. Zhang, D. Tsang, H. Kuwabara, Y. Hatae, B. Li, T. Takahashi, S. Y. Lee, T. Yasuda, C. Adachi, *Adv. Mater.* **2015**, *27*, 2096.
[47] I. H. Lee, W. Song, J. Y. Lee, *Org. Electron.* **2016**, *29*, 22.
[48] M. Liu, Y. Seino, D. Chen, S. Inomata, S. J. Su, H. Sasabe, J. Kido, *Chem. Commun.* **2015**, *51*, 16353.
[49] S. Y. Lee, T. Yasuda, Y. S. Yang, Q. Zhang, C. Adachi, *Angew. Chem., Int. Ed. Engl.* **2014**, *53*, 6402.
[50] P. Rajamalli, N. Senthilkumar, P. Gandeepan, P. Y. Huang, M. J. Huang, C. Z. Ren-Wu, C. Y. Yang, M. J. Chiu, L. K. Chu, H. W. Lin, C. H. Cheng, *J. Am. Chem. Soc.* **2016**, *138*, 628.
[51] T. Serevicius, T. Nakagawa, M. C. Kuo, S. H. Cheng, K. T. Wong, C. H. Chang, R. C. Kwong, S. Xia, C. Adachi, *Phys. Chem. Chem. Phys.* **2013**, *15*, 15850.
[52] K. Shizu, H. Noda, H. Tanaka, M. Taneda, M. Uejima, T. Sato, K. Tanaka, H. Kaji, C. Adachi, *J. Phys. Chem. C* **2015**, *119*, 26283.
[53] M. Kim, S. K. Jeon, S.-H. Hwang, J. Y. Lee, *Adv. Mater.* **2015**, *27*, 2515.
[54] T. Ahn, M. S. Jang, H.-K. Shim, D.-H. Hwang, T. Zyung, *Macromolecules* **1999**, *32*, 3279.
[55] D. R. Lee, M. Kim, S. K. Jeon, S. H. Hwang, C. W. Lee, J. Y. Lee, *Adv. Mater.* **2015**, *27*, 5861.
[56] W.-L. Tsai, M.-H. Huang, W.-K. Lee, Y.-J. Hsu, K.-C. Pan, Y.-H. Huang, H.-C. Ting, M. Sarma, Y.-Y. Ho, H.-C. Hu, C.-C. Chen, M.-T. Lee, K.-T. Wong, C.-C. Wu, *Chem. Commun.* **2015**, *51*, 13662.
[57] J. W. Sun, J. Y. Baek, K.-H. Kim, C.-K. Moon, J.-H. Lee, S.-K. Kwon, Y.-H. Kim, J.-J. Kim, *Chem. Mater.* **2015**, *27*, 6675.
[58] J. Ohshita, *Macromol. Chem. Phys.* **2009**, *210*, 1360.
[59] a) C. Mayr, S. Y. Lee, T. D. Schmidt, T. Yasuda, C. Adachi, W. Brütting, *Adv. Funct. Mater.* **2014**, *24*, 5232; b) S. Y. Lee, Y. Takuma, N. Hiroko, C. Adachi, *Appl. Phys. Lett.* **2012**, *101*, 093306.
[60] D. Yokoyama, *J. Mater. Chem.* **2011**, *21*, 19187.
[61] T.-A. Lin, T. Chatterjee, W.-L. Tsai, W.-K. Lee, M.-J. Wu, M. Jiao, K.-C. Pan, C.-L. Yi, C.-L. Chung, K.-T. Wong, C.-C. Wu, *Adv. Mater.* **2016**, *28*, 6976.
[62] R. Komatsu, H. Sasabe, Y. Seino, K. Nakao, J. Kido, *J. Mater. Chem. C* **2016**, *4*, 2274.
[63] T. Takahashi, K. Shizu, T. Yasuda, K. Togashi, C. Adachi, *Sci. Technol. Adv. Mater.* **2016**, *15*, 034202.
[64] K. Masui, H. Nakanotani, C. Adachi, *Org. Electron.* **2013**, *14*, 2721.
[65] J. W. Sun, K. H. Kim, C. K. Moon, J. H. Lee, J. J. Kim, *ACS Appl. Mater. Interfaces* **2016**, *8*, 9806.
[66] D. R. Lee, S. H. Hwang, S. K. Jeon, C. W. Lee, J. Y. Lee, *Chem. Commun.* **2015**, *51*, 8105.
[67] M. Y. Wong, G. J. Hedley, G. Xie, L. S. Kölln, I. D. W. Samuel, A. Pertegás, H. J. Bolink, E. Zysman-Colman, *Chem. Mater.* **2015**, *27*, 6535.
[68] P. Chen, L. P. Wang, W. Y. Tan, Q. M. Peng, S. T. Zhang, X. H. Zhu, F. Li, *ACS Appl. Mater. Interfaces* **2015**, *7*, 2972.
[69] K. Albrecht, K. Matsuoka, K. Fujita, K. Yamamoto, *Angew. Chem., Int. Ed.* **2015**, *54*, 5677.
[70] Y. H. Kim, C. Wolf, H. Cho, S. H. Jeong, T. W. Lee, *Adv. Mater.* **2016**, *28*, 734.
[71] W. Liu, C. J. Zheng, K. Wang, Z. Chen, D. Y. Chen, F. Li, X. M. Ou, Y. P. Dong, X. H. Zhang, *ACS Appl. Mater. Interfaces* **2015**, *7*, 18930.
[72] B. Li, H. Nomura, H. Miyazaki, Q. Zhang, K. Yoshida, Y. Suzuma, A. Orita, J. Otera, C. Adachi, *Chem. Lett.* **2014**, *43*, 319.
[73] W. J. Park, Y. Lee, J. Y. Kim, D. W. Yoon, J. Kim, S. H. Chae, H. Kim, G. Lee, S. Shim, J. H. Yang, S. J. Lee, *Synth. Met.* **2015**, *209*, 99.
[74] K. Shizu, H. Tanaka, M. Uejima, T. Sato, K. Tanaka, H. Kaji, C. Adachi, *J. Phys. Chem. C* **2015**, *119*, 1291.
[75] Y. J. Cho, S. K. Jeon, S.-S. Lee, E. Yu, J. Y. Lee, *Chem. Mater.* **2016**, *28*, 5400.
[76] Y. J. Cho, B. D. Chin, S. K. Jeon, J. Y. Lee, *Adv. Funct. Mater.* **2015**, *25*, 6786.
[77] Y. Kitamoto, T. Namikawa, D. Ikemizu, Y. Miyata, T. Suzuki, H. Kita, T. Sato, S. Oi, *J. Mater. Chem. C* **2015**, *3*, 9122.
[78] K. Suzuki, S. Kubo, K. Shizu, T. Fukushima, A. Wakamiya, Y. Murata, C. Adachi, H. Kaji, *Angew. Chem., Int. Ed. Engl.* **2015**, *54*, 15231.
[79] M. Numata, T. Yasuda, C. Adachi, *Chem. Commun.* **2015**, *51*, 9443.
[80] T. Hatakeyama, K. Shiren, K. Nakajima, S. Nomura, S. Nakatsuka, K. Kinoshita, J. Ni, Y. Ono, T. Ikuta, *Adv. Mater.* **2016**, *28*, 2777.
[81] C. Duan, J. Li, C. Han, D. Ding, H. Yang, Y. Wei, H. Xu, *Chem. Mater.* **2016**, *28*, 5667.
[82] H. Ohkuma, T. Nakagawa, K. Shizu, T. Yasuda, C. Adachi, *Chem. Lett.* **2014**, *43*, 1017.
[83] K. Nasu, T. Nakagawa, H. Nomura, C. J. Lin, C. H. Cheng, M. R. Tseng, T. Yasuda, C. Adachi, *Chem. Commun.* **2013**, *49*, 10385.
[84] L. Mei, J. Hu, X. Cao, F. Wang, C. Zheng, Y. Tao, X. Zhang, W. Huang, *Chem. Commun.* **2015**, *51*, 13024.
[85] I. Lee, J. Y. Lee, *Org. Electron.* **2016**, *29*, 160.
[86] J. Lee, K. Shizu, H. Tanaka, H. Nomura, T. Yasuda, C. Adachi, *J. Mater. Chem. C* **2013**, *1*, 4599.
[87] Y. J. Cho, K. S. Yook, J. Y. Lee, *Sci. Rep.* **2015**, *5*, 7859.
[88] M. Kim, S. K. Jeon, S. H. Hwang, S. S. Lee, E. Yu, J. Y. Lee, *Chem. Commun.* **2016**, *52*, 339.
[89] J. Luo, G. Xie, S. Gong, T. Chen, C. Yang, *Chem. Commun.* **2016**, *52*, 2292.
[90] I. H. Lee, W. Song, J. Y. Lee, S.-H. Hwang, *J. Mater. Chem. C* **2015**, *3*, 8834.
[91] Y. Liu, G. Xie, K. Wu, Z. Luo, T. Zhou, X. Zeng, J. Yu, S. Gong, C. Yang, *J. Mater. Chem. C* **2016**, *4*, 4402.
[92] D. Y. Chen, W. Liu, C. J. Zheng, K. Wang, F. Li, S. L. Tao, X. M. Ou, X. H. Zhang, *ACS Appl. Mater. Interfaces* **2016**, *8*, 16791.
[93] T. Takahashi, K. Shizu, T. Yasuda, K. Togashi, A. Chihaya, *Sci. Technol. Adv. Mater.* **2014**, *15*, 034202.
[94] K. Shizu, J. Lee, H. Tanaka, H. Nomura, T. Yasuda, H. Kaji, C. Adachi, *Pure Appl. Chem.* **2015**, *87*, 627.
[95] Y. J. Cho, S. K. Jeon, B. D. Chin, E. Yu, J. Y. Lee, *Angew. Chem., Int. Ed. Engl.* **2015**, *54*, 5201.
[96] a) R. Ishimatsu, S. Matsunami, K. Shizu, C. Adachi, K. Nakano, T. Imato, *J. Phys. Chem. A* **2013**, *117*, 5607; b) A. Niwa, T. Kobayashi, T. Nagase, K. Goushi, C. Adachi, H. Naito, *Appl. Phys. Lett.* **2014**, *104*, 213303.

[97] a) Y. Noguchi, H.-J. Kim, R. Ishino, K. Goushi, C. Adachi, Y. Nakayama, H. Ishii, *Org. Electron.* **2015**, *17*, 184; b) A. S. D. Sandanayaka, K. Yoshida, T. Matsushima, C. Adachi, *J. Phys. Chem. C* **2015**, *119*, 7631; c) A. S. D. Sandanayaka, T. Matsushima, C. Adachi, *J. Phys. Chem. C* **2015**, *119*, 23845.
[98] a) L. S. Cui, Y. M. Xie, Y. K. Wang, C. Zhong, Y. L. Deng, X. Y. Liu, Z. Q. Jiang, L. S. Liao, *Adv. Mater.* **2015**, *27*, 4213; b) C. W. Lee, J. Y. Lee, *ACS Appl. Mater. Interfaces* **2015**, *7*, 2899; c) B. S. Kim, J. Y. Lee, *ACS Appl. Mater. Interfaces* **2014**, *6*, 8396; d) Y. Im, J. Y. Lee, *Chem. Mater.* **2014**, *26*, 1413; e) M. P. Gaj, C. Fuentes-Hernandez, Y. Zhang, S. R. Marder, B. Kippelen, *Org. Electron.* **2015**, *16*, 109; f) Y. Im, W. Song, J. Y. Lee, *J. Mater. Chem. C* **2015**, *3*, 8061; g) Y. Zhao, C. Wu, P. Qiu, X. Li, Q. Wang, J. Chen, D. Ma, *ACS Appl. Mater. Interfaces* **2016**, *8*, 2635.
[99] a) R. Komatsu, H. Sasabe, S. Inomata, Y.-J. Pu, J. Kido, *Synth. Met.* **2015**, *202*, 165; b) H. Nakanotani, K. Masui, J. Nishide, T. Shibata, C. Adachi, *Sci. Rep.* **2013**, *3*, 2127; c) Y. Seino, S. Inomata, H. Sasabe, Y.-J. Pu, J. Kido, *Adv. Mater.* **2016**, *28*, 2638; d) D. P. Tsang, C. Adachi, *Sci. Rep.* **2016**, *6*, 22463.
[100] Y. J. Cho, K. S. Yook, J. Y. Lee, *Adv. Mater.* **2014**, *26*, 6642.
[101] M. Taneda, K. Shizu, H. Tanaka, C. Adachi, *Chem. Commun.* **2015**, *51*, 5028.
[102] T. Nakagawa, S. Y. Ku, K. T. Wong, C. Adachi, *Chem. Commun.* **2012**, *48*, 9580.
[103] G. Mehes, H. Nomura, Q. Zhang, T. Nakagawa, C. Adachi, *Angew. Chem., Int. Ed. Engl.* **2012**, *51*, 11311.
[104] K. Kawasumi, T. Wu, T. Zhu, H. S. Chae, T. Van Voorhis, M. A. Baldo, T. M. Swager, *J. Am. Chem. Soc.* **2015**, *137*, 11908.
[105] C. Tang, T. Yang, X. Cao, Y. Tao, F. Wang, C. Zhong, Y. Qian, X. Zhang, W. Huang, *Adv. Optical Mater.* **2015**, *3*, 786.
[106] H. Tanaka, K. Shizu, H. Miyazaki, C. Adachi, *Chem. Commun.* **2012**, *48*, 11392.
[107] H. Tanaka, K. Shizu, H. Nakanotani, C. Adachi, *J. Phys. Chem. C* **2014**, *118*, 15985.
[108] K. Shizu, M. Uejima, H. Nomura, T. Sato, K. Tanaka, H. Kaji, C. Adachi, *Phys. Rev. Appl.* **2015**, *3*, 014001.
[109] H. Tanaka, K. Shizu, H. Nakanotani, C. Adachi, *Chem. Mater.* **2013**, *25*, 3766.
[110] Y. Wada, K. Shizu, S. Kubo, K. Suzuki, H. Tanaka, C. Adachi, H. Kaji, *Appl. Phys. Lett.* **2015**, *107*, 183303.
[111] V. Jankus, P. Data, D. Graves, C. McGuinness, J. Santos, M. R. Bryce, F. B. Dias, A. P. Monkman, *Adv. Funct. Mater.* **2014**, *24*, 6178.
[112] J. H. Kim, S. H. Hwang, O. Y. Kim, J. Y. Lee, *SID Symp. Dig. Tech. Pap.* **2015**, *46*, 1658.
[113] H. Wang, L. Xie, Q. Peng, L. Meng, Y. Wang, Y. Yi, P. Wang, *Adv. Mater.* **2014**, *26*, 5198.
[114] L. Meng, H. Wang, X. Wei, J. Liu, Y. Chen, X. Kong, X. Lv, P. Wang, Y. Wang, *ACS Appl. Mater. Interfaces* **2016**, *8*, 20955.
[115] G. Xie, X. Li, D. Chen, Z. Wang, X. Cai, D. Chen, Y. Li, K. Liu, Y. Cao, S. J. Su, *Adv. Mater.* **2016**, *28*, 181.
[116] H. Tanaka, K. Shizu, J. Lee, C. Adachi, *J. Phys. Chem. C* **2015**, *119*, 2948.
[117] Y. Sagara, K. Shizu, H. Tanaka, H. Miyazaki, K. Goushi, H. Kaji, C. Adachi, *Chem. Lett.* **2015**, *44*, 360.
[118] T. Komino, Y. Sagara, H. Tanaka, Y. Oki, N. Nakamura, H. Fujimoto, C. Adachi, *Appl. Phys. Lett.* **2016**, *108*, 241106.
[119] S. Y. Lee, T. Yasuda, I. S. Park, C. Adachi, *Dalton Trans.* **2015**, *44*, 8356.
[120] H. Hirai, K. Nakajima, S. Nakatsuka, K. Shiren, J. Ni, S. Nomura, T. Ikuta, T. Hatakeyama, *Angew. Chem., Int. Ed. Engl.* **2015**, *54*, 13581.
[121] J. Li, Q. Zhang, H. Nomura, H. Miyazaki, C. Adachi, *Appl. Phys. Lett.* **2014**, *105*, 013301.
[122] K. Wu, T. Zhang, L. Zhan, C. Zhong, S. Gong, N. Jiang, Z.-H. Lu, C. Yang, *Chem.–Eur. J.* **2016**, *22*, 10860.
[123] Y. Xiang, S. Gong, Y. Zhao, X. Yin, J. Luo, K. Wu, Z. Lu, C. Yang, *J. Mater. Chem. C* **2016**, *4*, 9998.
[124] S. Y. Lee, T. Yasuda, H. Komiyama, J. Lee, C. Adachi, *Adv. Mater.* **2016**, *28*, 4019
[125] P. Data, P. Pander, M. Okazaki, Y. Takeda, S. Minakata, A. P. Monkman, *Angew. Chem., Int. Ed.* **2016**, *55*, 5739.
[126] A. E. Nikolaenko, M. Cass, F. Bourcet, D. Mohamad, M. Roberts, *Adv. Mater.* **2015**, *27*, 7236.
[127] Q. Zhang, H. Kuwabara, W. J. Potscavage, S. Huang, Y. Hatae, T. Shibata, C. Adachi, *J. Am. Chem. Soc.* **2014**, *136*, 18070.
[128] S. Wang, X. Yan, Z. Cheng, H. Zhang, Y. Liu, Y. Wang, *Angew. Chem., Int. Ed.* **2015**, *54*, 13068.
[129] J. Li, T. Nakagawa, J. MacDonald, Q. Zhang, H. Nomura, H. Miyazaki, C. Adachi, *Adv. Mater.* **2013**, *25*, 3319.
[130] a) R. D. Costa, E. Ortí, H. J. Bolink, F. Monti, G. Accorsi, N. Armaroli, *Angew. Chem., Int. Ed.* **2012**, *51*, 8178; b) R. D. Costa, E. Ortí, H. J. Bolink, *Pure Appl. Chem.* **2011**, *83*, 2115; c) J. D. Slinker, J. Rivnay, J. S. Moskowitz, J. B. Parker, S. Bernhard, H. D. Abruña, G. G. Malliaras, *J. Mater. Chem.* **2007**, *17*, 2976.
[131] a) C. Yang, H. Scheiber, E. J. W. List, J. Jacob, K. Müllen, *Macromolecules* **2006**, *39*, 5213; b) H. Suh, Y. Jin, S. H. Park, D. Kim, J. Kim, C. Kim, J. Y. Kim, K. Lee, *Macromolecules* **2005**, *38*, 6285; c) R. Grisorio, P. Mastrorilli, C. F. Nobile, G. Romanazzi, G. P. Suranna, G. Gigli, C. Piliego, G. Ciccarella, P. Cosma, D. Acierno, E. Amendola, *Macromolecules* **2007**, *40*, 4865; d) J.-K. Lee, R. R. Schrock, D. R. Baigent, R. H. Friend, *Macromolecules* **1995**, *28*, 1966; e) A. J. Sandee, C. K. Williams, N. R. Evans, J. E. Davies, C. E. Boothby, A. Köhler, R. H. Friend, A. B. Holmes, *J. Am. Chem. Soc.* **2004**, *126*, 7041; f) M. S. AlSalhi, J. Alam, L. A. Dass, M. Raja, *Int. J. Mol. Sci.* **2011**, *12*, 2036; g) J. H. Burroughes, D. D. C. Bradley, A. R. Brown, R. N. Marks, K. Mackay, R. H. Friend, P. L. Burns, A. B. Holmes, *Nature* **1990**, *347*, 539.
[132] K. Sun, X. Xie, Y. Liu, W. Jiang, X. Ban, B. Huang, Y. Sun, *J. Mater. Chem. C* **2016**, *4*, 8973.
[133] S. Xu, T. Liu, Y. Mu, Y.-F. Wang, Z. Chi, C.-C. Lo, S. Liu, Y. Zhang, A. Lien, J. Xu, *Angew. Chem., Int. Ed.* **2015**, *54*, 874.
[134] W. Song, I. Lee, J. Y. Lee, *Adv. Mater.* **2015**, *27*, 4358.
[135] a) J. Kido, M. Kimura, K. Nagai, *Science* **1995**, *267*, 1332; b) J. Chen, F. Zhao, D. Ma, *Mater. Today* **2014**, *17*, 175; c) Z. Chen, X.-K. Liu, C.-J. Zheng, J. Ye, C.-L. Liu, F. Li, X.-M. Ou, C.-S. Lee, X.-H. Zhang, *Chem. Mater.* **2015**, *27*, 5206; d) H. H. Chou, Y. K. Li, Y. H. Chen, C. C. Chang, C. Y. Liao, C. H. Cheng, *ACS Appl. Mater. Interfaces* **2013**, *5*, 6168; e) J. Ye, Z. Chen, F. An, M. Sun, H. W. Mo, X. Zhang, C. S. Lee, *ACS Appl. Mater. Interfaces* **2014**, *6*, 8964.
[136] a) G. Li, T. Fleetham, J. Li, *Adv. Mater.* **2014**, *26*, 2931; b) T. Fleetham, J. Ecton, Z. Wang, N. Bakken, J. Li, *Adv. Mater.* **2013**, *25*, 2573; c) E. L. Williams, K. Haavisto, J. Li, G. E. Jabbour, *Adv. Mater.* **2007**, *19*, 197; d) N. Bakken, *J. Photonics Energy* **2012**, *2*, 021203.
[137] S. Reineke, M. Thomschke, B. Lüssem, K. Leo, *Rev. Mod. Phys.* **2013**, *85*, 1245.
[138] J.-i. Nishide, H. Nakanotani, Y. Hiraga, C. Adachi, *Appl. Phys. Lett.* **2014**, *104*, 233304.
[139] T. Higuchi, H. Nakanotani, C. Adachi, *Adv. Mater.* **2015**, *27*, 2019.
[140] D. Zhang, L. Duan, Y. Zhang, M. Cai, D. Zhang, Y. Qiu, *Light: Sci. Appl* **2015**, *4*, e232.
[141] D. Zhang, M. Cai, Y. Zhang, D. Zhang, L. Duan, *ACS Appl. Mater. Interfaces* **2015**, *7*, 28693.
[142] W. Song, J. Y. Lee, *J. Phys. D: Appl. Phys.* **2015**, *48*, 365106.
[143] W. Song, I. H. Lee, S.-H. Hwang, J. Y. Lee, *Org. Electron.* **2015**, *23*, 138.
[144] B. Zhao, T. Zhang, W. Li, Z. Su, B. Chu, X. Yan, F. Jin, Y. Gao, H. Wu, *Org. Electron.* **2015**, *23*, 208.

[145] D. Zhang, L. Duan, Y. Li, D. Zhang, Y. Qiu, *J. Mater. Chem. C* **2014**, *2*, 8191.
[146] L. Meng, H. Wang, X. Wei, X. Lv, Y. Wang, P. Wang, *RSC Adv.* **2015**, *5*, 59137.
[147] B. S. Kim, J. Y. Lee, *Org. Electron.* **2015**, *21*, 100.
[148] B. S. Kim, K. S. Yook, J. Y. Lee, *Sci. Rep.* **2014**, *4*, 6019.
[149] W. Y. Hung, G. C. Fang, S. W. Lin, S. H. Cheng, K. T. Wong, T. Y. Kuo, P. T. Chou, *Sci. Rep.* **2014**, *4*, 5161.
[150] B. Zhao, T. Zhang, B. Chu, W. Li, Z. Su, Y. Luo, R. Li, X. Yan, F. Jin, Y. Gao, H. Wu, *Org. Electron.* **2015**, *17*, 15.
[151] X. K. Liu, Z. Chen, J. Qing, W. J. Zhang, B. Wu, H. L. Tam, F. Zhu, X. H. Zhang, C. S. Lee, *Adv. Mater.* **2015**, *27*, 7079.
[152] K. S. Yook, J. Y. Lee, *Chem. Rec.* **2016**, *16*, 159.
[153] a) P. Schrögel, M. Hoping, W. Kowalsky, A. Hunze, G. Wagenblast, C. Lennartz, P. Strohriegl, *Chem. Mater.* **2011**, *23*, 4947; b) D. Wagner, S. T. Hoffmann, U. Heinemeyer, I. Münster, A. Köhler, P. Strohriegl, *Chem. Mater.* **2013**, *25*, 3758; c) S.-C. Dong, L. Zhang, J. Liang, L.-S. Cui, Q. Li, Z.-Q. Jiang, L.-S. Liao, *J. Phys. Chem. C* **2014**, *118*, 2375.
[154] K. S. Yook, J. Y. Lee, *Adv. Mater.* **2014**, *26*, 4218.
[155] Y.-T. Chang, J.-K. Chang, Y.-T. Lee, P.-S. Wang, J.-L. Wu, C.-C. Hsu, I. W. Wu, W.-H. Tseng, T.-W. Pi, C.-T. Chen, C.-I. Wu, *ACS Appl. Mater. Interfaces* **2013**, *5*, 10614.
[156] C. Han, Y. Zhao, H. Xu, J. Chen, Z. Deng, D. Ma, Q. Li, P. Yan, *Chem.–Eur. J.* **2011**, *17*, 5800.
[157] Y.-S. Tsai, L.-A. Hong, F.-S. Juang, C.-Y. Chen, *J. Lumin.* **2014**, *153*, 312.
[158] D. Hu, P. Lu, C. Wang, H. Liu, H. Wang, Z. Wang, T. Fei, X. Gu, Y. Ma, *J. Mater. Chem.* **2009**, *19*, 6143.
[159] P. L. Dos Santos, J. S. Ward, M. R. Bryce, A. P. Monkman, *J. Phys. Chem. Lett.* **2016**, *7*, 3341.
[160] a) P. Schrogel, A. Tomkeviciene, P. Strohriegl, S. T. Hoffmann, A. Kohler, C. Lennartz, *J. Mater. Chem.* **2011**, *21*, 2266; b) T. Nishimoto, T. Yasuda, S. Y. Lee, R. Kondo, C. Adachi, *Mater. Horiz.* **2014**, *1*, 264.
[161] a) J. Huang, N. Sun, Y. Dong, R. Tang, P. Lu, P. Cai, Q. Li, D. Ma, J. Qin, Z. Li, *Adv. Funct. Mater.* **2013**, *23*, 2329; b) M. Zhu, C. Yang, *Chem. Soc. Rev.* **2013**, *42*, 4963.
[162] D. R. Lee, B. S. Kim, C. W. Lee, Y. Im, K. S. Yook, S. H. Hwang, J. Y. Lee, *ACS Appl. Mater. Interfaces* **2015**, *7*, 9625.
[163] Y. J. Cho, K. S. Yook, J. Y. Lee, *Adv. Mater.* **2014**, *26*, 4050.
[164] Y. Suzuki, Q. Zhang, C. Adachi, *J. Mater. Chem. C* **2015**, *3*, 1700.
[165] T. Zhang, Y. Liang, J. Cheng, J. Li, *J. Mater. Chem. C* **2013**, *1*, 757.
[166] J. Li, D. Ding, Y. Tao, Y. Wei, R. Chen, L. Xie, W. Huang, H. Xu, *Adv. Mater.* **2016**, *28*, 3122.
[167] L.-S. Cui, J. U. Kim, H. Nomura, H. Nakanotani, C. Adachi, *Angew. Chem., Int. Ed.* **2016**, *55*, 6864.
[168] M. Kim, J. Y. Lee, *ACS Appl. Mater. Interfaces* **2014**, *6*, 14874.
[169] M. Kim, S. K. Jeon, S.-H. Hwang, J. Y. Lee, *Synth. Met.* **2015**, *209*, 19.
[170] W. Li, J. Li, F. Wang, Z. Gao, S. Zhang, *ACS Appl. Mater. Interfaces* **2015**, *7*, 26206.
[171] J. Zhang, D. Ding, Y. Wei, F. Han, H. Xu, W. Huang, *Adv. Mater.* **2016**, *28*, 479.
[172] B. S. Kim, J. Y. Lee, *Adv. Funct. Mater.* **2014**, *24*, 3970.
[173] O. Y. Kim, B. S. Kim, J. Y. Lee, *Synth. Met.* **2015**, *201*, 49.
[174] Y. R. Cho, S. J. Cha, M. C. Suh, *Synth. Met.* **2015**, *209*, 47.
[175] C. Fan, C. Duan, Y. Wei, D. Ding, H. Xu, W. Huang, *Chem. Mater.* **2015**, *27*, 5131.
[176] T. Komino, H. Nomura, T. Koyanagi, C. Adachi, *Chem. Mater.* **2013**, *25*, 3038.
[177] T. Komino, H. Tanaka, C. Adachi, *Chem. Mater.* **2014**, *26*, 3665.
[178] D. Ding, Z. Zhang, Y. Wei, P. Yan, H. Xu, *J. Mater. Chem. C* **2015**, *3*, 11385.
[179] G. Méhes, K. Goushi, W. J. Potscavage, C. Adachi, *Org. Electron.* **2014**, *15*, 2027.
[180] D. Zhang, L. Duan, D. Zhang, Y. Qiu, *J. Mater. Chem. C* **2014**, *2*, 8983.
[181] D. Zhang, L. Duan, C. Li, Y. Li, H. Li, D. Zhang, Y. Qiu, *Adv. Mater.* **2014**, *26*, 5050.
[182] C. Li, L. Duan, D. Zhang, Y. Qiu, *ACS Appl. Mater. Interfaces* **2015**, *7*, 15154.
[183] S. Wang, Y. Zhang, W. Chen, J. Wei, Y. Liu, Y. Wang, *Chem. Commun.* **2015**, *51*, 11972.
[184] A. Pertegás, M. Y. Wong, M. Sessolo, E. Zysman-Colman, H. J. Bolink, *ECS J. Solid State Sci. Technol.* **2016**, *5*, R3160.
[185] H. Nakanotani, T. Higuchi, T. Furukawa, K. Masui, K. Morimoto, M. Numata, H. Tanaka, Y. Sagara, T. Yasuda, C. Adachi, *Nat. Commun.* **2014**, *5*, 4016.
[186] X. Y. Liu, F. Liang, Y. Yuan, L. S. Cui, Z. Q. Jiang, L. S. Liao, *Chem. Commun.* **2016**, *52*, 8149.
[187] J. P. Duan, P. P. Sun, C. H. Cheng, *Adv. Mater.* **2003**, *15*, 224.
[188] a) A. P. Kulkarni, S. A. Jenekhe, *J. Phys. Chem. C* **2008**, *112*, 5174; b) D. Wang, W. Li, B. Chu, Z. Su, D. Bi, D. Zhang, J. Zhu, F. Yan, Y. Chen, T. Tsuboi, *Appl. Phys. Lett.* **2008**, *92*, 053304.
[189] K. Goushi, K. Yoshida, K. Sato, C. Adachi, *Nat. Photonics* **2012**, *6*, 253.
[190] K. Goushi, C. Adachi, *Appl. Phys. Lett.* **2012**, *101*, 023306.
[191] J. Li, H. Nomura, H. Miyazaki, C. Adachi, *Chem. Commun.* **2014**, *50*, 6174.
[192] T. Zhang, B. Chu, W. Li, Z. Su, Q. M. Peng, B. Zhao, Y. Luo, F. Jin, X. Yan, Y. Gao, H. Wu, F. Zhang, D. Fan, J. Wang, *ACS Appl. Mater. Interfaces* **2014**, *6*, 11907.
[193] T. Zhang, B. Zhao, B. Chu, W. Li, Z. Su, L. Wang, J. Wang, F. Jin, X. Yan, Y. Gao, H. Wu, C. Liu, T. Lin, F. Hou, *Org. Electron.* **2015**, *24*, 1.
[194] L. Zhang, C. Cai, K. F. Li, H. L. Tam, K. L. Chan, K. W. Cheah, *ACS Appl. Mater. Interfaces* **2015**, *7*, 24983.
[195] Y.-S. Park, K.-H. Kim, J.-J. Kim, *Appl. Phys. Lett.* **2013**, *102*, 153306.
[196] X. K. Liu, Z. Chen, C. J. Zheng, C. L. Liu, C. S. Lee, F. Li, X. M. Ou, X. H. Zhang, *Adv. Mater.* **2015**, *27*, 2378.
[197] X. K. Liu, Z. Chen, C. J. Zheng, M. Chen, W. Liu, X. H. Zhang, C. S. Lee, *Adv. Mater.* **2015**, *27*, 2025.
[198] B. Zhao, T. Zhang, B. Chu, W. Li, Z. Su, H. Wu, X. Yan, F. Jin, Y. Gao, C. Liu, *Sci. Rep.* **2015**, *5*, 10697.
[199] D. Graves, V. Jankus, F. B. Dias, A. Monkman, *Adv. Funct. Mater.* **2014**, *24*, 2343.
[200] E. Hontz, W. Chang, D. N. Congreve, V. Bulovi , M. A. Baldo, T. Van Voorhis, *J. Phys. Chem. C* **2015**, *119*, 25591.
[201] W. Y. Hung, G. C. Fang, Y. C. Chang, T. Y. Kuo, P. T. Chou, S. W. Lin, K. T. Wong, *ACS Appl. Mater. Interfaces* **2013**, *5*, 6826.
[202] T. Furukawa, H. Nakanotani, M. Inoue, C. Adachi, *Sci. Rep.* **2015**, *5*, 8429.